Master Thesis

im Rahmen des
Universitätslehrganges „Geographical Information Science & Systems“
(UNIGIS MSc) am Zentrum für GeoInformatik (Z_GIS)
der Paris Lodron-Universität Salzburg

zum Thema

„Monitoring Mangrove Reforestation with TerraSAR-X in Senegal“

vorgelegt von

Mr. Keith D. Peterson

U102841, UNIGIS MSc Jahrgang 2012

Zur Erlangung des Grades
„Master of Science (Geographical Information Science & Systems) – MSc(GIS)”

Gutachter:
Ao. Univ. Prof. Dr. Josef Strobl

Langenargen, 15.11.2013

“Our journeys, we found, were to take us simultaneously to some of the least-charted regions of the planet and to the least-charted regions of our own minds”.

- Dr. Lawrence Blair

ACKNOWLEDGEMENTS

I would like to thank the Astrium Services GEO-Information Division for providing me with an interesting, challenging and at times frustrating thesis topic, for as Jon Krakauer stated in his book *Into the Wild*, "a challenge in which a successful outcome is assured isn't a challenge at all". In addition, I am grateful to Astrium for providing the numerous TerraSAR-X images as well as the soft- and hardware required for the research and analysis. Furthermore, I would especially like to thank my supervisor and advisor at Astrium, Mrs. Felicitas von Poncet. Your guidance in the field of SAR-analysis and interpretation was invaluable and I greatly appreciate the time you took for our lengthy discussions.

An additional thank you goes out to Polê Carto and the Livelihoods Fund for supplying the field data for this study. Based on personal experience, I know that the collection of the field samples was by no means an easy task, again, thank you.

I would also like to acknowledge the University of Salzburg UNIGIS Team for their support throughout my studies and making this program possible.

Finally, I would like to thank my family, and particularly my wife, for supporting me throughout the duration of my Masters studies. Your advice, motivation and occasional distractions, with the help of Juno, helped me immensely. I could not have done this without you.

EIGENSTÄNDIGKEITSERKLÄRUNG

Ich versichere, diese Master Thesis ohne fremde Hilfe und ohne Verwendung anderer als der angeführten Quellen angefertigt zu haben, und dass die Arbeit in gleicher oder ähnlicher Form noch keiner anderen Prüfungsbehörde vorgelegen wurde. Alle Ausführungen der Arbeit die wörtlich oder sinngemäß übernommen wurden, sind entsprechend gekennzeichnet.

Langenargen den 15. November, 2013 Keith Peterson

ZUSAMMENFASSUNG

Monitoring von Mangrovenwaldaufforstung mit TerraSAR-X im Senegal

Diese Studie erforscht die Reichweite eines Terra SAR-X basierten Monitoring Mechanismus, sowie das Maß zu welchem dieser effizient als zusätzliche Maßnahme zu traditionellen Feld Messungen für kontinuierliche Beobachtungen junger Mangroven Plantagen eingesetzt werden kann. Hierfür wurde ein Forschungsgebiet im südwestlichen Senegal entlang des Casamance Flusses gewählt und erforscht.

Mangrovenwälder sind anfällige und empfindliche Ökosysteme, welche eine bedeutende Rolle im Lebenszyklus zahlreicher Spezies spielen; zudem bieten sie natürliche Ressourcen für menschliche Populationen und schützen Küstenregionen vor den Einflüssen des Klimawandels. Leider sind diese Wälder weltweit gefährdet und deren Flächenanzahl sink rapide. Um das Aussterben dieses wertvollen Ökosystems zu vermeiden, wurden großflächige Aufforstungsmaßnahmen unternommen. Der Livelihoods Fund initiierte ein Mangroven Aufforstungsprojekt im Jahre 2008 im Rahmen eines Clean Development Mechanism. Um den Fortschritt Ihrer Investitionen erfolgreich zu überwachen, ist ein effizientes Monitoring Programm notwendig.

TerraSAR-X StripMap Szenen wurden zeitgleich mit einer Feldkampagne Ende 2012 aufgenommen. Ein statistisches Inversionsmodell wurde von diesen Daten erstellt, um eine objektbasierte Stratifizierung der Wachstumsqualität innerhalb der Plantagen zu entwickeln. Die resultierenden Klassifikationen, die auf zwei TS-X- Szenen umgesetzt wurden, erzielten eine kumulierte Gesamtgenauigkeit von 77% und ein Kappa von 75%. Zusätzlich konnte die Methodik in knapp über 70% des Forschungsgebietes verwendet werden.

Die Ergebnisse dieser Studie sind aktuell hauptsächlich durch die extremen Fluktuationen in der Wassertiefe, verursacht durch die Gezeiten, sowie die Komplexität der Hydrologie der Flussmündungen, eingeschränkt. Diese unbekannten Variablen beeinflussen vor allem die Stratifizierung der Wachstumsqualität.

Nichtsdestotrotz bietet diese Studie eine exzellente Grundlage für zukünftige Forschungsprojekte und beweist, dass ein TerraSAR-X basiertes Monitoringsystem durchaus verwendet werden kann, um flächendeckende Informationen über Mangroven Aufforstungsbemühungen zu erhalten.

ABSTRACT

Monitoring Mangrove Reforestation with TerraSAR-X in Senegal

Keywords: mangrove, reforestation, monitoring, TerraSAR-X, SAR

This study examined to what extent a TerraSAR-X based monitoring mechanism can efficiently supplement traditional field-measurement based monitoring plans for the continuous monitoring of young mangrove plantation environments. For this purpose, a study site in southwestern Senegal, along the Casamance River, was examined.

Mangrove forests are fragile and sensitive ecosystems that play an important role in the lifecycles of numerous species, provide natural resources to human populations and protect coastal areas from the impacts of climate change. Unfortunately, these forests are threatened worldwide and declining at an alarming rate. In order to prevent this valuable ecosystem from completely disappearing, large scale reforestation efforts have been started. The Livelihoods Fund initiated a mangrove reforestation project in 2008 within the framework of a Clean Development Mechanism. To successfully track the progress of their investment, an efficient monitoring program is required.

TerraSAR-X StripMap scenes were acquired over the study area to temporally coincide with a field campaign in late 2012. A statistical inversion model was derived from the data to allow for an object-based stratification of growth quality within the plantations. The resulting image classification, performed on two separate TS-X footprints, yielded a cumulative overall accuracy of 77% and a Kappa of 75%. In addition, the methodology could be applied to just over 70% of the study area.

The results of this study are, at this time, limited mostly by the extreme fluctuations in water depth caused by tidal conditions and the complex hydrology of the estuary. These unknown variables particularly impact the growth quality strata.

Nevertheless, the study provides an excellent foundation for future research and demonstrates that a TerraSAR-X based monitoring system can be utilized to gain valuable wall-to-wall information on the state of mangrove reforestation efforts.

TABLE OF CONTENTS

LIST OF FIGURES

Appendix Figures:

LIST OF TABLES

Appendix Tables:

LIST OF ACRONYMS & ABBREVIATIONS

AGB	Aboveground Biomass
C	Carbon
CDM	Clean Development Mechanism
CER	Certified Emission Redection
CO_2	Carbon dioxide
dB	Decibel
DBH	Diameter at Breast Height
DGPS	Differential Global Positioning System
DLR	Deutsches Zentrum für Luft- und Raumfahrt / German Aerospace Center
EAARL	Experimental Advance Airborne Research LiDAR
EEC-RE	Enhanced Ellipsoid Corrected-Radiometrically Enhanced
EO	Earth Observation
FAO	Food and Agriculture Organization of the United Nations
GHG	Greenhouse Gas
GIM	Geocoded Incidence Angle Mask
GIS	Geographic Information System
GLOMIS	Global Mangrove database and Information System
GVCF	Green Vegetation Cover Fraction
GVI	Green Vegetation Index
HH	Horizontal-Horizontal
HS	High Resolution SpotLight
ISME	International Society for Mangrove Ecosystems
ITD	Infoterra GmbH
ITTO	International Tropical Timber Organization
IUCN	International Union for Conservation of Nature
LiDAR	Light detection and ranging
NDVI	Normailized Differenced Vegetation Index
PDD	Project Design Document
R^2	Coefficient of Determination
RADAR	Radio Detection and Range
REDD+	Reducing Emissions from Deforestation and Degradation
RMSE	Root Mean Square Error
SAR	Synthetic Apature Radar
SC	ScanSAR
SL	SpotLight
SM	StripMap
SSC	Single look Slant range Complex
tDW	tons dead weight
TD-X	TanDEM-X
TS-X	TerraSAR-X
TS-X NG	TerraSAR-X Next Generation
UNFCCC	United Nations Framework Convention on Climate Change
VHR	Very High Resolution
VV	Vertical-Vertical
WASS	Wide Area Augmentation System

1 INRODUCTION

1.1 Motivation & Background

1.1.1 Mangrove Forests – Status & Trends

Mangrove forests are found in coastal areas bordering river banks and lagoons in the tropics and subtropics. The term "mangrove" can be used to describe both the plant family and the ecosystem where the plants are found (FAO, 2007). The *World Mangrove Atlas* defines mangrove plants as "trees and shrubs (the term also includes ferns and palms)" which colonize the fluvial floodplains and river banks in the tropical and subtropical parts of the world (Spalding, Blasco, & Field, 1997). In addition, the term commonly describes salt-tolerant trees and shrubs that have developed "morphological adaptations" to the harsh tidal environment such as "aerial roots, salt excretion glands and vivipary of seeds" (FAO, 2007). Although mangrove forests occur throughout the world, their geographic extent is defined by an approximate latitudinal range between 30° North and 30° South, as well as by a mean sea-surface temperature isotherm of 15° C (Woodroffe & Grindrod, 1991). According to Sakho et al. (2011), mangrove forests occupy 150,000 km^2 (42% the size of Germany) worldwide, representing 75% of the world's tropical coast. As of 2005, they were present in 124 countries and areas throughout the world; the majority of which are in Asia and Africa (FAO, 2007).

Mangroves are an important habitat and one of the most productive natural ecosystems in the world (FAO, 2007). They play a critical role as a natural "nursery" for a variety of birds, mammals, fish, crustaceans, shellfish and reptiles; they additionally enhance the accumulation of sediments and nutrients (Alongi, 2008). According to Adeel and Pomeroy (2002), approximately "90% of all marine organisms spend some portion of their life cycle within mangrove systems". In recent years the role of mangroves, as well as other coastal wetland environments, as a natural buffer zone, protecting coastal areas from sea-level rise, storm surges, shoreline erosion and even tsunamis has gained increasing support among the international community (Adeel & Pomeroy, 2002; Duke et al., 2007; Mazda et al., 2007; Alongi, 2008).

One of the most significant aspects of mangrove forests, in regards to this study, is the fact that they can contain a large amount of biomass (Alongi, 2008), making them a decisive atmospheric CO_2 sink (Duke et al., 2007). According to research by Alongi (2002), these tidal forests can contain biomass levels rivaling those of tropical

rainforests, often having a "standing crop" of 300 – 500 tDW ha^{-1}. This abundance of biomass makes mangroves a high-carbon ecosystem, which has recently become a focal point of the United Nations Framework Convention on Climate Change (UNFCCC) – prioritizing mangrove forests will create opportunities for conservation and "raise awareness that threats to these ecosystems also pose threats to the atmosphere" (Mollins & Verchot, 2013).

In addition to their ecological importance, mangrove forests also play an important role in human sustainability and livelihoods (Alongi, 2008). Mangrove ecosystems are a plentiful source of wood, food and medicine for local communities; the surrounding waters often offer valuable fisheries (Spalding et al., 1997). Historically, mangrove forests were viewed as "inhospitable, unhealthy and dangerous" environments to live in and very few local populations settled in the forest areas themselves, creating a biological balance according to the *World Mangrove Atlas*. Today, the tables have turned, the pressures of rapid population growth, food production and land development are heavily impacting mangrove environments (Spalding et al., 1997), particularly in developing countries, where more than 90% of the world's mangroves are found (Duke et al., 2007).

Figure 1-1: Degraded mangrove forest in Casamance, Senegeal. Photo from Livelihoods (2012a).

Currently, the worldwide surface area occupied by mangrove ecosystems is declining due to anthropogenic and natural causes (Spalding et al., 1997; Valiela et al., 2001; FAO, 2007; Alongi, 2008). Some researchers predict that if the current rate of

mangrove deforestation (1 to 2% annually) continues unabated, mangrove ecosystems may disappear completely within the next 100 years (Duke et al., 2007). In an extensive review of the status of the world's mangroves between 1980 and 2005, the FAO (2007) stated that the global area of mangroves decreased from roughly 18.8 million hectares in 1980 to 15.2 million hectares in 2005 (*Table **1-1***). The general trend in all five regions of the world where mangroves occur is clearly negative. This resilient, yet sensible, ecosystem is severely threatened by the increasing effects of climate change coupled with rapid population growth in coastal areas. Currently, nearly 55% of the world's population is living in coastal zones (Adeel & Pomeroy, 2002), which is associated with an increased pressure on the ecosystems there, with land competition and growing exploitation of natural resources (FAO, 2007). As the use of mangrove ecosystems increases, they become smaller and more fragmented, which leads to a decline in species richness, since the number of mangrove plant species is related to the forest size (Duke et al., 2007).

Table 1-1: Extent of mangrove forest by region between 1980-2005 (FAO, 2007).

Region	1980 1000 ha	1990 1000 ha	Annual change 1980-1990		2000 1000 ha	Annual change 1990-2000		2005 1000 ha	Annual change 2000-2005	
			1000 ha	%		1000 ha	%		1000 ha	%
Africa	3670	3428	-24	-0.68	3218	-21	-0.63	3160	-12	-0.36
Asia	7769	6741	-103	-1.41	6163	-58	-0.89	5858	-61	-1.01
North & Central America	2951	2592	-36	-1.29	2352	-24	-0.97	2263	-18	-0.77
Oceania	2181	2090	-9	-0.42	2010	-8	-0.38	1972	-8	-0.39
South America	2222	2073	-15	-0.69	1996	-8	-0.38	1978	-4	-0.18
World	**18794**	**16925**	**-187**	**-1.04**	**15740**	**-118**	**-0.72**	**15231**	**-102**	**-0.66**

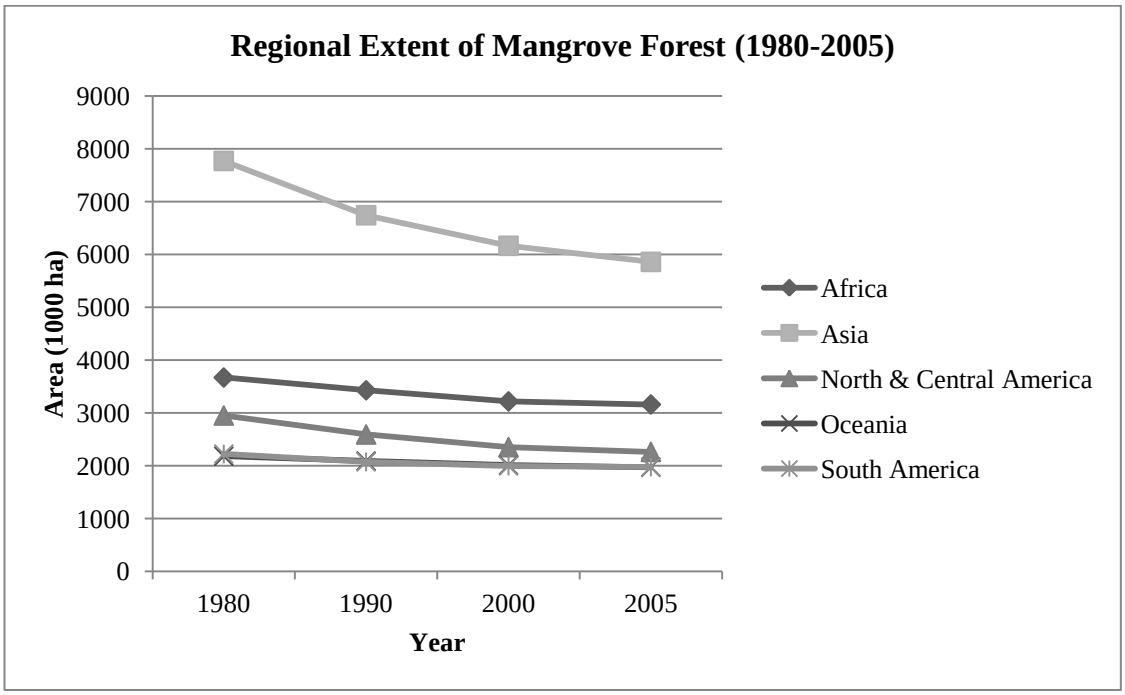

Figure 1-2: Regional extent of mangrove forests between 1980 and 2005 (figure developed by author based on statistics from the FAO (2007)).

Despite the negative trends in forest size and the increased level of threat, some regions of the world are experiencing a localized growth in mangroves and the rate of loss is decreasing (Adeel & Pomeroy, 2002; FAO, 2007). The regional decline in mangrove forest loss, or even growth in forest area, can be attributed to three key factors: (1) an increased level of awareness through educational activities; (2) legislation prohibiting the commercial exploitation of mangrove resources; and (3) the introduction of mangrove reforestation and rehabilitation programs (FAO, 2007). According to Bosire et al. (2008), roughly 150,000 ha of mangrove forest must be restored annually to achieve "no-net-loss".

Mangrove reforestation initiatives have become popular throughout the world and are currently being practiced in the countries of Indonesia, Vietnam, Singapore, Mauritius, Ivory Coast and Senegal, to name a few. The plantation program in Mauritius, implemented in 1980, has become a model of successful mangrove rehabilitation. This small island nation has, according to the FAO (2007), "nearly balanced the considerable previous net loss" of mangrove forest and recent projections call for further growth.

The achievements of such reforestation programs have inspired the West African nation of Senegal, which is one of the African nations experiencing "major losses" in mangrove forest area (FAO, 2007). Due to a series of climatic events (i.e. drought) beginning in the 1970s and increasing anthropogenic pressure that negatively impacted the local mangrove ecosystems, the Senegalese government, local populations and development partners are determined to restore the mangroves throughout the country

(Ndour, Diédiou, & Fall, 2009). Together, they have "put in place cooperation and intervention mechanisms and developed restoration techniques for the degraded areas"(Ndour et al., 2009).

1.1.2 The Livelihoods Fund & Mangrove Reforestation

One such development partner is the Livelihoods Fund (referred to from here out as the Fund), an international carbon investment fund. The Fund, officially established in 2011, grew out of the Danone Fund for Nature, which began in 2008 (Livelihoods, 2012c). According to the Livelihoods Charter (2012b), the Fund "acts as a platform providing the means to restore or preserve ecosystems that are degraded or threatened by mobilizing in particular carbon offset mechanisms". Thereby, the Fund functions as a link between economic bodies and institutions which aim to reduce and offset their greenhouse gas (GHG) emissions through activities that demonstrate a "strong" ecological and social value-added component, on the one side, and local communities "for whom these actions are vital", on the other side (Livelihoods, 2012b).

In this regard, the goals and actions of the Fund can be closely, if not directly, related to those of the Clean Development Mechanism (CDM) established and defined by Article 12 of the Kyoto Protocol in 1998. Article 12 states that the purpose of the CDM "shall be to assist Parties not included in Annex I in achieving sustainable development and in contributing to the ultimate objective of the Convention, and to assist Parties included in Annex I in achieving compliance with their quantified emission limitation and reduction commitments" (UNFCCC, 1998). Within the framework of the CDM, developing countries (Parties not included in Annex I) are stimulated economically and ecologically (e.g. sustainable development) through project activities that generate certified emission reductions (CERs) and industrialized countries (Parties included in Annex I) gain flexibility in how they meet their emission limitation and reduction commitments (UNFCCC, 1998). The CDM allows emission-reduction projects in developing countries, like those established by the Fund, to earn CER credits (each credit is equivalent to 1 tonne of CO_2). The CERs can, in turn, be traded and sold (carbon trading) by industrialized countries.

The Livelihoods Fund, as carbon investment fund, has established CDM projects throughout the world. One of the first "investments" the Fund made was in mangrove reforestation in Senegal. The project, co-managed by a partnership between Danone, the Ramsar Convention on Wetlands and the International Union for Conservation of Nature (IUCN), began in February 2008 and has an expected lifetime of 30 years

(Livelihoods, 2010). The project goals are clearly documented in the "Clean Development Mechanism Project Design Document Form" (CDM-PDD) developed in 2010:

- "To restore degraded wetlands and to improve productivity and environmental condition through reforestation, restoring ecological, economic and social services of a significant part of degraded Senegalese mangroves.
- To mitigate Climate Change by the removal of GHG through biomass growth.
- To reduce poverty of the local communities through employment creation in the short-term and the improvement of sustainable collection of mangrove products in the mid-term."

To meet the project objectives, the Fund proposes a three-phase implementation scheme: (1) the establishment of *Rizophora mangles* (red mangrove) plantations for ecosystem restoration; (2) the development of an awareness program to teach local people about mangrove establishment, conservation and sustainable management; (3) the generation of a monitoring and management system for the duration of the project (Livelihoods, 2010).

The Fund proposes the establishment of 1,700 ha of mangrove plantations located throughout currently degraded mangrove-lands in the Sine Saloum and Casamance estuaries of Senegal. Hereby, they hope to eventually remove 67,851 tCO_2e during the first crediting period (Livelihoods, 2010).

In order to assure the success of the extensive reforestation plan, an accurate and efficient monitoring regime is required to "determine any changes in carbon stocks" (Livelihoods, 2010). The CDM-PDD currently relies on an intensive field measurement based monitoring plan in which the "Carbon Unit" must collect reliable field measurements with GPS throughout the vast project area. To accurately report the project status, the CDM-PDD called for a total of 283 field samples between 2008 and 2009 (see *Figure **1-3***).

	2008			2009			
	GEC	REC	Total	GEC	REC	Total	Total
Area of the stratum (ha)	143,39	5,79	149,18	1003,90	546,80	1550,69	1699,88
Area of the plot(ha)	0.025	0.025		0.025	0.025		
st_i/mean (%)	50	50		50	50		
Number of sample plots	**24**	**1**	**25**	**167**	**91**	**258**	**283**

Figure 1-3: Estimated number of field samples for 2008 and 2009. GEC = Good ecological conditions; REC = Regular ecological conditions (Livelihoods, 2010).

The field sampling was conducted by Pôle Carto, a Marseille based GIS and cartography company, in conjunction with locally trained field personnel. To-date, the field campaigns have not been able to collect the number of field plots called for in the CDM-PDD. The actual number and distribution of field samples collected during the first field campaign (conducted in 2011), which focused primarily on plantations established in 2008 and 2009, was significantly lower; Pôle Carto delivered a total of 36 field samples. The second field campaign, conducted in 2012, resulted in the collection of 85 filed samples.

1.1.3 Mangrove Reforestation Monitoring

According to Field (1999), five practical considerations have to be made when planning the reforestation of a mangrove ecosystem: (1) identification of site degradation causes, (2) evaluation of site selection criteria, (3) sourcing of seedlings and planting, (4) site monitoring and (5) maintenance of the restored mangrove ecosystem. To-date, the Fund has successfully carried out three of the five steps (1 – 3) and has, as discussed in chapter 1.1.2, defined and begun the initial field-based monitoring strategy. As demonstrated above, the goals of the initial CDM-PDD monitoring strategy were impractical. Field (1999) shares this view and states that ground based monitoring techniques are of limited use, as the navigation of mangrove environments is difficult. The article goes on to say that remote sensing based techniques would avoid such problems and the transfer of data to a GIS enables fast actualization as well as the potential for multiple data source combination (Field, 1999). Field (1999) concludes, that the use of such technologies remains practically unexplored, yet "have important roles to play in quantifying the extent, structure and development of mangrove ecosystems and, though it is a relatively expensive activity, it deserves more attention".

To account for the difficulties posed by a purely field-measurement-based monitoring system, the Fund contracted Astrium Services to conduct a feasibility study to examine whether remote sensing products could be used to accurately monitor the young mangrove plantations. Astrium Services, as operator and commercial distributor of the TerraSAR-X (TS-X) and TanDEM-X (TD-X) missions, delivered a comparative analysis of a Very High Resolution (VHR) optical imagery based and a TerraSAR based monitoring method.

The study considered a limited number of select plantations near three communities (Thiobon, Ziguinchor and Cap Skiring) in the Casamance estuary for which three multispectral color WorldView-2 (1.84 m resolution) and five TS-X (1 - 3 m resolution

depending on acquisition mode) images were acquired (Tewkesbury, Von Poncet, & Brown, 2012). The report concluded that "early stage trees" (i.e. canopy footprint < 1 m^2) cannot be directly counted in the WorldView-2 imagery given the spatial resolution, yet it was possible to visually distinguish regions of poor growth from good growth (Tewkesbury et al., 2012). Nevertheless, the Astrium report goes on to say that the attempted optical-based quantification of healthy trees yielded mixed results and that the observed correlation in one area could not be applied to the other two. What is more, the quality and usability of the imagery was severely impacted and limited by cloud and haze which could potentially lead to significantly higher processing costs.

The TS-X based analysis of the same three areas first of all examined which acquisition mode (i.e. High Resolution SpotLight, SpotLight and StripMap) was best suited for the detection of the small trees and the project requirements. The feasibility study concluded that "single mature or small groups of mangroves can be clearly indentified" in both High Resolution SpotLight (up to 1 m resolution) and StripMap (up to 3 m resolution) modes, "thus providing sufficient spatial detail for the assessment of within plot variations" (Tewkesbury et al., 2012). More importantly, the study demonstrated a "strong" correlation between TerraSAR backscatter and tree density in plantations up to four years in age, "where backscatter explains up to 90% of the plant density variance measured in the field" (Tewkesbury et al., 2012).

1.2 Research Statement & Objectives

The primary goal of this Masters thesis is to investigate to what extent a TerraSAR-X based monitoring mechanism can efficiently supplement the traditional field-measurement based monitoring plan currently being implemented for the continuous monitoring and evaluation of young mangrove plantations in Senegal, Africa. Thereby the following research questions will be addressed:

- What is the validity range for the proposed approach?
- How many field samples are required to accurately stratify plantation growth quality? And, what parameters must the field survey fulfill for optimum results?
- To what level of accuracy can tree growth quality be determined and what are the major sources of error that need to be considered?
- Can an efficient and transferable TerraSAR-based monitoring methodology be developed for the continuous evaluation of the CDM project?

1.3 Methodology & Approach

1.3.1 Data Used

The characteristics of the TerraSAR sensor, aboard the TS-X and TD-X satellites, are well suited for the monitoring of young mangrove trees. Unlike optical sensors, SAR operates weather independently and scenes are not impeded by cloud cover or haze. In addition, SAR systems are capable of capturing imagery in both day- and nighttime conditions as it is an active sensor and does not rely on the sun for energy. Furthermore, the TerraSAR system provides an unrivaled geometric accuracy in comparison to other currently available commercial sensors and a flexible resolution (1 – 18.5 m). The TerraSAR system operates in the X-band with a short wavelength of 3 cm, advantageous for the detection of small vegetation (Woodhouse, 2006).

For the purpose of this thesis, a series of TerraSAR StipMap images were acquires over the study area, providing wall-to-wall coverage of the plantations established by the Livelihoods Fund. The images were delivered in two formats (1) Single Look Slant Range Complex (SSC) and (2) Enhanced Ellipsoid Corrected-Radiometrically Enhanced (EEC-RE). To utilize the interferometric coherence (derived from the SSC images), repeat pass acquisitions were captured at the minimum revisit time (11 days) for all footprints.

A limited amount of VHR optical imagery, previously acquired for the feasibility study, was used in conjunction with up-to-date Google Earth imagery (i.e. GeoEye) during the validation phase of the study.

Field data was provided by Pôle Carto in the form of GPS points, MS Excel spreadsheets and extensive photographs.

1.3.2 Study Area

The study area is located in the West African nation of Senegal and encompasses the Casamance Estuary between the nations of Gambia to the North and Guinea-Bissau to the South. A detailed description of the study area is provided in chapter 3.1.

1.3.3 Approach

Based on the data available, the research questions and goals, the methodology will be built around an object-based image analysis procedure. This will be conducted using the Trimble eCognition software. The TS-X images will be segmented and subsequently classified, using a hierarchal classification scheme, into four growth quality strata. The

classification parameters are to be based on a correlation between field measurements and TS-X observations.

1.4 Expected Results

The ultimate goal of this research is to develop an efficient method for monitoring the condition of young mangrove plantations within the study area. Hereby, it is expected that the condition of the plantations (recorded in the field) will correlate to the backscatter and coherence values derived from the TS-X data.

The author expects to establish a relationship between the TerraSAR backscatter signal and the ground truth data that will allow for an accurate supervised classification of the TS-X images. Due to the well-established relationship between SAR backscatter and biomass it is anticipated that the backscatter signal will reveal differences in either plant density or growth quality within individual plantation plots.

A further aspect of this investigation is the transferability of the method. For efficient monitoring the method must be applicable throughout the entire study area and to other sites, given minor adjustments.

As this research strives to develop a service-oriented methodology, the results will need to meet certain accuracy criteria. In general, the classification of the plantations should have an overall accuracy of at least 80%. According to Olson (2008), current computer remote sensing techniques "seldom achieve accuracies above 85%, and 80% is becoming the accepted norm".

1.5 Topics Not Covered

This study concentrates primarily on the quantitative and qualitative stratification of the plantations and does not examine the biophysical parameters of the mangrove plantations or the more mature mangroves. Plantation biomass and carbon stock are not an output of this study.

In addition, it is not the goal of this study to develop a methodology that will replace the need for field surveying, rather to supplement field sampling techniques and increase the efficiency of monitoring efforts.

Finally, this study does not attempt to judge the successfulness of the mangrove reforestation project within the context of the CDM-PDD.

1.6 Target Group

This thesis research is directed towards the remote sensing community and is particularly oriented for colleagues and peers active in the fields of forest monitoring and assessment with remote sensing technologies. Nevertheless, the methodologies and results used and generated by this research should be comprehensible for those with little or no experience in the fields of SAR and remote sensing based environmental monitoring. This thesis should provide a foundation for on-going research on mangrove reforestation monitoring with remote sensing techniques.

1.7 Thesis Structure

The thesis has been divided into seven chapters. The first chapter provides an introduction to the elements covered by this research, research objectives, sub-objectives and research questions. The second chapter introduces the key components of radar imaging, in regards to the thesis topic, to provide readers not familiar with SAR technologies supplemental background information for a clearer understanding of the presented methods and results. Chapter three presents the information on the study area. The data used and the applied methodology has been detailed in the fourth chapter. The fifth chapter presents and explains the results obtained from the methodology through different data analyses. A detailed discussion of the results is described in chapter six. The thesis concludes with a summary of the research and results as well as recommendations for future studies in the field of mangrove reforestation monitoring.

2 INTRODUCTION TO RADAR IMAGING

This chapter provides a general introduction to several key elements of radar imaging, beginning with a brief overview of the development of radar and SAR systems and an explanation of principle terms and characteristics, followed by a brief examination of the TerraSAR-X system. The chapter concludes with a short discussion of the use of SAR in restored mangrove environments.

The science of remote sensing is founded on the principal of data and information collection of features on the Earth's surface without physical contact with the objects. When confronted with providing an explanation supporting the use of microwaves for remote sensing, Ian Woodhouse (2006) simply argued, because "they are different". Woodhouse goes on to say that utilizing the microwave region of the electromagnetic (EM) spectrum expands remote sensing analysis capabilities beyond other more traditional spectral regions (i.e. visible). This is not to say that microwave remote sensing is superior to optical remote sensing, rather that it provides a useful extension to optical analysis techniques due to the manner in which the radar signal interacts with objects on the Earth's surface.

2.1 A Brief History of Radar Imaging

The first space borne radar imaging satellite, Seasat, was launched by NASA in 1978 with the primary objective of studying the oceans (Woodhouse, 2006). Despite its brief 110-day lifetime, the Seasat instrument "revolutionized active microwave remote sensing" according to Woodhouse (2006). Radar imaging has advanced considerably since its beginnings in 1978 and been one of the most exciting fields of remote sensing over the past two decades. The European Space Agency (ESA) launched ERS-1 and 2 into orbit in 1991 and 1995 respectively. The ERS satellites carried Synthetic Aperture Radar (SAR) and provided a combined data set for over 20 years (ERS-2 was retired in 2011). The ERS satellites were followed by Envisat in 2002. Japan's space agency (JAXA) launched JERS-1 in 1992 and ALOS, in 2006, with three different instruments on board, including the L-band radar PalSAR. Unfortunately, the ALOS satellite experienced an unknown error and went offline in 2011. Canada launched Radarsat-1, its first commercial Earth observation (EO) satellite, in 1995 and Radarsat-2 in 2007, both of which operate in the C-band. The Italian Ministry of Research and Ministry of Defense, in cooperation with the Italian Space Agency (ASI), launched four satellites,

equipped with SAR X-band sensors, beginning with COSMO-SkyMed-1 in 2007. COSMO-SkyMed-4 was sent into orbit in 2010. TerraSAR-X (TS-X), the first commercially-oriented radar satellite, was launched in 2007 by Astrium Services and the German Aerospace Center (DLR) and operates in the X-band. The launch of TanDEM-X (TD-X) followed shortly after in 2010.

The steady advancement of radar imaging platforms, according to Woodhouse (2006), has brought microwave sensing "to a level of maturity that affords it a unique place in the observation of Earth". The value of SAR sensors, technologies and information is strongly shared by ESA. The Sentinel missions, composed of five satellites, of which two will be equipped with SAR sensors, are slated to begin in late 2013. Sentinel-1 is outfitted with a C-band sensor and Sentinel-3 will have a dual-frequency Ku- and C-band sensor. The Sentinel missions are part of Europe's Global Monitoring for Environment and Security (GMES or Copernicus) program, on which ESA and the EU have together invested approximately 2.3 billion Euros (Sendling, 2012).

2.2 Basic Principles of Radar Imaging

2.2.1 Microwaves

Radar remote sensing makes use of the microwave portion of the EM spectrum from 1 mm to 1.3 m wavelengths (Massonnet & Souyris, 2008). Microwave interactions are governed by considerably different physical parameters than those of visible EM radiation (Woodhouse, 2006). The differences in the physical properties of microwaves, in comparison to visible wavelengths, can be seen in *Figure **2-1***. The microwave portion of the EM spectrum operates at a much longer wavelength and the intensity of the backscattered EM waves is governed by the geometric and dielectric properties of the scattering objects rather than the chemical makeup of the objects. The penetration capability of an EM wave depends on the length of its wave – the penetration increases with wavelength (Cafforio, Prati, & Rocca, 1991). Therefore, the P-band, operating at wavelengths between 30 and 100 cm, results in a deeper penetration of the surface (i.e. soil or forest canopy) than that of the X-band, which has a wavelength of approximately 3 cm. The long wave characteristics of radar imaging sensors result in the ability of radar waves to penetrate clouds, light rain and smoke, yielding an all-weather remote sensing system.

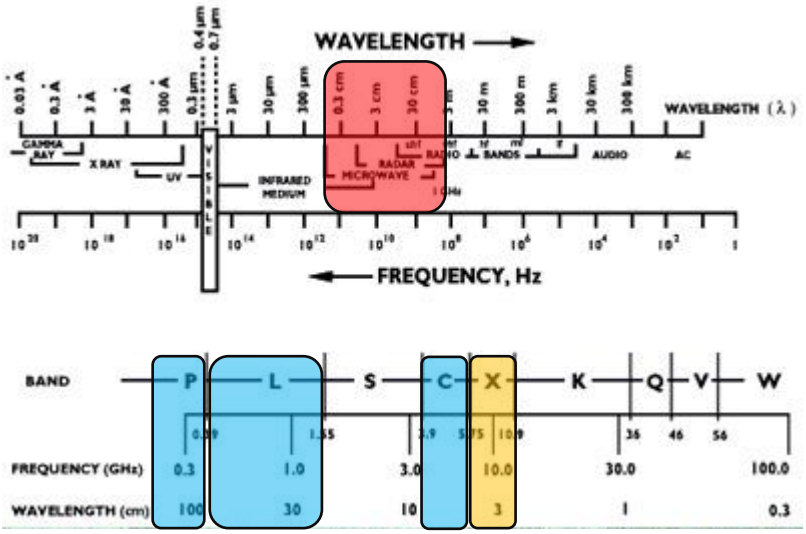

Figure 2-1: The electromagnetic spectrum – the microwave portion of the EM spectrum is highlighted in red. The prominent SAR bands (C, L, P and X) are highlighted in blue and the X-band is shown in orange. Graphic adapted from ESA (2008).

Currently, there are seven commercial- or research-oriented operational SAR satellites in orbit. These satellites operate in either the C- (Radarsat-2) or X-band (TerraSAR-X and COSMO-Sky-Med). The L-band ALOS PALSAR satellite malfunctioned unexpectedly in 2011 and is no longer operational. The P-band is not currently available on any SAR satellite, but is used by some airborne (i.e. aircraft-mounted) SAR providers such as the DLR's F-SAR (DLR). The different microwave bands have, like visible EM bands, different wavelengths (see *Figure **2-1*** above) and the wavelength influences the interaction of energy with a target object. *Figure **2-2*** demonstrates the difference in wavelength penetration in a forest environment. Tree foliage results in increased absorption at shorter wavelengths which minimizes the penetration of the radar beam and therefore minimizes the double-bounce trunk response (Richards, 2009).

Figure 2-2: Differences in microwave band penetration for an Austrian Pine. Graphic reproduced from (Le Toan, 2005).

Yet, it should be noted that scattering properties "scale in proportion to the wavelength", so that the response from smaller trees at shorter wavelengths (i.e. X-band) should be similar to the response from larger trees at longer wavelengths (i.e. L- or P-band) (Woodhouse, 2006).

2.2.2 Synthetic Aperture Radar

Synthetic Aperture Radar (SAR) is a form of radar that was developed to provide accurate azimuth resolution at high altitudes (i.e. satellite orbits). The increase in resolution accuracy is achieved by synthesizing a long antenna by utilizing the forward movement of the satellite (Richards, 2009). According to Richards (2009), the "length of the synthetic aperture is defined by the time that a particular spot on the ground is irradiated by the radar", hence, the longer the spot on the ground is captured by the SAR satellite, the higher the accuracy. This is achieved by using a broad beam in azimuth, as depicted in *Figure **2-3*** (Richards, 2009).

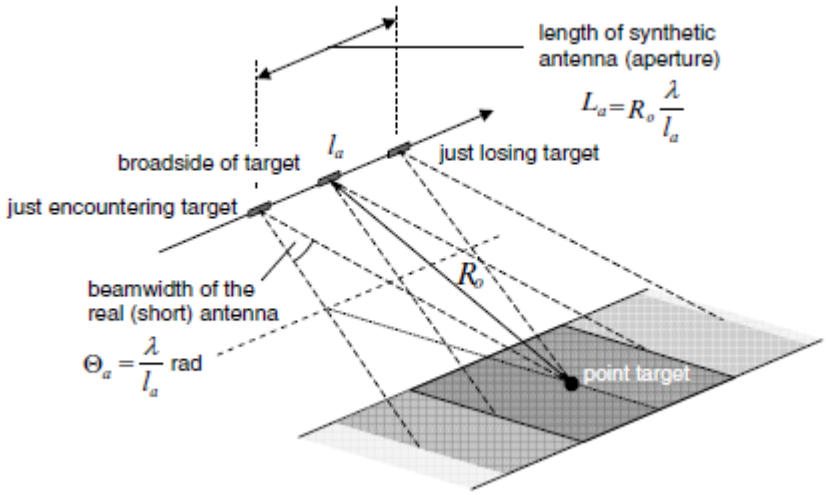

Figure 2-3: The utilization of satellite motion to synthesize a long antenna – the footprint is shown as a rectangle for reasons of simplicity (Richards, 2009).

2.2.3 SAR Polarimetry

The term polarization describes the behavior of the electric field of an EM wave. Electromagnetic waves are transverse, meaning the oscillations are perpendicular to the direction in which the wave is travelling (see ***Figure 2-4***) and the perpendicular polarization planes are typically described as horizontal or vertical with reference to the Earth's surface (Woodhouse, 2006).

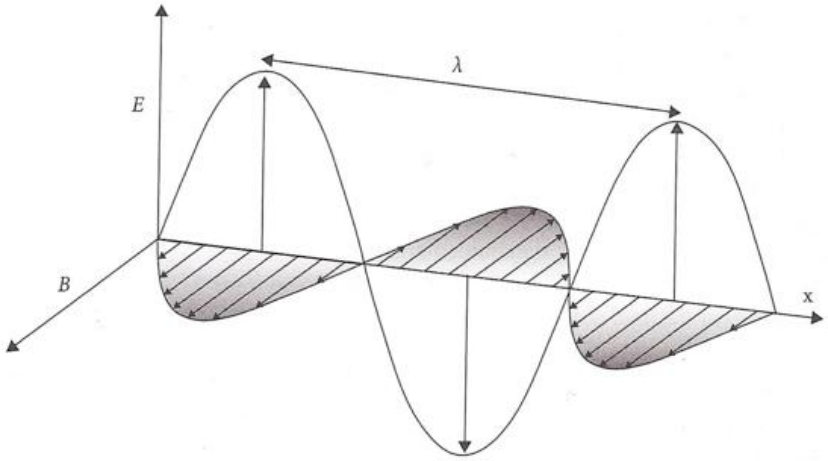

Figure 2-4: Propagation of electromagnetic plane wave. Source:Jones and Vaughan (2010).

The use of polarimetric information is particularly important in SAR remote sensing activities, since the physical characteristics (i.e. size) of an object can be related to the polarimetric properties of the object (Woodhouse, 2006). SAR systems create polarized waves through antennas designed to transmit and receive EM waves of specific polarizations. Single-polarization antennas transmit and receive either horizontal (H) or vertical (V) polarization, whereas dual-polarized SAR systems, such as TerraSAR-X, are capable of transmitting H and receiving both H or V, or transmitting V and receiving both V or H. Since objects on the Earth's surface can change the polarization of the scattered wave (i.e. wave sent back to the sensor) to a different polarization than that of the incident wave, radar antennas are often designed to receive different polarization components at the same time (Canada Centre for Remote Sensing, 2007). Thus, a SAR system using H and V polarizations can have the following channels:

1. HH – horizontal transmit and horizontal receive
2. VV – vertical transmit and vertical receive
3. HV – horizontal transmit and vertical receive
4. VH – vertical transmit and horizontal receive.

Multiple polarizations help in distinguishing the physical structure of the scattering structures, enabling the identification of multiple backscattering mechanisms (Schmitt, Leichtle, Huber, & Roth, 2012).

2.2.4 Backscatter

Woodhouse (2006) explains the concept of scattering as the "redirection of electromagnetic energy by an object". The redirected energy from such objects that is captured by the SAR sensor is referred to as backscatter (symbolized by the Greek letter *sigma*, σ). Unlike the incident energy in the visible or near infrared wavelengths, which

is primarily scattered by the surface of an object being imaged, microwave energy used in SAR remote sensing has a comparatively long wavelength and can therefore often penetrate objects so that scattering can occur from within the object itself as well as from the surface (Richards, 2009). The amount of scattering, and therefore the value of σ, depends on a variety of target characteristics such as shape, dielectric properties, orientation and roughness (Woodhouse, 2006). Therefore, SAR imagery looks different than optical imagery and such effects must be considered during interpretation, as to relate the received energy to an object's biophysical characteristics (Richards, 2009).

Richards (2009) defines the three most common scattering mechanisms from land surfaces as (1) surface scattering, where energy is reflected from a well-defined interface, (2) volume scattering, where reflections come from a variety of scattering elements (i.e. branches, leaves and trunks within a tree canopy) and (3) corner reflector scattering, where the reflection is increased by the relative angle of the object to the sensor. ***Figure 2-5*** provides a simplified depiction of the three scattering mechanisms.

The relative strength of each of these contributions depends on two key factors: (1) the surface roughness and (2) the dielectric properties of the object, and all of these factors depend on the radar frequency, polarization and incidence angle (i.e. looking angle of the SAR sensor) (Toan, 2005).

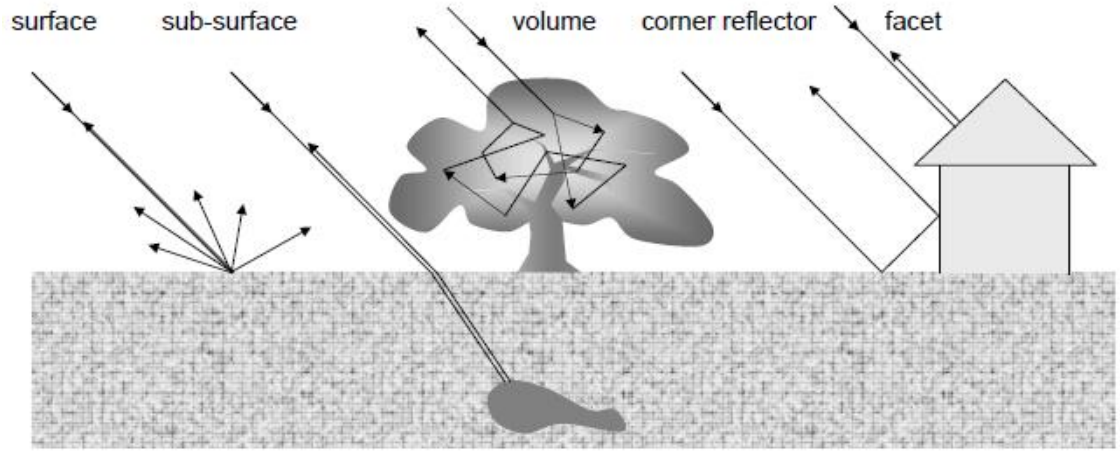

Figure 2-5: The three common most scattering mechanisms. Graphic reproduced from Richards (2009).

2.2.5 Interferometric Coherence

In addition to recording the amplitude of the return signal, SAR systems also record information on the phase of the backscattered echoes. This is a particularly interesting characteristic that differentiates microwave- from optical remote sensing, for which only the intensity (equivalent to amplitude squared) is returned (Richards, 2009). The concept of phase in radar remote sensing is typically applied to the oscillation of EM waves and described as the "stage of the cycle the wave is in" according to Woodhouse

(2006). Interferometry is the technique of measuring differences in the phase resulting from two satellite passes and is often used to detect surface changes. Such information is stored in a raster known as an interferogram or coherence image.

If the relationship between two waves is constant over time, they are said to be coherent (Woodhouse, 2006). In the field of microwave remote sensing, coherency describes the preservation of the phase of the return signal (ESA, 2013); it is a comparative quantity and a "measure of similarity between two waves separated in space or time" (Woodhouse, 2006). The quality of the interferogram is measured by the coherence (magnitude of the complex correlation of both amplitude and phase information), values range from 0 (incoherent) to 1 (fully coherent). The coherency value is, according to the ESA *RADAR and SAR Glossary*, affected by a number of parameters such as:

- Local slope – steep slopes result in low coherence
- Surface properties and land cover – moving surfaces and vegetation have relatively low coherence due to their naturally changing characteristics
- Temporal difference between acquisitions – typically, the larger the time interval between images, the lower the coherence
- Baseline size – large baselines lead to lower coherence
- Technical parameters for the generation of the interferogram – the poorer the quality of the co-registration or resampling of the images, the lower the coherence.

Woodhouse (2006) concludes in his discussion of interferometric coherence that, its use is advantageous, as the analysis and interpretation of decorrelation information can be used for inferring surface conditions or image classification.

2.3 The TerraSAR-X Satellite System

The TerraSAR-X satellite system, jointly operated by Astrium Services and the DLR, currently consists of two fully operational satellites: TerraSAR-X (TS-X) and TanDEM-X (TD-X). The TS-X satellite was launched in June 2007 and has been commercially operational since January 2008. TD-X joined its sister satellite in orbit in October 2010.

Both the TS-X and TD-X instruments are side-looking X-band SAR with an active antenna that allows for multi-mode image capture (i.e. ScanSAR, StripMap and SpotLight). *Table **2-1*** and *Table **2-2*** summarize the characteristic values of the satellite and sensor as stated in the *TerraSAR-X Ground Segment Basic Product Specification Document* (Eineder et al., 2010). ***Figure 2-6*** shows an artist's rendering of the two

satellites in orbit. The two satellites fly in helix formations with a cross-track distance of 200 m which allows for bistatic acquisitions (Eineder et al., 2010).

Table 2-1: TerraSAR-X orbit parameters.

Orbit & Attitude Parameters	
Nominal orbit height at the equator	514 km
Orbits/day	15 2/11
Revisit time (orbit repeat cycle)	11 days
Inclination	97.44°
Ascending node equatorial crossing time	18:00 ± 0.25 h (local time)
Attitude steering	”Total Zero Doppler Steering”

Table 2-2: TerraSAR-X system parameters.

System Parameters	
Radar carrier frequency	9.65 GHz
Radiated RF Peak Power	2 kW
Incidence angle range for StripMap / Scan-SAR	20° – 45° full performance (15°-60° accessible)
Polarizations	HH, VH, HV, VV
Antenna length	4.8 m
Nominal look direction	Right
Antenna width	0.7 m
Number of StripMap /ScanSAR elevation beams	12 (full performance range) 27 (access range)
Number of SpotLight elevation beams	91 (full performance range) 122 (access range)
Number SpotLight azimuth beams	229
Incidence angle range for spotlight modes	20° – 55° full performance (15°-60° accessible)
Pulse Repetition Frequency (PRF)	2.0 kHz – 6.5 kHz
Range Bandwidth	max. 150 MHz (300 MHz experimental)

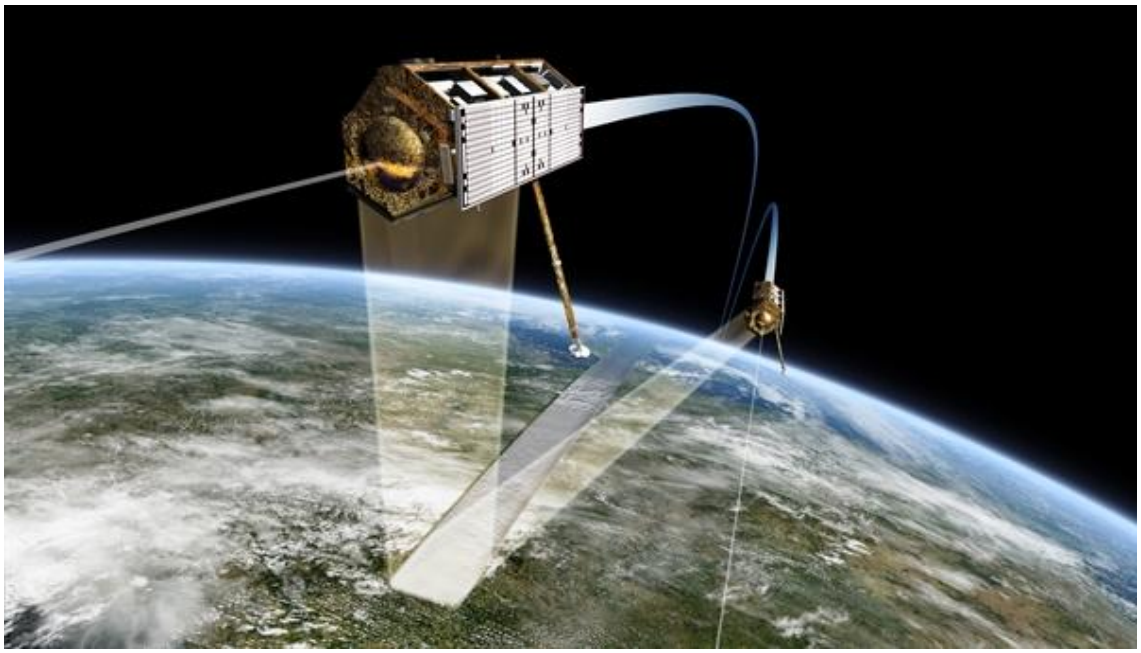

Figure 2-6: Artist’s rendering of the TerraSAR-X and TanDEM-X satellites. Graphic reproduced from DLR (2011).

The TerraSAR Basic Image Products are available in three main image modes and are described as follows by in the *TerraSAR-X Services – Image Product Guide* (Infoterra, 2009):

1. SpotLight (SL) – the SL imaging modes utilize a phased array beam steering technique to increase the illumination time and hence the size of the synthetic aperture, making it possible to acquire data with up to 1 m resolution in the High Resolution SpotLight (HS) mode and 2 m in the standard SL mode. The scene size in the SL and HS acquisition modes are technically restricted to 10 km x 10 km for SL and 10 km x 5 km (width x length) for HS.
2. StripMap (SM) – the SM mode is the standard imaging mode, comparable to that of the ERS-1 satellite. The satellite illuminates a ground swath with a continuous series of pulses resulting in an image strip with consistent quality in the flight direction. The SM mode has a spatial resolution of up to 3 m and a swath width of 30 km. It is possible to extend the acquisition length up to 1,650 km, but the standard scene size is 30 km x 50 km (for manageable image files).
3. ScanSAR (SC) – the SC mode uses electronic antenna elevation steering to capture neighboring and slightly overlapping coverages with different incident angles. The coverages are then processed into a single scene with up to 18 m resolution. The standard scene size is 100 km x 150 km but the acquisition length can be extended to 1,650 km, like that of SM.

*Figure **2-7*** shows how the acquisition of the three different modes vary from one another as well as the difference in surface illumination.

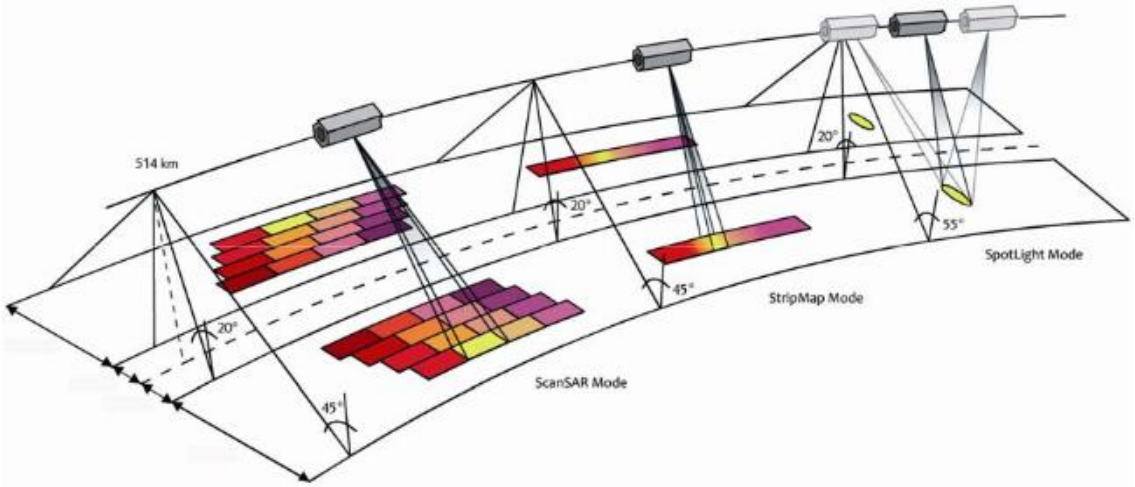

Figure 2-7: TerraSAR-X acquisition modes. Graphic reproduced from TerraSAR-X Services – Image Product Guide (Infoterra, 2009).

2.4 Radar imaging in a mangrove environment

The use of SAR for monitoring wetland environments is widely accepted due to the temporal reliability of the sensor and especially because SAR demonstrates an acute sensitivity to surface water and flooded vegetation, often providing information "unavailable from optical sensors" (Brisco, Schmitt, Murnaghan, Kaya, & Roth, 2011). The advantages of SAR for wetland vegetation monitoring can be, as stated by Brisco et al. (2011), primarily attributed to the dominance of the double-bounce scattering mechanism. The increase of double-bounce scattering due to flooded conditions in forests has been well established in current literature (Hess et al., 1995; Kasischke et al., 1997; Townsend, 2001; Townsend, 2002).

"Flooded vegetation is expected to show a strong double-bounce backscattering", making it distinguishable from other vegetation covers (Schmitt et al., 2012). According to Proisy et al. (2000), the increase in backscattering occurs "when the incident wave propagates through the entire canopy and reaches an underlying highly reflecting surface", which, in a mangrove environment, is the water surface. Hence, mangrove forest typically demonstrate "well pronounced microwave signatures" (Proisy et al., 2000).

Particularly the use of HH polarization is advantageous in a mangrove plantation environment. Kasischke et al. (1997) state that the X-band HH polarization is an optimal parameter for monitoring "coastal/low stature wetlands". This premise can also be inferred from a study by Lopez-Sanchez et al. (2012) which investigated the use of TS-X for rice cultivation monitoring. The structural characteristics of rice plants during the vegetative stage are principally comparable with that of young mangrove saplings, despite their plant density, and the environmental parameters are similar. The study demonstrated a "significant" correlation between the backscatter coefficients at HH channels and plant development (Lopez-Sanchez et al., 2012). According to Lopez-Sanchez et al. (2012), the X-band backscattering at an incidence angle of 30° is dominated by the double-bounce interaction between the flooded surface and the near-vertical plant stems and that thicker stems lead to higher HH backscatter.

The TS-X satellite system is well suited for the monitoring of young mangrove environments. It provides both high temporal and spatial image resolution in the X-band and is available in various polarizations, including HH.

3 STUDY AREA

This chapter provides a geographic and environmental description of the study area where this research was performed. In addition, the mangrove plantation environment is introduced.

3.1 The Casamance Study Area

The study area spreads across southwestern Senegal and comprises a large portion of the Casamance estuary. The size of the study area is, in this case, defined by the available TS-X coverage. The study area is located along the Atlantic coast, an area made up of a multitude of low lying saltwater wetlands and lush mangrove forest. The local climate is characterized as a Sudano-Sahelian type, dominated by two seasons: a dry season from October to June and a rainy season from July to September (Faye, Faye, Ndyoe, & Faye, 2003). A climate diagram for Ziguinchor, Senegal is shown in *Figure **3-1***. The Casamance estuary system is semi-diurnal microtidal, with a maximum tidal range (vertical difference between high and low tide) of approximately 2 m (Sakho et al., 2011).

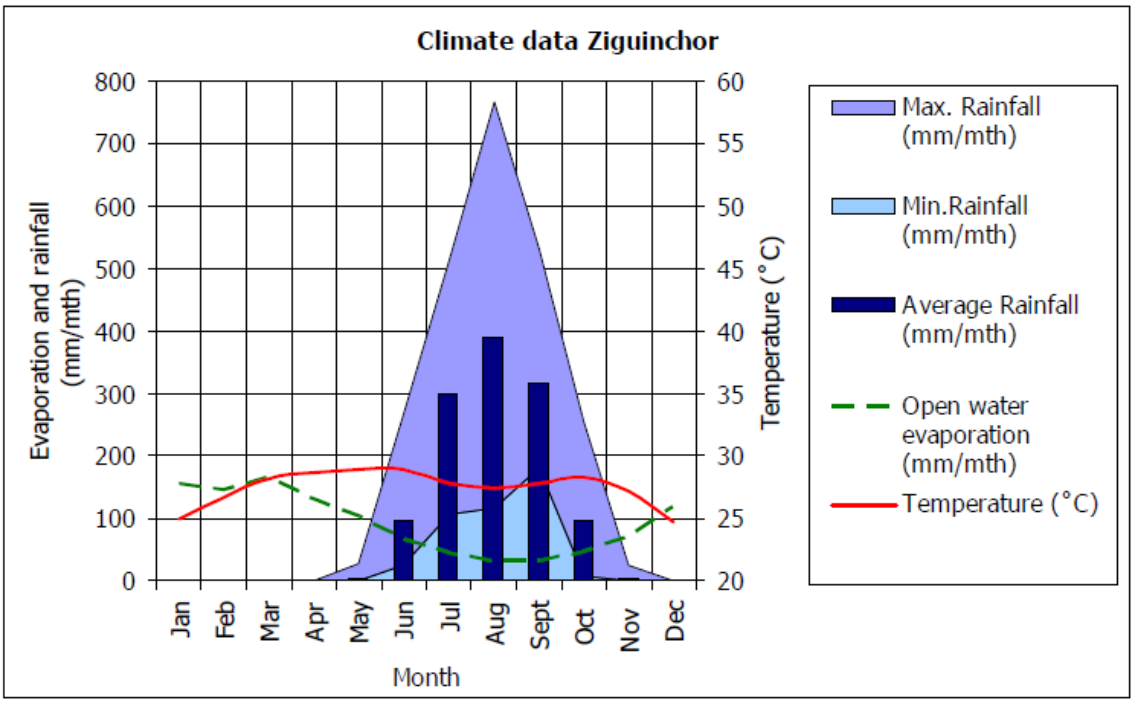

Figure 3-1: Climate diagram for Ziguinchor, Senegal. The mean monthly temperature is from the period 1971 – 1989 and precipitation data is from the interval 1970 – 2004 Graphic reproduced from (Blesgraaf, Geilvoet, van der Hout, Smoorenburg, & Sottewes, 2006).

The Casamance study area (6,131.57 km^2) is located in southern Senegal, bordering the countries of Gambia to the North and Guinea-Bissau to the South. The study area is located in the wettest part of Senegal with up to 200 mm of rainfall per month

(McSweeney, New, & Lizcano, 2010), between 12° 15' and 13° 06' North and 16° 15' and 16° 48' West. The Casamance estuary consists of floodplains with a multitude of mangrove-bounded channels as well as large bare zones (salt flats), referred to as *tannes* by the local inhabitants (Conchedda, Durieux, & Mayaux, 2008). The estuary is heavily influenced by tidal parameters, the tide propagates 240 km upstream from the mouth of the Casamance River (Blesgraaf et al., 2006). Therefore, the mangroves grow in a seawater dominated environment with low freshwater influence; the increasing salinity levels favor the more salt-tolerant *Avicennia nitida* (Conchedda et al., 2008), one of two species that comprise the mangrove forests in the estuary (the other being the *Rhizophora racemosa*) (FAO, 2007).

The plantations considered by this study are defined by data made available by Pôle Carto and were planted between 2008 and 2012. The Livelihoods Fund has established a total of 1,300 mangrove plantations within the study area defined by the TS-X coverage. 871 plantations are located north of the Casamance River, whereas 430 can be found south of the river. The plantations cover a total area of approximately 51.61 km^2. The majority of plantations being examined in this study were established in 2010 (see *Figure **3-2***). At the time of this study, the locations of only 12 plantations established in 2011 were available and no information on the location of 2012 plantings was obtainable. *Figure **3-3*** shows the spatial distribution of the plantations throughout the study area.

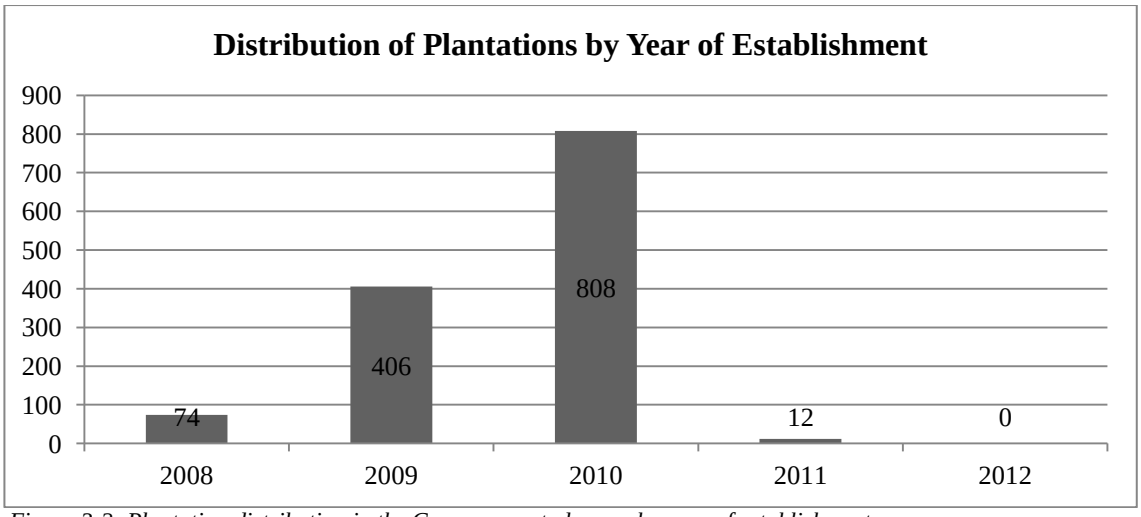

Figure 3-2: Plantation distribution in the Casamance study area by year of establishment.

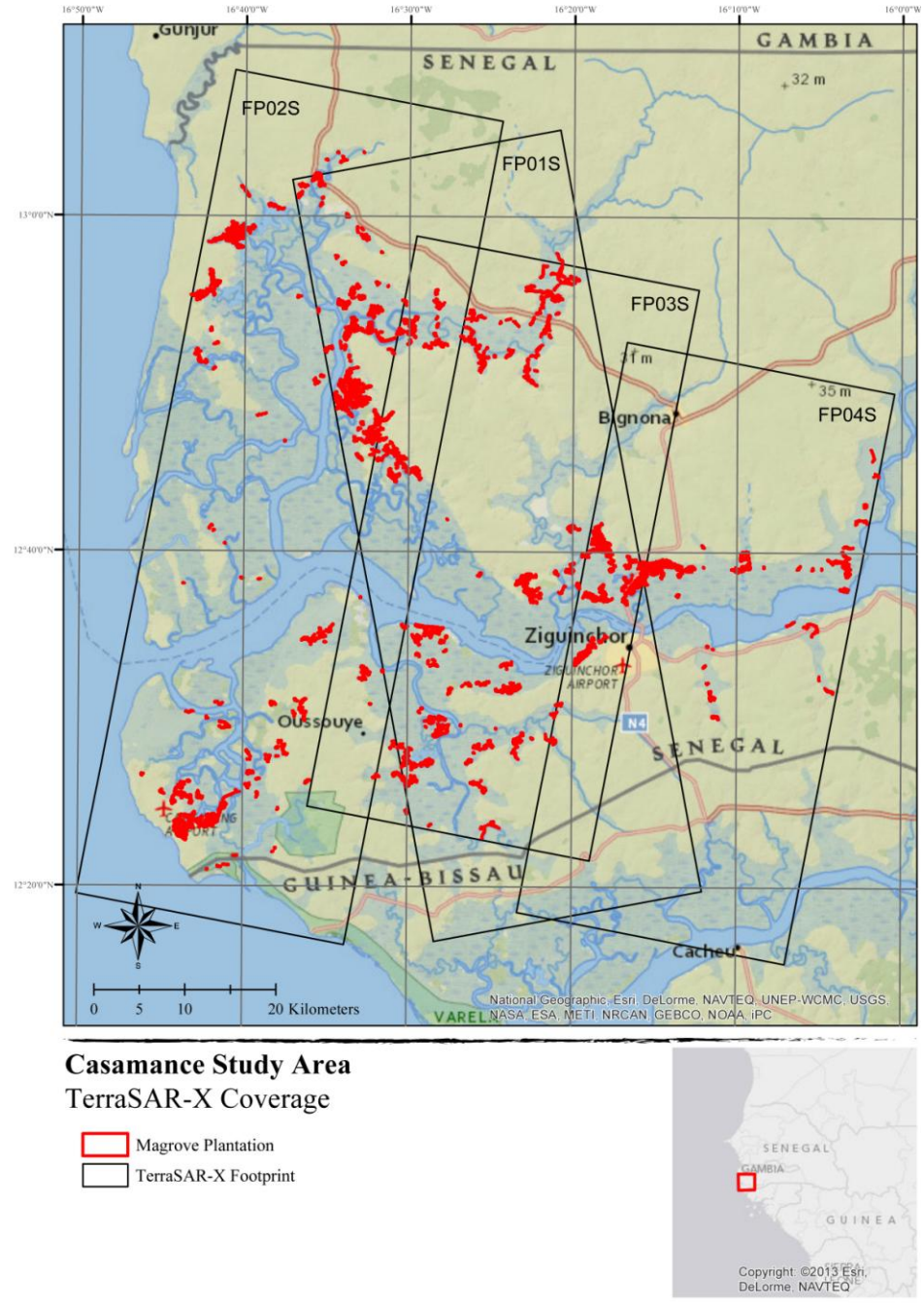

Figure 3-3: Map of the Casamance study area with TS-X coverage and plantation sites.

3.2 Mangrove Plantations – environmental conditions & physical characteristics

The establishment of the mangrove plantations in the study area by the Livelihoods Fund is well documented in the Project Design Document (PDD). The document states that mangrove plantations are to be established in degraded mangrove lands which meet the following three criteria:

1. Soil conditions – preferably muddy and silty-loam with a salinity rate less than 44 ppt and pH between 4.5 and 6.5
2. Tidal immersion – preferably within the intertidal zone an immerged at least four hours a day during both wet and dry seasons
3. Ecological conditions – optimal ecological conditions are determined by the good state of health of mature mangroves and presence of the selected species (*Rhizophora mangle*) in the vicinity.

Additionally, the PDD (2010) states that no seedling preparation (i.e. germination and establishment) is required, as the propagules "will be collected directly from the mature mangrove" near the plantation sites; if there are no propagules in the area, they will be gathered in other regions with "similar ecological conditions". Healthy propagules are then planted manually in a 1 m x 1 m raster, resulting in a theoretical planted density of 10,000 trees/ha (Livelihoods, 2010). The plantations are established in areas that meet the general criteria listed above.

Figure 3-4: Planting of mangrove propagules by local inhabitants. Photo from the Livelihoods (2012a).

a)  b) 

Figure 3-5: Mangrove propagules: a) propagules collected near plantation site; b) planted propagule (photo taken during the 2012 field survey by Pôle Carto field team).

The young mangrove plantations (up to four years in age) considered by this study vary in their growth rates, from freshly planted propagules (see *Figure **3-5b***) to well-developed saplings with a measurable crown and stilt-roots. Representative mangrove plantations in the study area are depicted in *Figure **3-6***. As the trees age they grow in height and diameter and begin to develop branches and eventually stilt roots.

Figure 3-6: Representative mangrove plantations, left a plantation established in 2011 and right a plantation planted in 2009 (photos taken by the Pôle Carto field team during the 2012 field survey).

4 MATERIALS & MEHTODOLOGY

This chapter is divided into two sub-sections, the first of which provides a detailed description of data used, while the second presents the methodology adopted for this research. ***Figure 4-1*** depicts the generalized workflow used to derive the qualitative stratification information from the TerraSAR-X data. The procedural details are shown later in separate diagrams devoted to the specific processing steps.

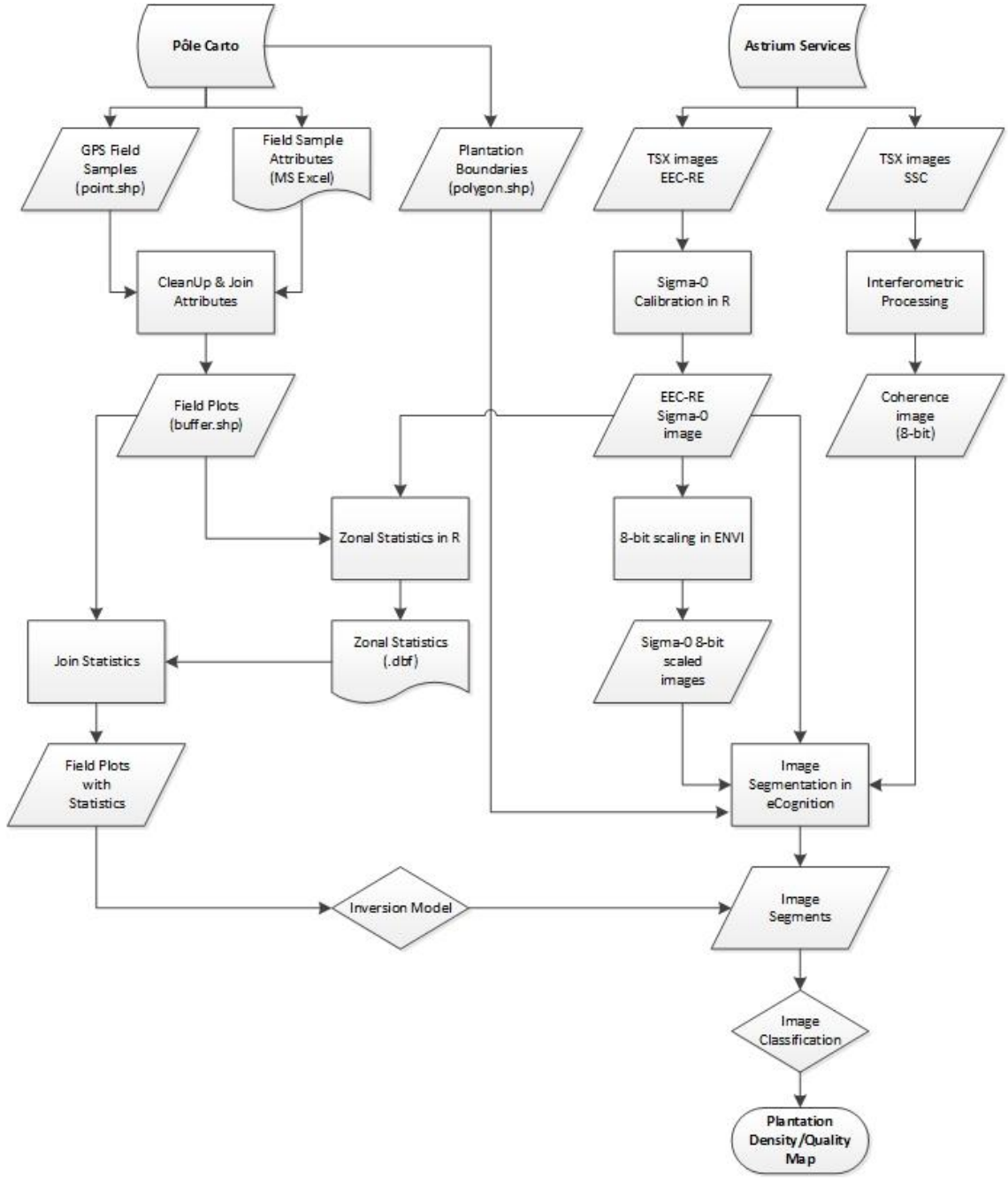

Figure 4-1: Generalized methodology workflow diagram.

4.1 Materials

The primary data source for this study was TS-X and TD-X satellite remote sensing data. Field data, provided by a project partner, was the secondary data source. Additionally, Very High Resolution (VHR) optical remote sensing data was used to attain additional sample plots and to validate the stratification results.

4.1.1 TerraSAR-X Remote Sensing Data

The TerraSAR-X (TS-X) data was acquired in StripMap (SM) mode, as the preliminary feasibility study demonstrated that SM mode provides sufficient detail for the discrimination of variation within individual plantations and also delivers wide area coverage (30 km x 50 km), resulting in significantly lower operational costs for the end user than possible with SpotLight (SL) data (Tewkesbury et al., 2012).

Ten TS-X SM images were acquired for this study to provide the needed spatial and temporal coverage of the study area. The study area was positioned to allow for an efficient and seamless north-to-south acquisition in single flight paths. Four TS-X footprints were used to fully cover the plantation sites (see ***Figure 3-3***). The choice of TS-X footprints was important for achieving maximum area coverage with the minimum possible revisit time (11 days). The images were acquired between late October 2012 and February 2013 to correspond with the dry season in Senegal (see ***Figure 4-2***). A complete list of the TerraSAR scenes used in this study is provided in ***Table 4-1***.

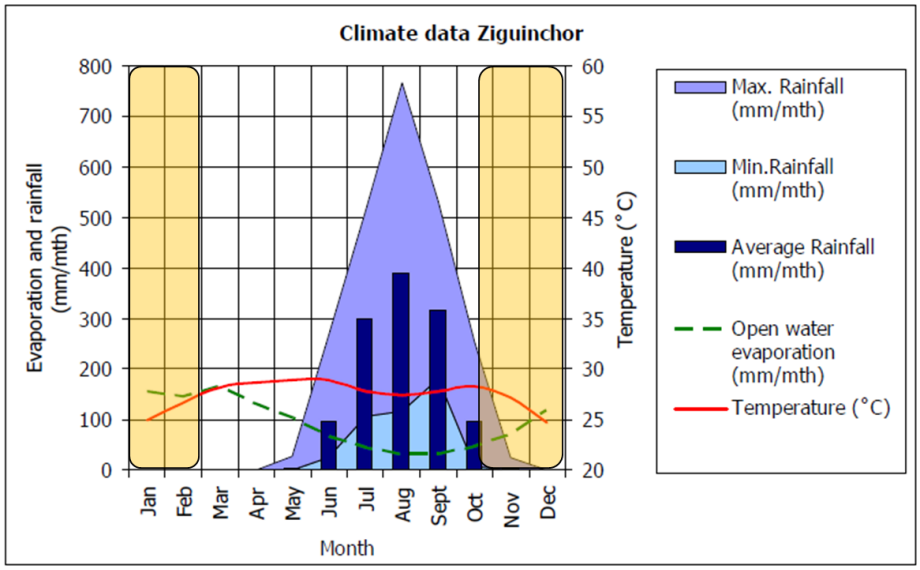

Figure 4-2: TerraSAR acquisition period (highlighted in orange) planned to coincide with the local dry season. Graphic reproduced from Blesgraaf et al. (2006) and modified by the author.

The images were captured with a single HH polarization. The HH polarization was chosen based on the physical characteristics of the mangrove plantations and the general

operating conditions (see section 3.2). The operating conditions in young mangrove plantations in the study area are similar to those found in rice patties – the plants grow in an environment dominated by flooding and have comparable physical parameters.

Two images were acquired for each of the four footprints in order to generate interferometric coherence images. The acquisitions were made with a time interval of 11 days (the minimum revisit time) to increase the probability of coherence - large temporal gaps lead to low coherence (ESA, 2013). An additional two images were acquired on 17.02.2013 and 28.02.2013 for FP04S and FP02S respectively.

Table 4-1: TerraSAR imagery acquired for the study.

Sensor	Footprint ID	Acquisition Date	Acquisition Time	Incidence Angle*
TS-X	FP01S	24.10.2012	19:08	27.20 – 30.24
TD-X	FP01S	04.11.2012	19:08	27.20 – 30.24
TD-X	FP02S	30.10.2012	7:02	31.76 – 34.56
TS-X	FP02S	10.11.2012	7:02	31.76 – 34.56
TS-X	FP02S	28.02.2013	7:02	31.76 – 34.56
TS-X	FP04S	21.11.2012	7:02	27.20 – 30.24
TS-X	FP04S	02.12.2012	7:02	27.20 – 30.24
TS-X	FP04S	17.02.2013	7:02	27.20 – 30.24
TS-X	FP03S	13.12.2012	7:02	29.52 – 32.44
TS-X	FP03S	24.12.2012	7:02	29.52 – 32.44

*Note: the incidence angle is provided here as the range (minimum - maximum).

The images were ordered in two formats: (1) Single Look Slant Range Complex (SSC) and (2) Enhanced Ellipsoid Corrected-Radiometrically Enhanced (EEC-RE). The SSC product is designed for SAR applications requiring both the amplitude and phase information, such as SAR interferometry. In addition, the images do not contain radiometric artefacts which could be caused by spatial resampling (Infoterra, 2009). The EEC product provides the highest level of geometric accuracy available for the TS-X Basic Image Products (Infoterra, 2009), making it easily compatible with other types of geo-information. The images were ordered in UTM and come terrain corrected (the terrain correction is based on an external DEM product). The radiometric enhancement (RE) decreases the range and azimuth, and in turn reduces the speckle – 5 to 7 looks are averaged to generate a radiometric resolution of 1.5 dB (Infoterra, 2009). This calibration is essential when working with low backscattering values (Lopez-Sanchez et al., 2012), as is the case in the mangrove plantation environment.

4.1.2 Optical Remote Sensing Data

A limited amount of VHR optical satellite remote sensing data was acquired during the initial feasibility study, performed by Astrium, in order to compare the analysis potential of radar and optical remote sensing data. Three small WorldView-2 images

were acquired throughout the study area near Thiobon, Ziguinchor and Cap Skiring (see ***Figure 4-3***). The WorldView-2 images have 4 bands: red, green, blue and near-infrared (NIR).

In addition, imagery from Google Earth was used in areas where there was no WorldView-2 coverage available. The Google Earth imagery available in the study area at the time was primarily from GeoEye and coincidently acquired during the same general time period (± 6 months) as the TS-X images. *Table **4-2*** provides information about the VHR optical imagery used in the study.

The optical imagery was used for the generation of additional reference sample plots for specific land cover types not included in the field survey by Pôle Carto and for the validation of the classification results.

Table 4-2: VHR optical imagery used for the study.

Sensor Type	Acquisition Date	Resolution	Extent (km^2)	Area
WorldView-2	26.12.2011	0.5 m	120	Ziguinchor
	31.12.2011		31	Thiobon
	03.01.2012		31	Cap Skiring
Google Earth (Digital Globe)	21.03.2012	NA	2834	NA
	01.04.2012		1650	
	21.09.2012		325	

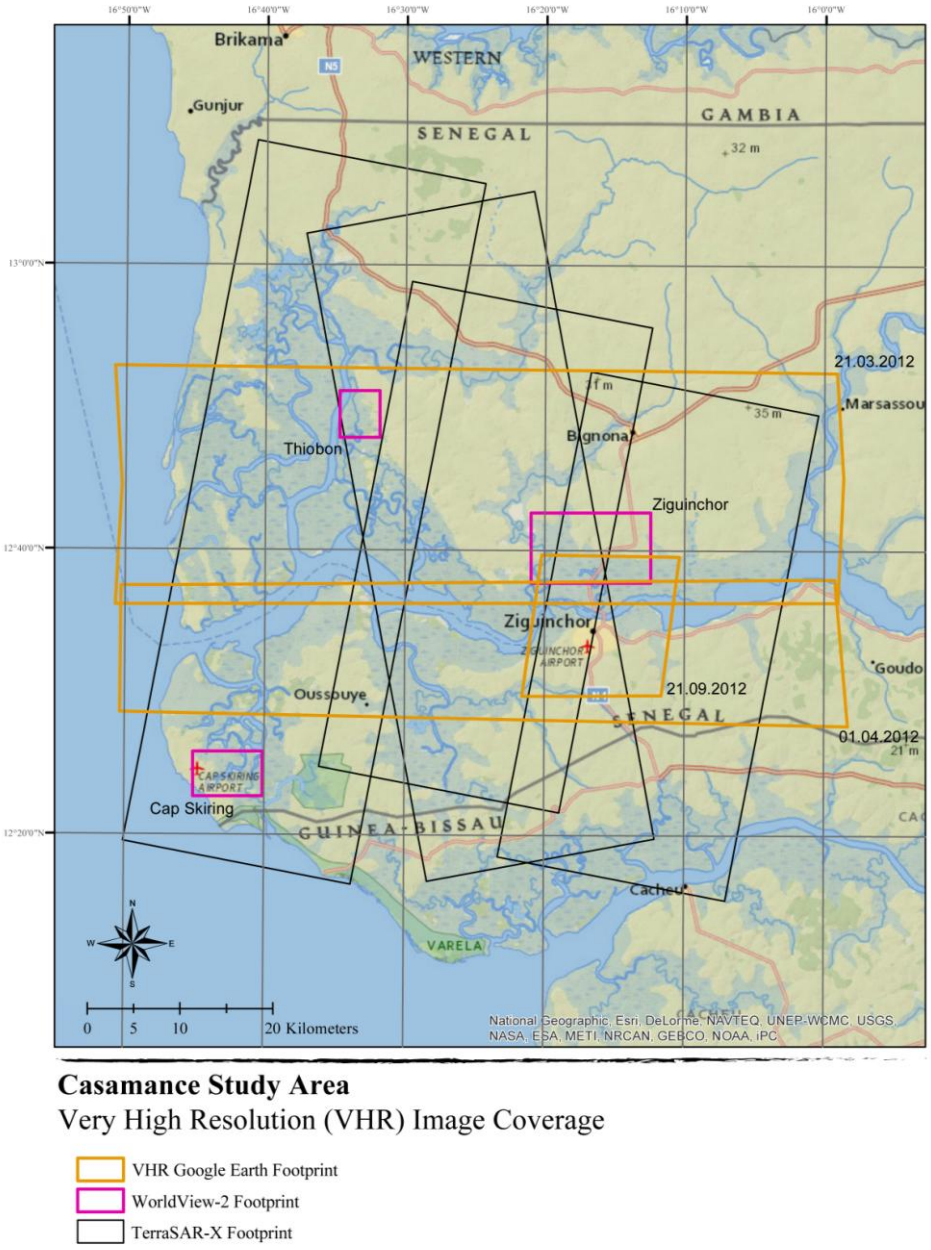

Figure 4-3: VHR optical data coverage in the study area.

4.1.3 Field Data

Field data was collected and provided by Polé Carto. They performed a field survey in December 2012 and provided 85 field samples within the study area. The field survey was planned in conjunction with Astrium to provide the reference data needed for the correlation between ground-based measurements and radar backscatter. However, field measurements were preformed during a routine field campaign and therefore had to be focused on the plots planted in 2012 in order to plan for the re-planting of gaps where plants were dead or growing poorly. Hence, the resulting measurements could not fully meet the field data requirements defined by Astrium. The survey team used a handheld GPS device (Garmin eTrex) with a GPS accuracy of 15 m and a DGPS (WAAS) accuracy of <3 m (GARMIN, 2006). The field samples were circular with a 10 m

radius, hence a total area of 314 m^2. The extent of the plot was regulated through the use of a 10 m length of rope; one team member stood at the center of the plot with one end of the rope while a second team member stretched the rope to its full length and walked the perimeter of the circle (see ***Figure 4-4***).

Figure 4-4: Photos provided by the field team showing the measurement of the field plot (left) recording of measurements in the field sheets (right).

Several different types of plots were recorded during the December 2012 field campaign (see *Table **4-3***). The field survey recorded the following information for plantation density plots:

- Year – the year in which the plantation was planted
- Density – the number of planted trees per plot
- Tree height – the tree height was measured for representative trees (typically 3 to 5 trees)
- Tree diameter – the tree diameter was measured for representative trees (typically 3 to 5 trees)
- Water depth – water depth was recorded for select sample plots acquired on the same day as a TS-X image acquisition (13.12.2012).
- Comments – comments were recorded when necessary on atypical plot characteristics (i.e. growth quality, presence of other vegetation types within plot, presence of water, etc.)
- Photos – digital photos were taken in each plot, the photo numbers were recorded for each plot.

Two "biomass" plots recorded the same type of information as the plantation density plots, only that they included the height, stem diameter and crown diameter for *every*

tree within the plot. The biomass plots were smaller in size than the other sample plots. They were square in form and approximately 104 m^2 and 83 m^2 in size.

All the other plot types were recorded to provide additional ground truth information to be analyzed in the TS-X images and typically included comments on ground cover, vegetation and photos.

Table 4-3: Field sample plot category collected in December 2012.

Plot Type	Number of Plots
Plantation Density	72
Plantation (Dead)	2
Plantation Biomass	2
Other Vegetation	6
Other	2
Mud-Flat (Field)	1
TOTAL	***85***

To bolster the data measured in the field, a biomass (or tree volume) attribute was added. The calculation of the biomass was based on the findings of Medeiros and Sampaio (2007), who performed an extensive study of aboveground biomass (AGB) for several different species of mangrove trees, including the *Rhizophora mangle*, in Brazil. Equations to estimate AGB were developed specifically for each species type based on destructive sampling (i.e. trees were harvested in order to make measurements) and even included trees with a minimum diameter at breast height (DBH) of 2 cm (Medeiros & Sampaio, 2007). The study found that the AGB significantly correlates to tree diameter and that the biomass estimation can be improved by considering the tree height as well (Medeiros & Sampaio, 2007). The authors (2007) developed the following formula for the estimation of *Rhizophora mangle* biomass (kg) with a coefficient of determination (R^2) of 0.94:

$$AGB = 0.2752(D^2H)^{0.8529}$$

The field measured tree heights and diameters, although they could not be measured at breast height due to the small size of trees, were input into the formula to estimate AGB for the field plots. Although the equation was developed for Brazilian mangroves, it can be applied to the project area due to the characteristics of the allometric equation for mangroves which is, according to Komiyama et al. (2008) more species-specific and less site-specific.

An analysis of the information collected in the field revealed that the majority of field samples in the study area were taken in plantations established in 2011 and 2012 (77.2%) and that no data was collected in plantations planted in 2010 (see *Figure **4-5***).

Due to the field surveys concentration on plantations established in 2011 and 2012, 71% of the plots contained trees <41 cm in height (see ***Figure 4-6***).

The majority (74.7%) of plots had a plant density <301 trees/plot (see ***Figure 4-7***). These measurements correspond well with the estimated mortality rate (see *Table **4-4***) calculated by the Livelihoods Fund (Livelihoods, 2010).

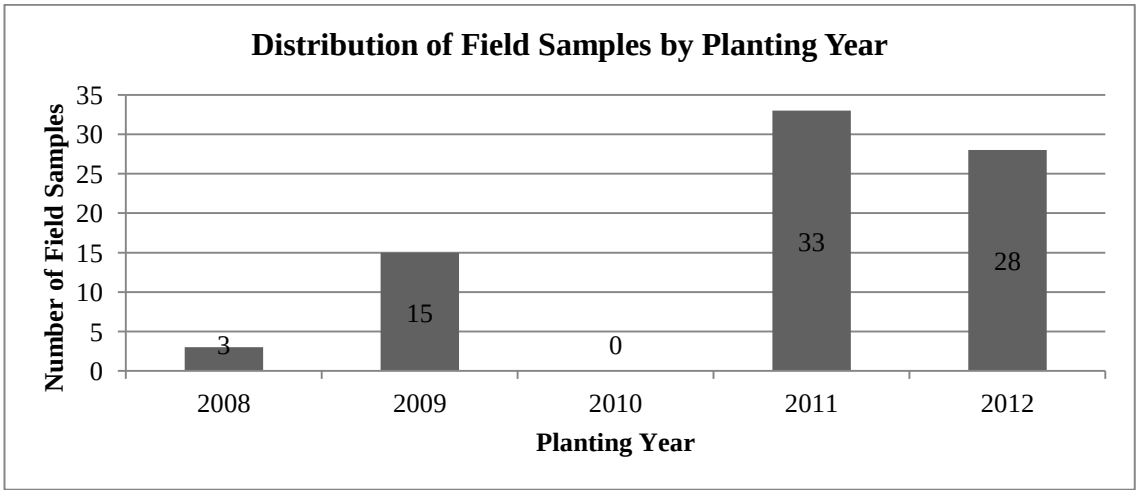

Figure 4-5: Field sample distribution by year of plantation establishment.

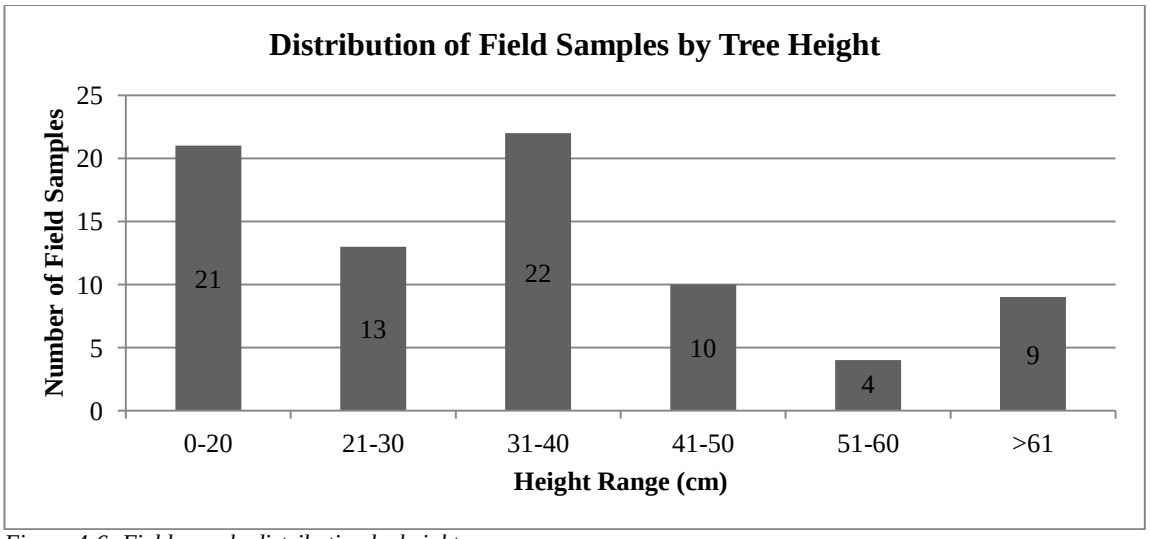

Figure 4-6: Field sample distribution by height range.

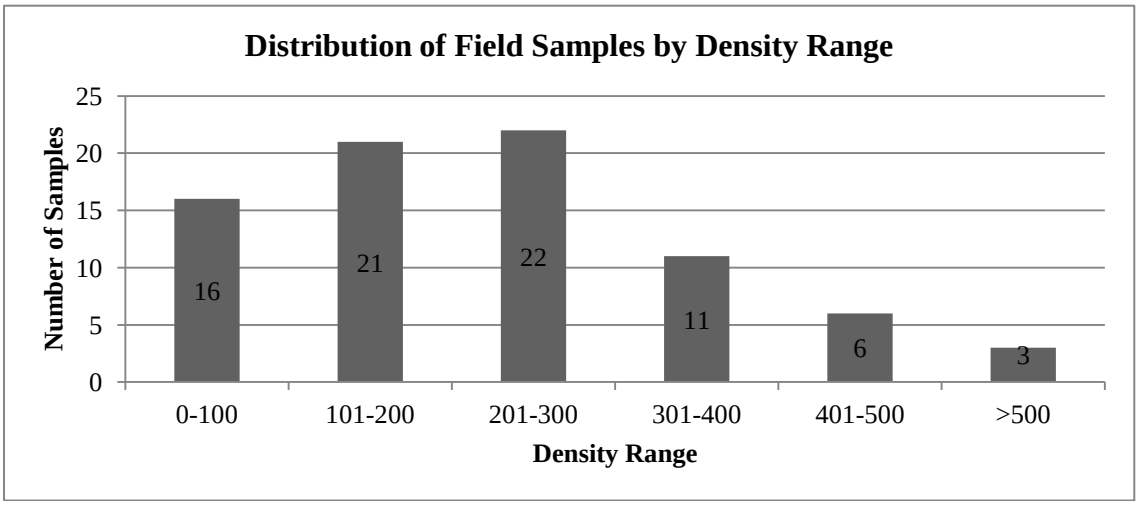

Figure 4-7: Field sample distribution by density range.

Table 4-4: Estimated tree mortality rates for mangrove plantations (Livelihoods, 2010).

Age (year)	Density (trees/plot)	Density (trees/ha)	Mortality Rate (%)
1	314	10,000	50
2	157	5,000	50
3	78.5	2,500	50
4	58.86	1,250	25
5	44.14	938	25

4.2 Methodology

The methodology is divided into two main steps: (1) data pre-processing and (2) data processing. The pre-processing was performed to prepare the remote sensing and field data for analysis. After the completion of the pre-processing stage the data was processed. This involved a detailed analysis of the field survey and image data as well as the generation of a qualitative image classification solution.

4.2.1 Data Pre-Processing

The pre-processing is split into three parts. First, the pre-processing steps taken to prepare the TS-X imagery for the extraction of zonal statistics and object-based image analysis are described. Secondly, the ArcGIS-based pre-processing procedure for the development of the field plot data set is discussed and finally the statistical pre-processing steps are presented.

4.2.1.1 Image Pre-Processing

In total, 10 TerraSAR SM mode EEC-RE images were acquired for this study (see *Table **4-1*** in Section 4.1.1 for a detailed list of imagery acquired). Before the imagery could be analyzed and integrated into the processing procedure it had to undergo several pre-processing steps. The pre-processing procedure is represented in ***Figure 4-8***. The overall goal of the pre-processing procedure was the generation of three image file types required for image processing and analysis: (1) an EEC-RE sigma-0, (2) an 8-bit EEC-RE sigma-0 image and (3) an interferometric coherence image.

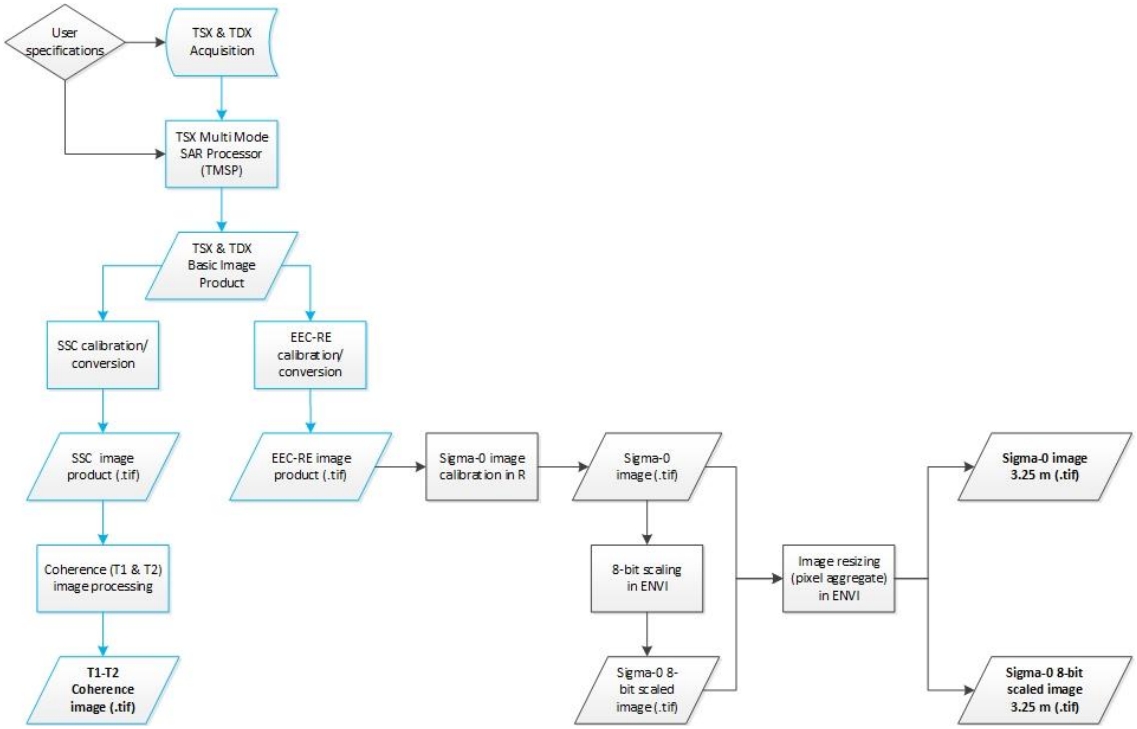

Figure 4-8: Pre-processing workflow for the TerraSAR-X imagery. Tasks highlighted in blue are part of the user defined Astrium ordering process; tasks in black were performed post-order.

A majority of the image pre-processing is part of the automated ordering service provided by Astrium Services[1]. The pre-processing steps conducted during the ordering were specified by the author and include the generation of EEC-RE and SSC-derived interferometric coherence images. The TerraSAR-X images were delivered in GeoTiff format (EEC-RE images in 32-bit floating point and coherence images in 8-bit).

The EEC-RE images were then calibrated using a script developed within the open source statistical software, R, to generate sigma nought (sigma-0) images. The sigma-0 calibration is needed to normalize the backscatter coefficient and provides a "unitless measure of the scattering cross-section per unit area of surface", thus reflecting target object properties rather than measurement geometry properties (Woodhouse, 2006). This is, according to Woodhouse (2006), "the property we are actually interested in since it quantifies something about the ground surface rather than being instrument specific". The sigma-0 calibration in R resulted in a 32-bit floating point GeoTiff file.

Subsequently, the sigma-0 calibrated EEC-RE images were converted from 32-bit floating point to 8-bit scaled GeoTiff files in ENVI. The 8-bit scaling was necessary for future analysis and processing in the Trimble eCognition software. The scale conversion was done using a formula developed within the ENVI Band Math tool:

[1] For detailed explanations of the TS-X products please refer to the *TerraSAR-X Services – Image Product Guide* available online at:
http://www2.astrium-geo.com/files/pmedia/public/r459_9_20091208_TS-Xx-itd-ma-0009_TS-X-productguide_i1.00.pdf)

BYTSCL(*b1*, MAX=P_{max}, MIN=P_{min})

where, *b1* is the image band to be calibrated (the SAR images only had a single band). P_{max} is the user defined maximum pixel value which is to be scaled to 255 and P_{min} is the user defined minimum pixel value which is to be scaled to 0. The goal was to establish an image where water pixel values become 0, or very near to it, and mature mangrove forest pixel values become 255 or close to it.

In order to define P_{max} and P_{min} representative control points were collected for water and mature mangrove forest within the TS-X imagery. The selection of the control points was aided by the use of VHR optical imagery from WoldView-2 and Google Earth (only imagery acquired in 2011 and 2012 was considered). In total, 18 control points were collected; 10 representing water and 8 mature mangroves. For the selection of the control point location, it was important to find areas in the image showing little temporal change to assure as pure a sample as possible. Therefore, each TS-X image was inspected for every potential control point location. This multi-temporal examination prevented, in the case of water control points, the selection of a point that was water at the time of the first acquisition (T_1) and soil, or soil-influenced shallow water, at the time of the second acquisition (T_2).

*Figure **4-9*** provides a representative example of such control point generation. Here, the selection of the control point location was based on a WorldView-2 image and two TS-X images. The image is in the left-hand column were typical for the establishment of P_{min} values associated with water, whereas the images in the right-hand column were used for P_{max} (mature mangrove).

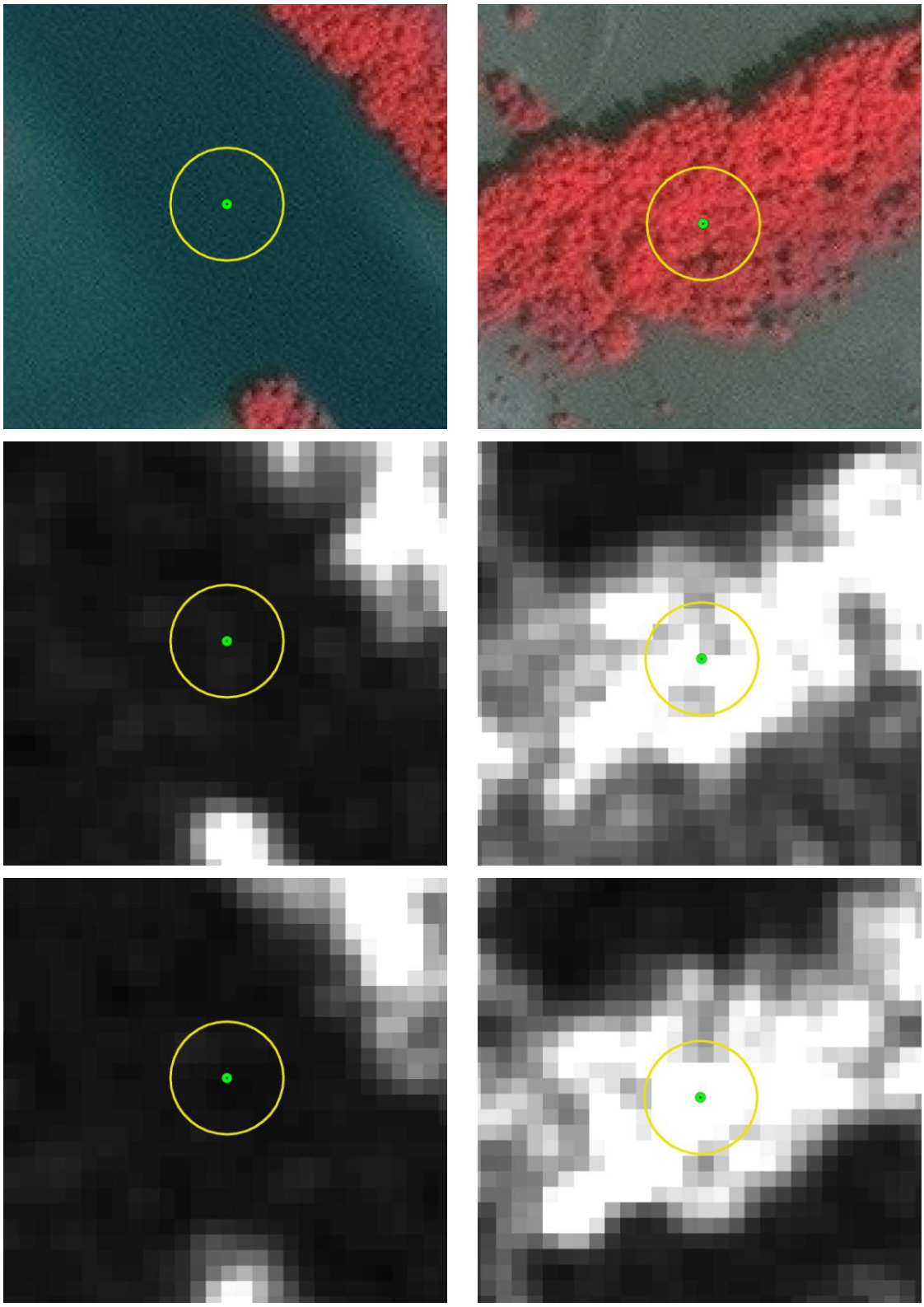

Figure 4-9: Examples of control points with 10 m buffer used to determine P_{max} and P_{min} for water (left) and mature mangrove forest (right): WorldView-2 image (top), 2012-10-30 TS-X image (middle) and 2012-11-10 TS-X image (bottom).

The P_{max} and P_{min} values were derived from the analysis of the sigma-0 calibrated EEC-RE images and based on a detailed examination of the range in pixel values within various plantation boundaries as well as throughout the entire image.

A 10 m buffer was applied to each control point and zonal statistics where extracted from each TS-X image for the buffer area (314 m^2) using a script developed within the R program. The script calculated the average backscatter for each buffered control point polygon and exported the results in .dbf file format. The 18 control points yielded a total of 87 multi-temporal measurements; 51 measurements of water and 36 of mature mangroves. *Figure **4-10*** graphically depicts the mean backscatter values for both water and mature mangrove control points. The P_{max} value was conservatively assigned -1 decibel (dB) and the P_{min} value was set to -23 dB. These values were applied to the scaling of all images to insure consistency.

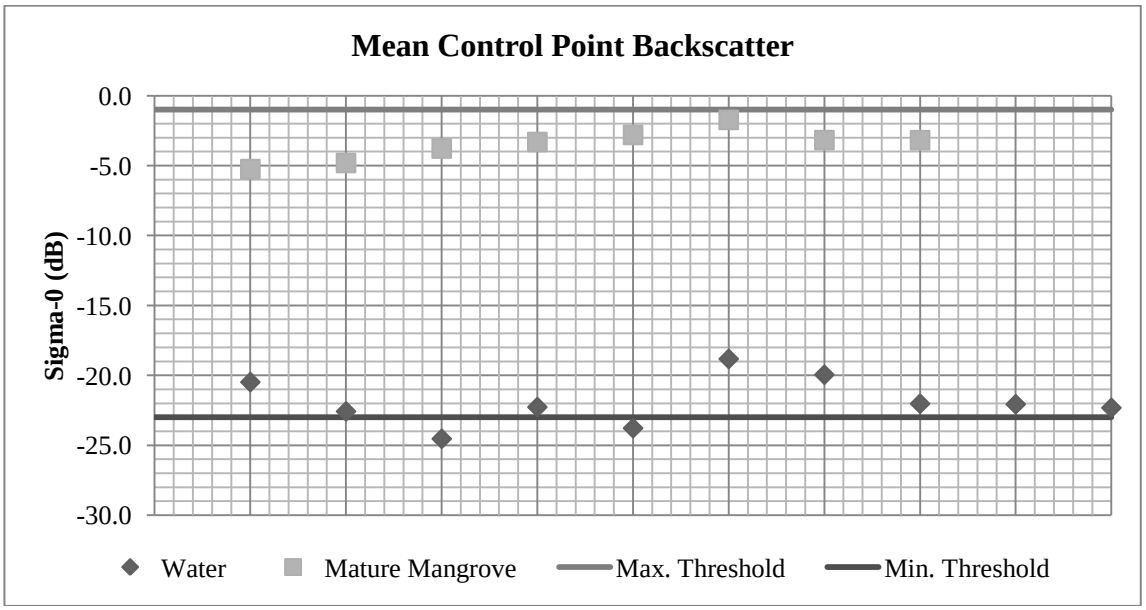

Figure 4-10: Graphical analysis of control points for the definition of P_{max} and P_{min}.

Finally, the EEC-derived sigma-0 images were resized to match the resolution of the coherence image. The coherence image has a 3.25 m resolution, whereas the EEC images, and there products, have a resolution of 2.75 m. The processing in eCognition requires the input images to have the same spatial resolution. The image resizing was performed in ENVI. Rather than resampling the images, the pixel values were aggregated – all the pixel values that contribute to the output pixel were averaged (Exelis Visual Information Services, 2004).

The interferometric coherence images did not require any additional pre-processing, as they were delivered in the required 8-bit format.

4.2.1.2 GIS Pre-Processing

The Field data collected by Pôle Carto was provided in three parts: (1) ESRI shapefile format, (2) tabular MS Excel field sheets and (3) digital photographs.

Four separate ESRI shapefiles were supplied for the Casamance study area containing information on 2008 and 2009 plantation field samples, 2011 and 2012 plantation field samples, tide level field samples and biomass field samples. The configuration of the four shapefiles is shown in *Table A **1*** of the Appendix.

Four tabular field sheets were provided in a single MS Excel document: one for information on 2012 plantations, one for information on 2011 plantations, one for information on 2008 and 2009 plantations and one for biomass monitoring. The information contained in the tabular sheets is listed in *Table A **2*** and ***Table A 3*** of the Appendix.

A series of pre-processing steps were necessary before a detailed analysis of the data could be performed. These steps are depicted in ***Figure 4-11***. To begin with, the three point-shapefiles were combined and subsequently buffered in ArcGIS. A 10 m buffer was applied to each point location to create a 314 m^2 circular polygon representing the true size of the plot in the field, as described in see Section 4.1.3. The next step was to combine the buffered field plot file with the biomass field plot file (also a polygon-shapefile), resulting in a total of 85 field samples.

In order to incorporate data from the field sheets into the field sample shapefile, the attributes from the field sheets had to be formatted to allow for a seamless join in ArcGIS. For example, the multiple tree height and diameter measurements recorded for each plot were averaged. In addition, a hyperlink was generated for the first photo in each range. The information about mature mangrove trees inside and outside the plot was noted in the "comment" field.

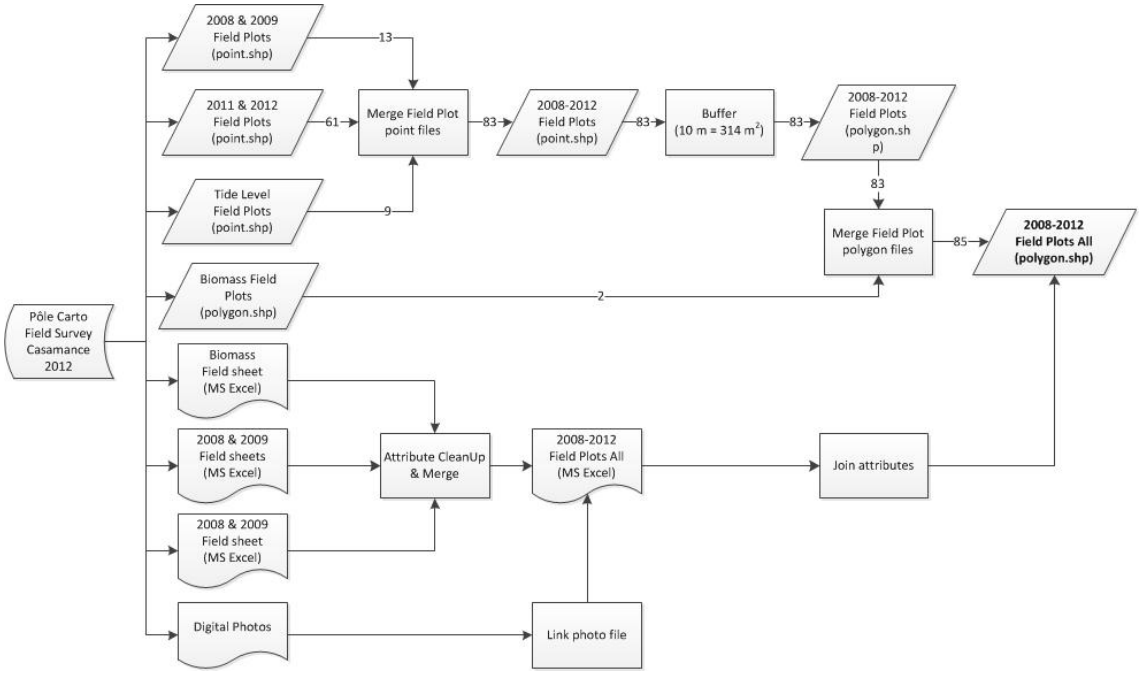

Figure 4-11: GIS-based pre-processing workflow.

The result was a single polygon-shapefile containing all the field measured information for each field sample. This shapefile would then be used as input for the generation of zonal statistics.

4.2.2 Statistical Pre-Processing

The statistical pre-processing consisted of two steps: (1) the extraction of zonal statistics from the TS-X imagery, followed by (2) the analysis of the zonal statistics and development of an inversion model to establish a correlation between the field-measured values and data captured by the TerraSAR system (i.e. EEC-RE and interferometric coherence images).

4.2.2.1 Zonal Statistics

In order to investigate whether a relationship exists between the field measurements and the data contained in the TS-X images, zonal statistics were extracted from each EEC-RE sigma-0 calibrated image and interferogram based on the buffered field sample locations using the R statistical computing software (R Development Core Team, 2008). From the EEC-RE sigma-0 calibrated TS-X images, the mean backscatter was computed for each 314 m^2 field sample polygon. From the coherence image, the mean coherence, or measure of correlation between T_1 and T_2, was calculated. The R extraction tool includes all raster cells (i.e. pixels) that are covered by the extraction feature (i.e. buffered field sample locations); a pixel is considered "covered" if its center is inside the extraction feature (Hijmans & Etten, 2013). ***Figure 4-12*** shows an example of the raster cell selection within a buffered field sample.

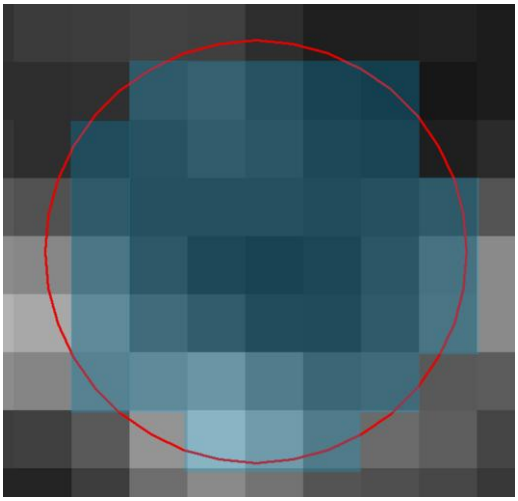

Figure 4-12: Example of raster cell selection for computation of zonal statistics in R. Cells highlighted in blue are considered covered by the extraction feature (outlined in red).

The results for each extraction feature, from each input image, are then exported as a .dbf file. If an extraction feature is outside the image footprint, it receives a value of 0.

A total of 850 (85 samples x 10 TS-X images) image-derived backscatter measurements and 340 (85 samples x 4 coherence images) coherence measurements were calculated for the Casamance study area. The 85 field samples were distributed throughout the coverage area so that some points were within multiple footprints and yielded backscatter data for multiple acquisition dates (see *Figure **4-13***); each field sample location was recorded at least three times. Such points are advantageous because they provide more information on the field sample site (i.e. during different operating conditions: submerged, flooded and dry).

The individual .dbf files were combined and joined to the shapefile containing the field survey measurement locations.

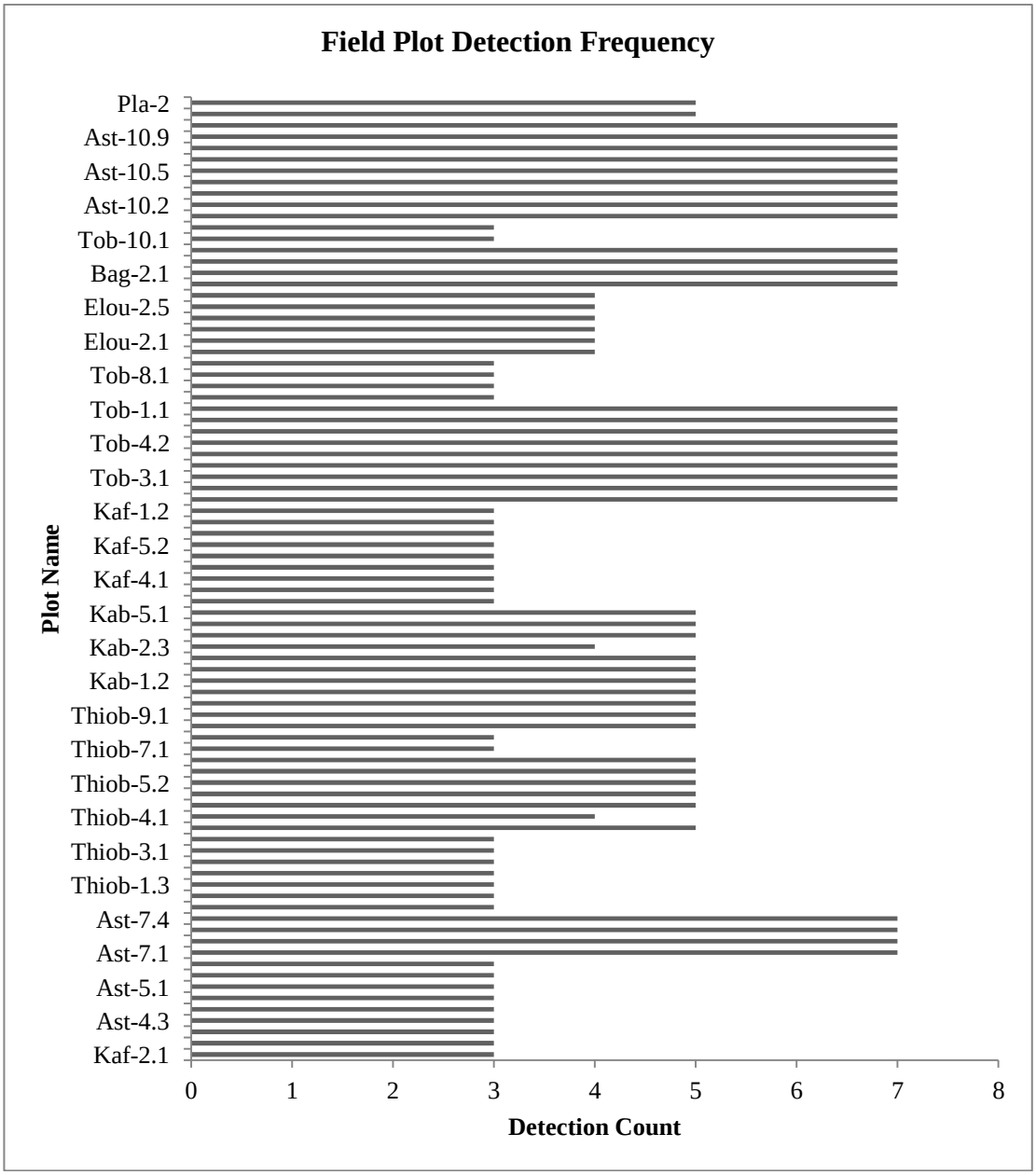

Figure 4-13: Field sample detection frequency.

4.2.2.2 Development of an Inversion Model

A fundamental part of the proposed monitoring method depends on the establishment of a robust correlation between the field-observed measurements and the information recorded by and derived from the TS-X sensor. The zonal statistics were used to explore the relationship between several key data elements in order to develop an inverse model that could be integrated into the image analysis.

To generate a representative inverse model, the zonal statistics calculated for each field sample were carefully analysed to establish which backscatter value truly resulted from young mangrove trees rather than soil, water or mature mangrove vegetation. To identify such modelling points, a set of selection criterion were defined.

The initial investigation analyzed the correlation between TS-X backscatter (sigma-0 calibrated) and observed tree density, with the goal of generating a model for a quantitative classification. The modeling points were initially selected based on the general criterion listed in *Table **4-5***. The selection criterion in *Table **4-5*** reduced the number of sample points from 850 to 93, at which point a detailed analysis of the sample points began to determine which samples represented favourable operating conditions (i.e. flooded). This process was primarily based on TS-X image interpretation as well as a detailed inspection of the ground photos taken by the field team and resulted in the final selection of 35 potential modelling points.

Table 4-5: General field sample selection criterion with a brief explanation of reasoning.

Criteria	**Explanation**
Within Image Coverage	Only sample points within a TS-X footprint were considered. If a point was not within the TS-X footprint it resulted in mean backscatter value of 0.
Density > 0	Some sample points were taken for reference purposes (i.e. to identify mud-flats, additional photo locations and mature vegetation) and did not include density measurements. Only points with a density measurement can be considered.
Area = 314 m^2	Biomass plots (2) were not included in the analysis because they were considerably smaller (80-100 m^2) than the density plots.
Tree Height ≥ 40 cm	Only sample points with a mean tree height of ≥ 40 cm were included as smaller trees do not provide enough vegetation volume to solely influence the backscatter.
Mean Backscatter > -18 dB	Sample points with a mean backscatter value ≤ -18 dB are representative of water or reflect submerged trees.

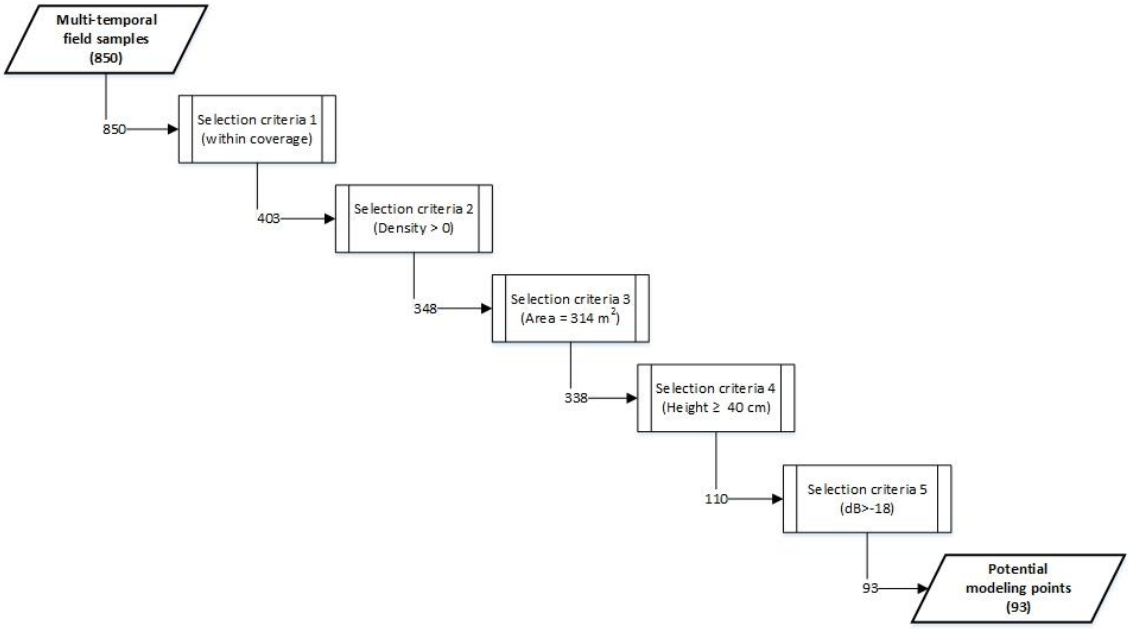

Figure 4-14: General sample point selection process.

4.2.2.2.1 Quantitative Model

The 35 potential modelling points were split into two equal sized groups via random sampling; 18 points were used to develop the inverse model and 17 were used for validation. The modeling results revealed an exponential model with a R^2 of 0.642 (see *Figure **4-15***). The model validation demonstrates a general over estimation of tree density, particularly in areas with higher tree density (although only one point was available for such conditions). A Root-Mean-Square Error (RMSE) of 17% was achieved (see *Figure **4-16***).

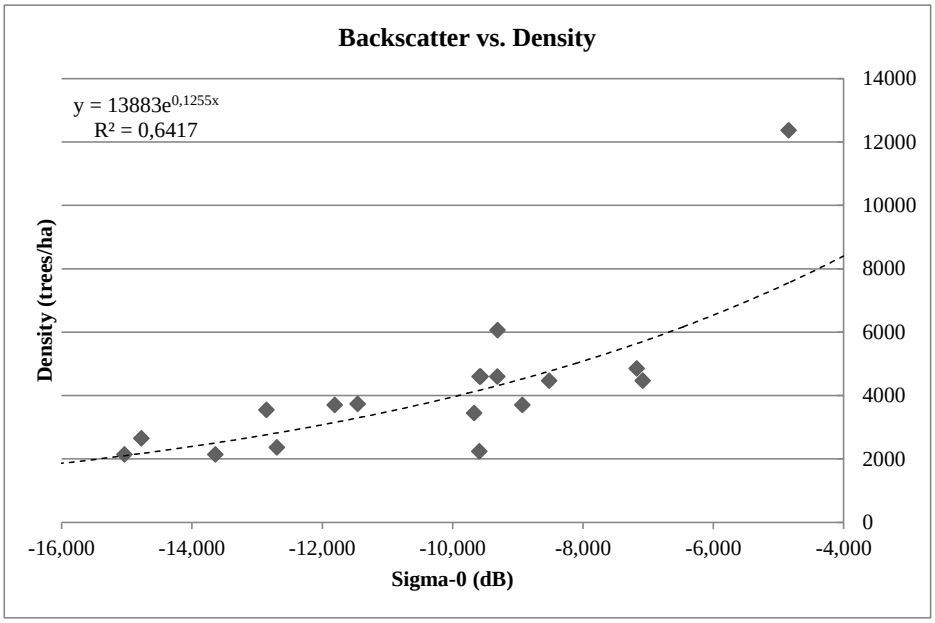

Figure 4-15: Quantitative tree density model.

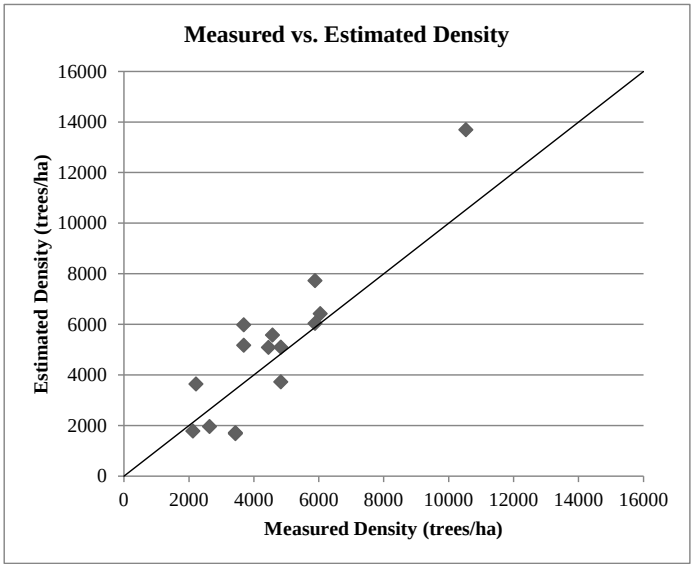

Figure 4-16: Validation results for quantitative modeling.

4.2.2.2.2 Qualitative Model

A second analysis examined the relationship between TS-X backscatter (sigma-0) and stand biomass (= tree biomass * tree density) to be used for a qualitative (i.e. tree growth quality) stratification. For the purpose of this investigation, only sample points with TS-X coverage on 24.10.2012 and 17.02.2013 were considered due to the generally favorable operating conditions on these dates; both images reflected primarily "flooded" conditions within the plantation areas (see *Figure A **1*** and *Figure A **2*** in the Appendix).

After the general selection process (see *Table **4-5***), points reflecting dry conditions or the presence of mature mangrove vegetation within the plot were removed. Unlike the selection process for the establishment of the quantitative model, the selection of points for the qualitative model considered all field samples regardless of plot size and measured tree height. In total, 38 modeling points were selected (16 from 24.10.2012 and 22 from 17.02.2013). The 38 modeling points were split into two equal sized groups via random sampling for modeling and validation.

Three qualitative models were generated, considering (a) only field samples from 24.10.2012, (b) only field samples from 17.02.2013 and (c) both groups of field samples. Both the linear and exponential trends were calculated for each model. As can be seen in *Table **4-6***, the linear trend model proved to be the better fit in all three cases and a fairly similar R^2 was achieved by in all linear modeling scenarios. Nevertheless, scenario c produced a significantly lower RMSE (32%). ***Figure 4-17*** depicts the qualitative modeling results achieved with scenario c. *Figure **4-18*** depicts the two validation cases for modeling scenario c. Both modeling scenarios demonstrate a

tendency to underestimate the amount of biomass, especially in areas with a higher field measurement-based biomass.

Table 4-6: Summary of modeling and validation results.

Modeling Scenario	Linear R^2	Exponential R^2	Linear RMSE	Exponential RMSE
(a) 24.10.12 only	0.6078	0.5815	68%	89%
(b) 17.02.13 only	0.5965	0.4096	52%	56%
(c) 24.10.12 & 17.02.13	0.5683	0.4069	31%	32%

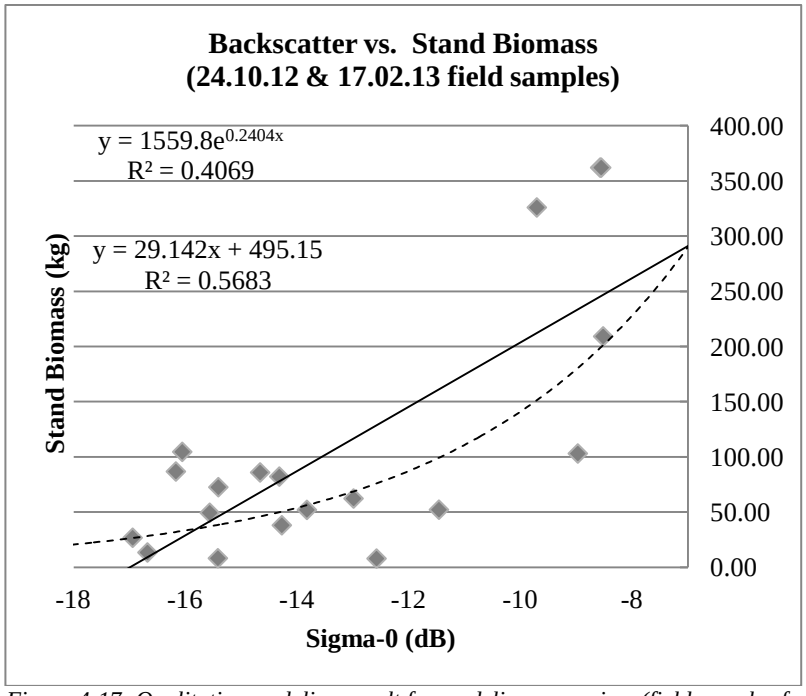

Figure 4-17: Qualitative modeling result for modeling scenario c (field samples from 24.10.2012 and 17.02.2013).

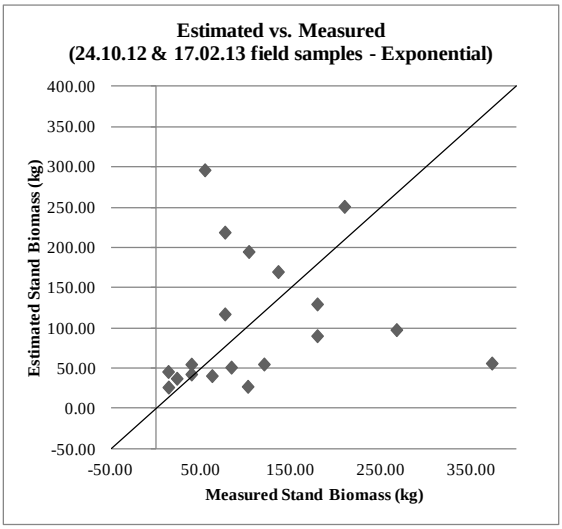

RMSE = 31%

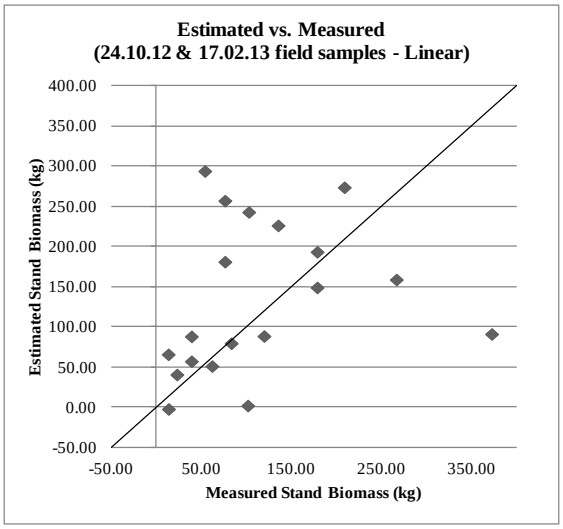

RMSE = 32%

Figure 4-18: Validation of the scenario c modeling results based on linear (right) and exponential (left) inversion models.

The underestimation of higher stand biomass values (> 200), present in *Figure **4-18***, is primarily a result of the underrepresentation of field samples collected in plantations established in 2008 and 2009 (see *Figure **4-5***). The majority of samples were acquired

in very young plantations, established between 2011 and 2012, and result in low stand biomass values, the estimated values for which can be easily overestimated due to surface reflections during low tide (dry) conditions. Nevertheless, the model is applicable to the entire study area, given the appropriate operating conditions (i.e. flooded but not submerged plantations).

Although the quantitative model resulted in a lower RMSE (17%) and a comparable R^2 (0.64), it lacks in transferability and efficiency. The generation of the model currently relies too heavily on the individual's image interpretation skills and statistical assumptions. Furthermore, the field samples used for the model are not representative of the study area as a whole, rather only micro environments within it.

Based on these findings, the image analysis will concentrate on a qualitative investigation of the plantations. The growth quality of the young mangrove trees within the plantations will be assessed based on the linear model from scenario c.

4.2.3 Data Processing

4.2.3.1 Object-based Image Analysis

In order to efficiently, objectively, and consistently analyze the TS-X images, a supervised object-based image analysis approach was chosen. For this purpose, the Trimble eCognition Developer software was implemented. A segment-based classification method, based on a predefined hierarchical rule-set, was chosen. This approach builds groups of spatially adjacent pixels with similar characteristics (i.e. backscatter values), which eCognition calls "image objects", rather than analyzing individual image pixels. This method consists of three basic procedures:

1. Class hierarchy design – involves the definition of classes as well as inheritance rules between parent and child classes (e.g. sub-classes)
2. Image segmentation – development of a segmentation regime of the input raster data set(s) into homogeneous image objects according to image characteristics (i.e. backscatter or coherence values)
3. Image classification – comprises the allocation of image objects into the predefined classes according to decision rules which can be based on various image object characteristics such as backscatter and coherence values, shape, spatial relationship, topologic criteria and association with thematic layers.

The object-based image analysis was conducted for each TS-X footprint individually to allow for image-specific adjustments and improved processing. For this purpose, the

image pairs (see *Table **4-1***), acquired with an 11 day time interval, as well as the resulting coherence image were used as inputs in eCognition. In addition, the plantation boundary polygon-shapefile from Polê Carto was used as a thematic layer.

4.2.3.1.1 Class hierarchy

The class hierarchy designed for this study is illustrated in ***Figure 4-19***. It is founded on a multi-facetted segmentation approach (i.e. multiple segmentations) to increase the image processing efficiency by reducing the amount of data to be processed through a pyramid progression. The image object analysis procedure can therefore be tailored to the unique characteristics of specific classes.

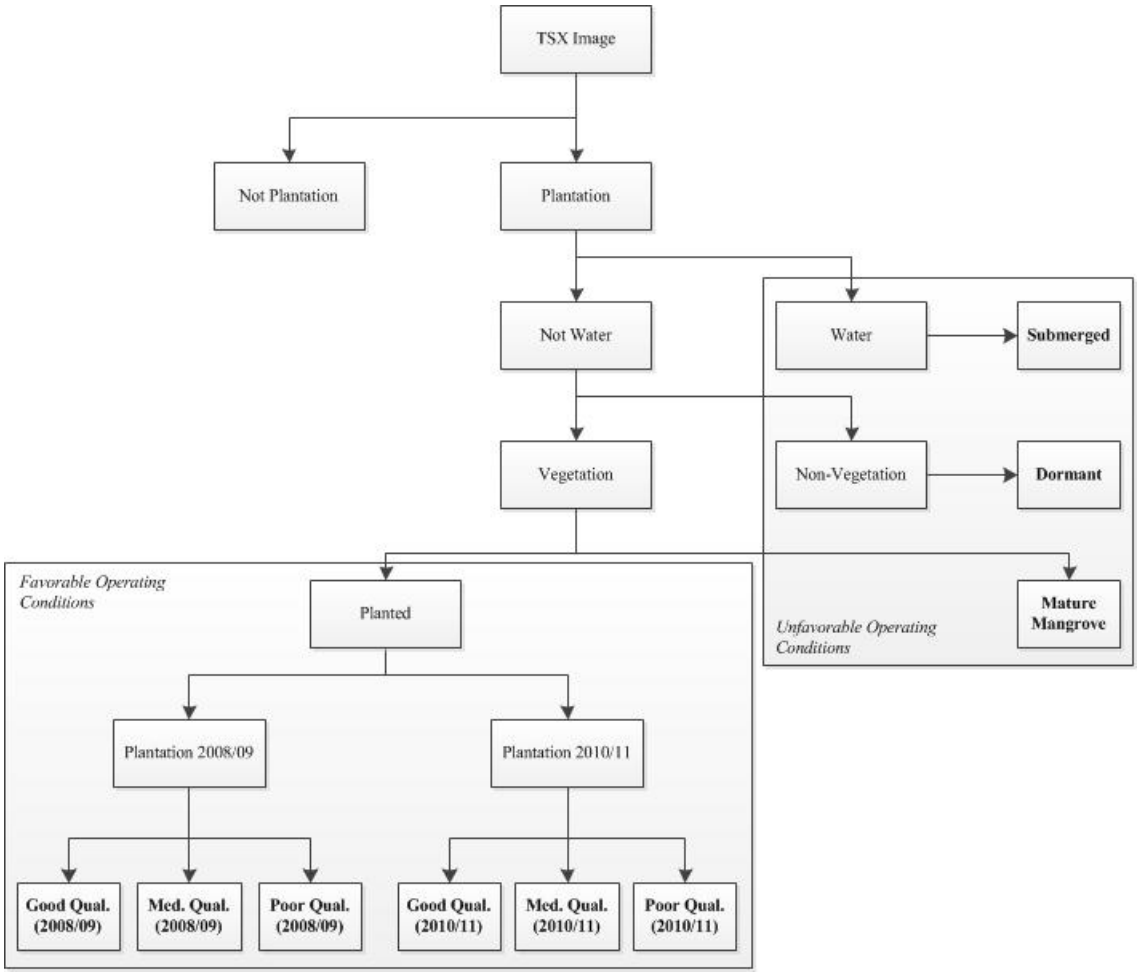

Figure 4-19: Class hierarchy design, target classes are marked in bold.

The initial goal of this hierarchal classification scheme is to separate the image objects in to two main categories: (1) favorable operating conditions and (2) unfavorable operating conditions. The classification begins with the removal of image objects representing unfavorable operating conditions into three target classes: submerged, dormant and mature mangrove. The remaining image objects, representing favorable operating conditions, are then stratified into the three growth quality classes. The classification process is described in detail in section 4.2.3.1.3 below.

4.2.3.1.2 Image segmentation

For this study, two different segmentation techniques, (1) "multi-resolution" and (2) "quad tree", were analyzed to determine which is best fitted to qualitatively analyze the plantations. For this purpose, a representative subset region, north of Ziguinchor, with 300 plantations was chosen for the comparative analysis (see ***Figure 4-20***).

After the isolation of the plantation polygons, using a chessboard segmentation, a second segmentation was performed specifically on the "mangrove plantation" image objects within two separate "map" environments. The class hierarchy design was then applied to both segmentations. Identical classification parameters were implemented to assure that any differences in results would stem only from the different segmentation types.

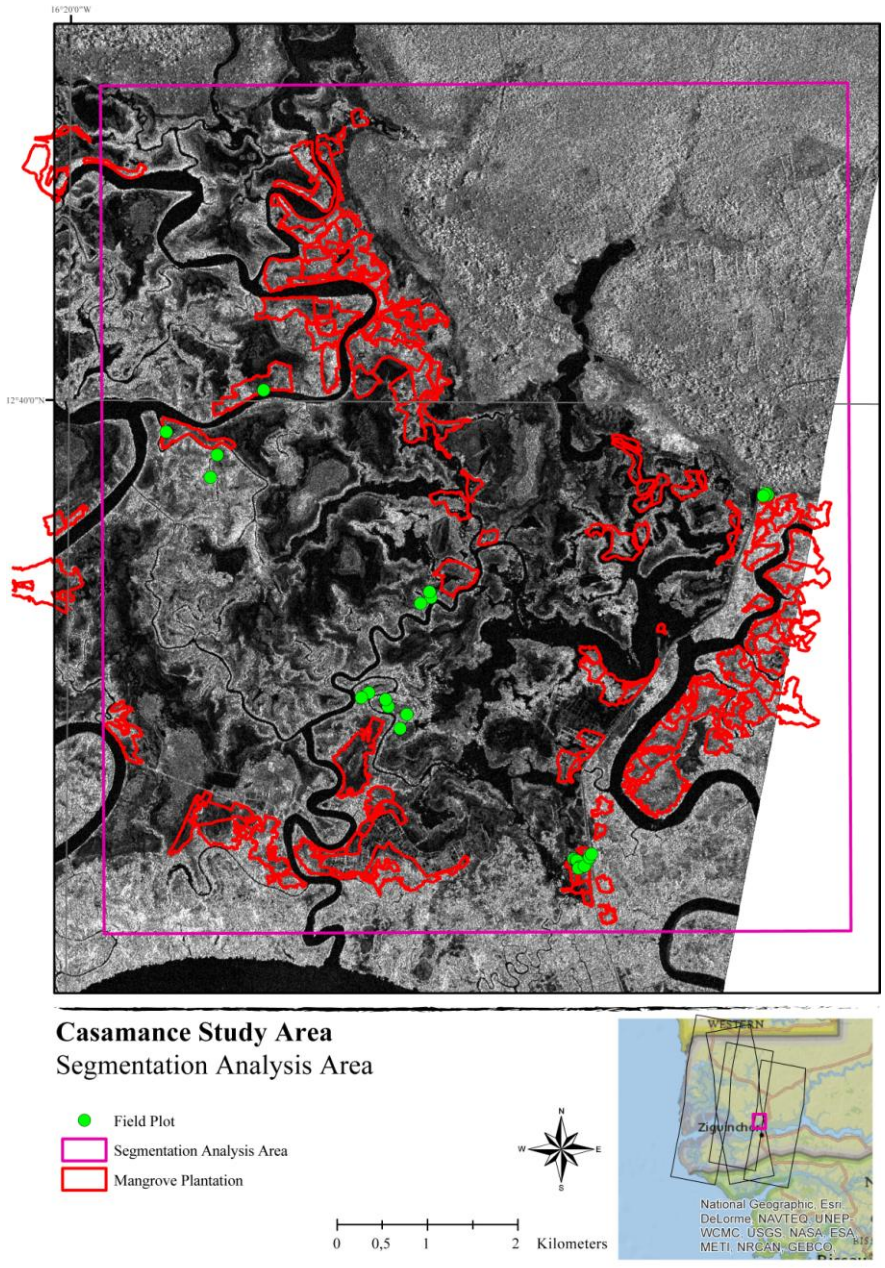

Figure 4-20: Subset region used for testing the segmentation parameters.

As described in the *eCognition Developer 8.8 User Guide* (2012), the multi-resolution segmentation algorithm merges pixels or existing image objects based on their relative homogeneity criterion, a combination of spectral and shape characteristics. The segmentation results can be modified to fit the input data by altering the scale (the higher the value the larger the image objects), shape and compactness parameters. The algorithm is especially well-suited for the extraction of features that are characterized by both color and shape homogeneity (Trimble, 2012). The best results were generated using a scale factor of 40, a shape parameter of 0.3 and a compactness parameter of 0.6. *Figure **4-21*** compares the four different multi-resolution segmentation results.

The segmentation with a scale factor of 100 yielded large image objects with a fairly wide range of backscatter values (see ***Figure 4-21a***). There is a general separation of vegetated (green) from non-vegetated (magenta) areas. Nevertheless, the variation, especially within vegetated image objects, is too large. The segmentations based on scale factors of 50 (***Figure 4-21b***) and 30 (***Figure 4-21d***) both resulted in well-formed image objects. Objects with higher backscatter values in T_1 are particularly well-defined in the segmentation calculated with a scale factor of 50, whereas vegetated objects with lower backscatter (i.e. young mangrove trees) still demonstrate a higher level of variance than desired. The segmentation generated with a scale factor of 30, created relatively fragmented segments in areas with high backscatter in T_1, yet performed much better in the areas with low backscatter vegetation. Therefore, a compromise was made and a scale factor of 40 was chosen (***Figure 4-21c***).

a)

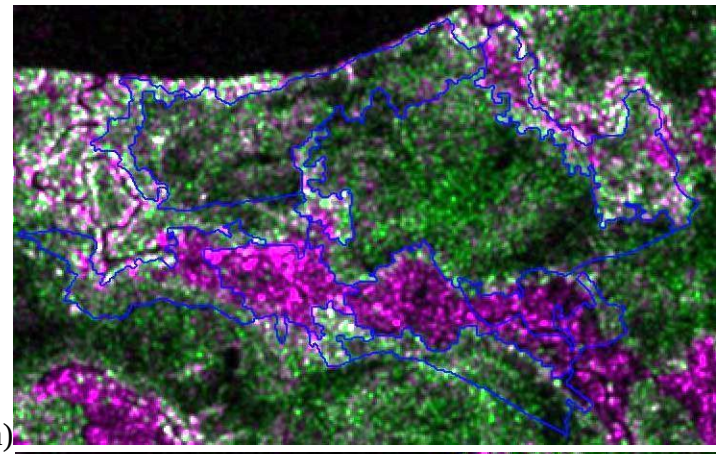

b)

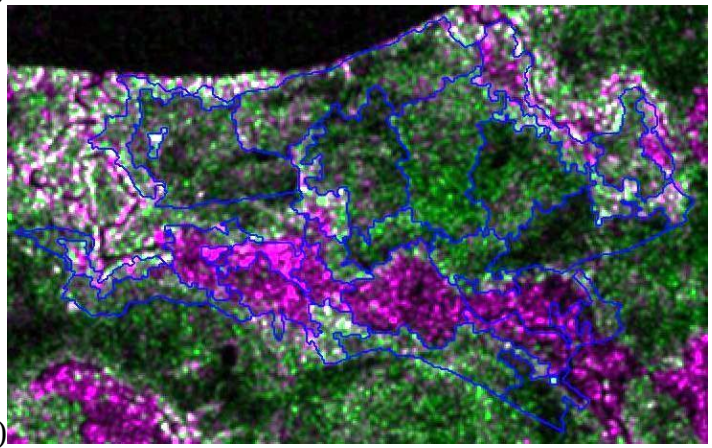

c)

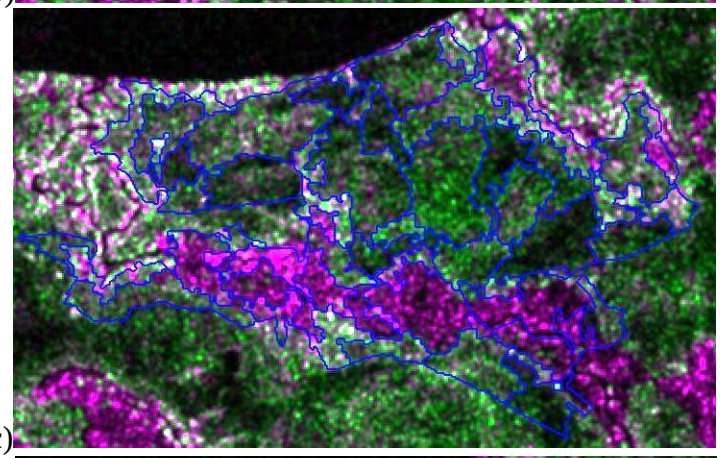

d)

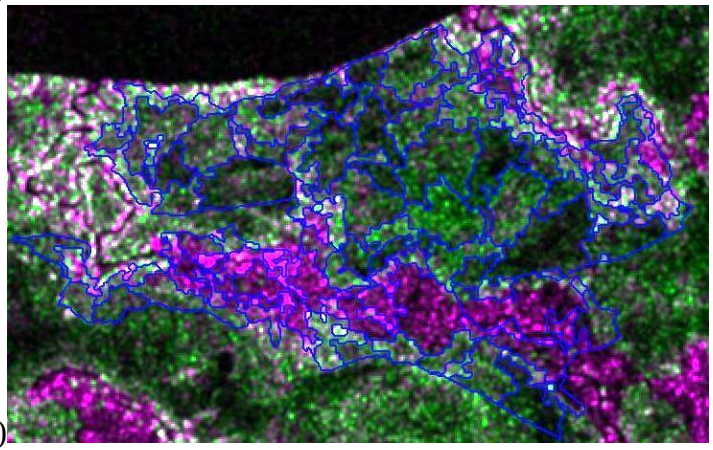

Figure 4-21: Comparison of multi-resolution segmentation results. Image objects are outlined in blue with the multi-temporal TS-X images (R:T1, G:T2, B:T1) in the background: a) scale = 100, b) scale = 50, c) scale = 40 and d) scale = 30.

The quad tree segmentation utilizes a quad tree-based segmentation algorithm to build image objects. It generates square objects with differing sizes depending on the defined upper limit (i.e. scale parameter) of color differences within each object (Trimble, 2012). This type of segmentation is particularly well-suited for images with a "well-separated background and foreground" (Trimble, 2012). A scale parameter of 60 resulted in the best segmentation of the plantations (see ***Figure 4-22***). Nevertheless, the quad tree segmentation caused an over-segmentation of high backscatter areas, generating an extremely large number of image objects. In addition, the square object shape is not particularly well suited for this type of natural environment.

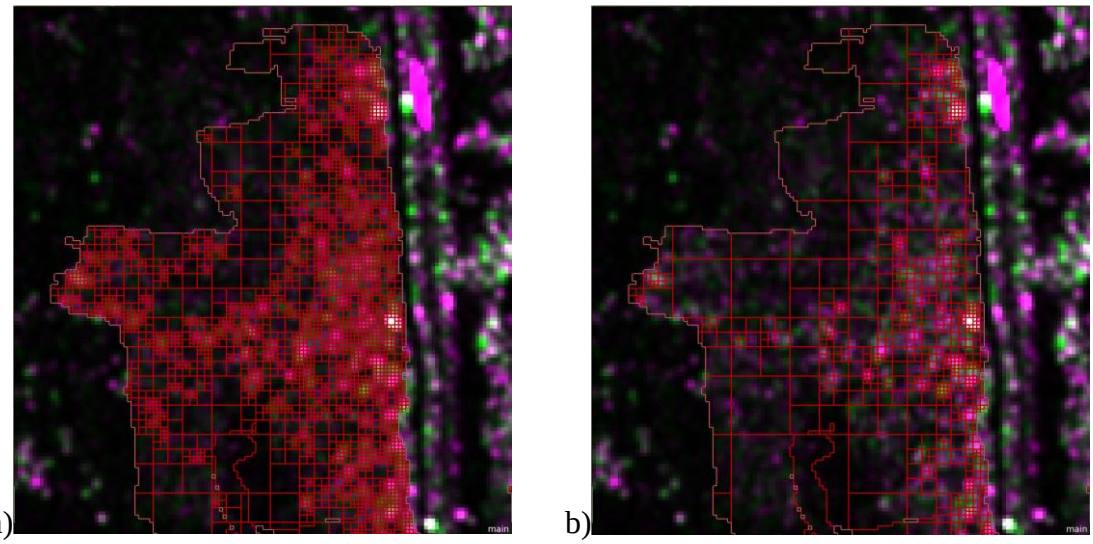

Figure 4-22: Comparison of quad-tree segmentation results. Image objects are outlined in red with the multi-temporal TS-X images (R:T_1, G:T_2, B:T_1) in the background: a) scale = 15, b) scale = 60.

The segmentation results differed significantly. The multi-resolution segmentation generated a total of 2,066 image objects, whereas the quad tree method resulted in 268,729 image objects. Even after the application of the classification rule set (including the merger of neighboring objects with the same classification), the difference in the number of image objects remained; the multi-resolution segmentation based classification contained 621 image objects while the quad tree segmentation based classification had 12,699. For the purpose of this comparative analysis, the classification was only performed to the point of separating planted mangrove trees from non-vegetation and mature mangrove stands. The quad tree segmentation resulted in a much more fragmented classification (see *Figure **4-23***). The fragmentation is particularly present in the non-vegetated class, as such pixels demonstrate a significant color difference; the quad tree segmentation considers only the color difference within the image object for segmentation, whereas the multi-resolution segmentation considers the actual "spectral" information, shape and compactness (Trimble, 2012).

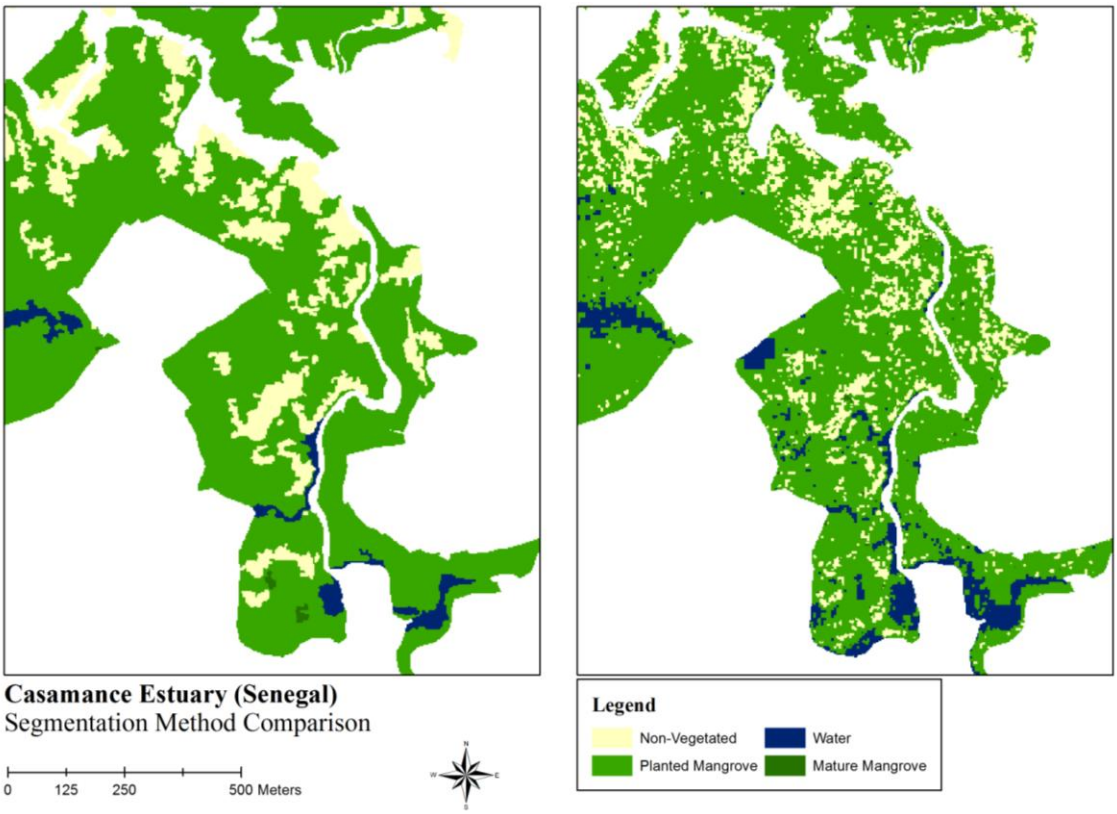

Figure 4-23: Comparison of classification results based on a) multi-resolution and b) quad tree segmentations.

In order to combine the advantages of both segmentation methods - the naturalness of the multi-resolution segmentation with the detail of the quad tree segmentation in high backscatter areas (i.e. mature mangroves) – a multi-threshold segmentation was applied after the multi-resolution segmentation. The multi-threshold segmentation algorithm uses a combination of histogram-based and multi-resolution methods to calculate a threshold for dividing a set of pixels into two subsets (Trimble, 2012). The multi-threshold segmentation was performed to isolate small patches of high backscatter within the plantation segments that were not accounted for by the initial multi-resolution segmentation, as these values have a significant influence on the objects mean backscatter value and can potentially lead to misclassifications during the growth quality stratification (see ***Figure 4-24***).

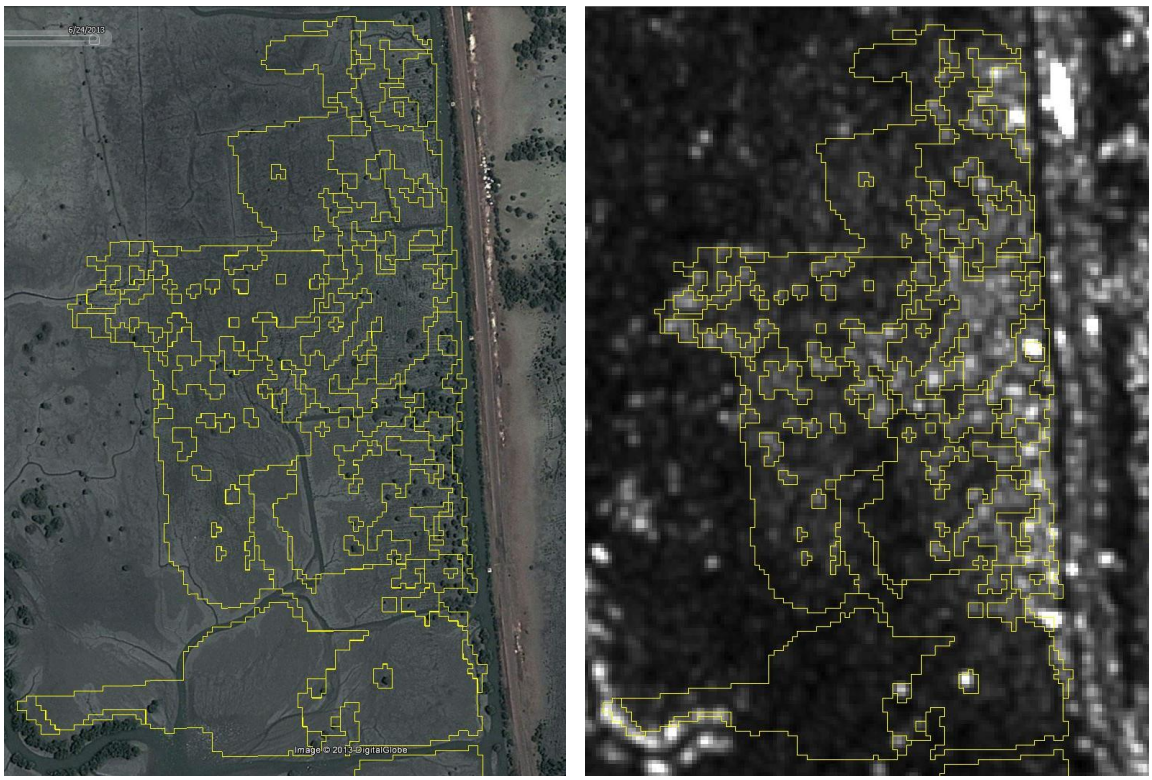

Figure 4-24: Multi-threshold segmentation results. The resulting image object polygons are overlain on a Google Earth image from 21.09.2012 (left) and on the TS-X image from 24.10.2012 (right). Patches of mature vegetation and dry hummocks are well segmented.

4.2.3.1.3 Image classification

The rule set for the image classification is based on the class hierarchy scheme illustrated in *Figure **4-19***, which ultimately classifies the image into nine target classes: mature mangrove, submerged, dormant, poor growth 2008/09 and 2010/11, medium growth 2008/09 and 2010/11 and good growth 2008/09 and 2010/11.

For this purpose, three growth quality classes have been defined for areas with favorable operating conditions and three classes with unfavorable operating conditions (see ***Table 4-7***). The growth quality definitions account for the natural differences in the two planting periods (2008/09 and 2010/11) that result from tree age. The general definitions in ***Table 4-7*** are based on field observation. Representations of the growth quality stratum for each planting period are depicted in *Figure **4-25*** and *Figure **4-26*** (photos taken during the 2012 field survey by Pôle Carto). For the purpose of the classification, the quality of tree growth is based on a combination of vegetation tree biomass and density – stand biomass (see the inversion model established in section 4.2.2.2.2).

Table 4-7: Mangrove plantation growth quality class definitions.

Growth Class	Class Definition
Good	Well-developed trees: 2008/09 - defined crowns with multiple branches and aerial roots; tree height generally > 50 cm. 2010/11 – development of first branches
Medium	Moderately developed trees: 2008/09 – early stages of branch development, no definable crown: tree height generally between 40 and 60 cm. 2010/11 – well formed leaves are present with 1 to 2 nodes; tree height generally between 30 and 40 cm.
Poor	Limited tree growth and under developed trees with depressed foliage: 2008/09 – little branching and restricted foliage; tree height is variable. 2010/11 – no sign of branching and very little leaf mass; tree height typically < 25 cm.
Dormant	No or sparse tree growth, the image object is dominated by bare soil.
Submerged	No tree grows observable, the trees are either completely submerged or the objects backscatter is dominated by water. No stratification possible.
Mature Mangrove	Fully developed mangrove vegetation.

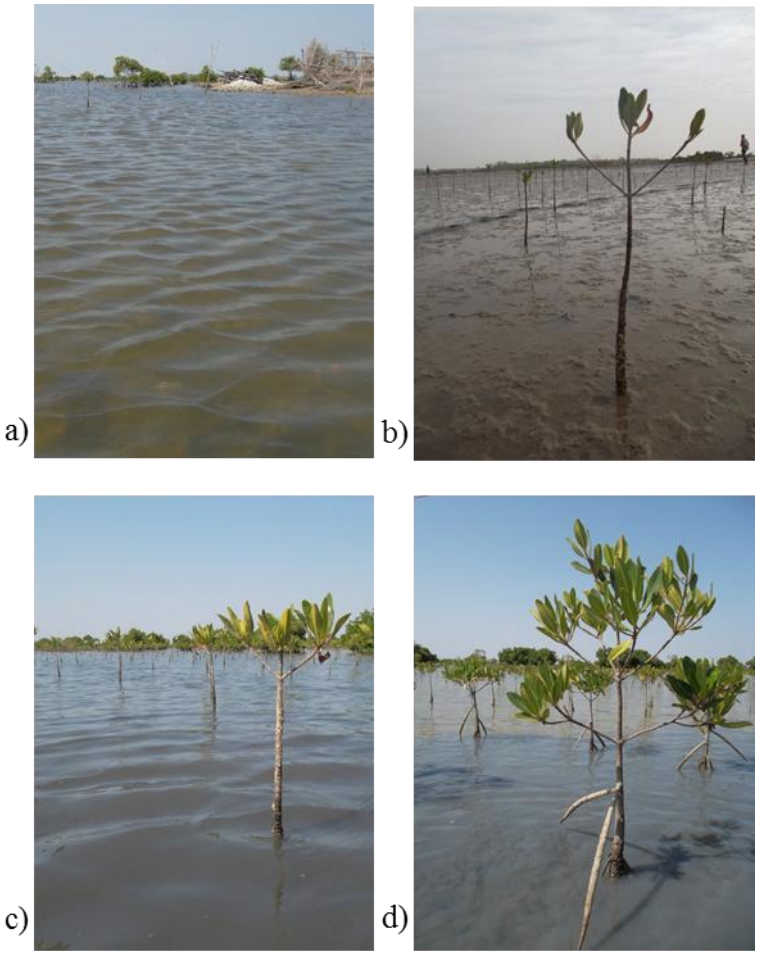

Figure 4-25: Representative field photos of the four growth quality classes for plantations established between 2008 and 2009: a) dormant, dead trees or no tree growth; b) poor growth, majority of trees are under developed; c) medium growth, trees have formed several branches; d) good growth, initial canopy and hanging roots established.

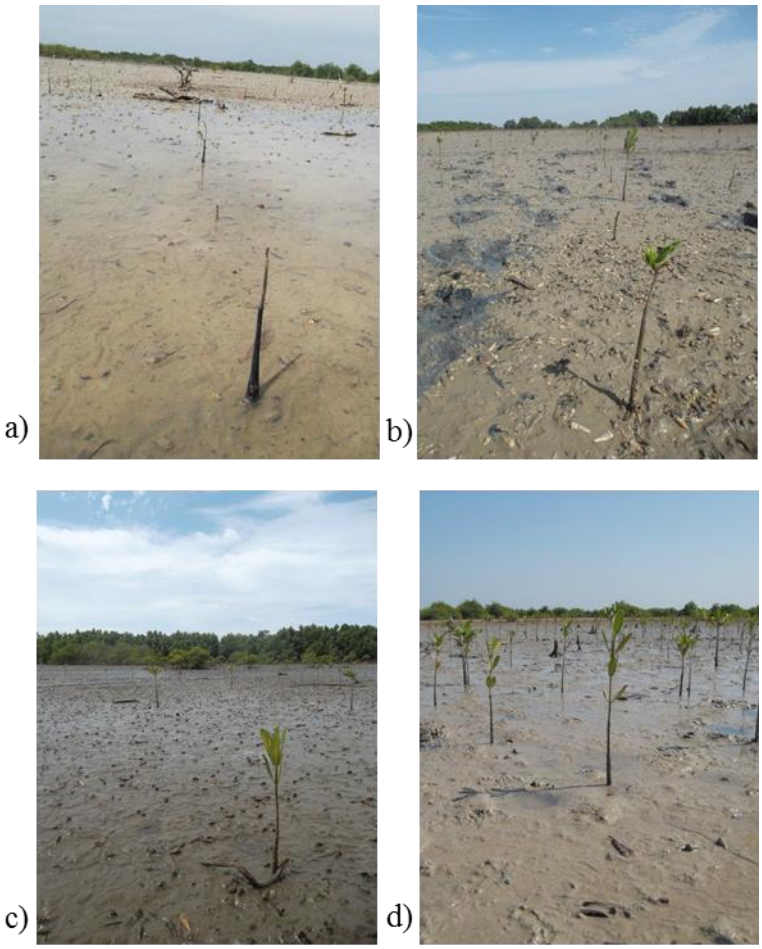

Figure 4-26: Representative field photos of the four growth quality classes for plantations established between 2010 and 2011: a) dormant, dead trees or no tree growth; b) poor growth, majority of trees are under developed with only a few leaves; c) medium growth, trees have well-formed leaves and 1 to 2 nodes; d) good growth, initial branches forming and 3 to 4 nodes.

The rule set developed for the classification is comprised of 11 general steps (see ***Table 4-8***). Each step is assigned its own level within eCognition to improve the organization of the rule set and allow for increased flexibility (i.e. the operator can easily adjust classification parameters without permanently changing preceding results).

The first three steps are primarily used for image segmentation. To account for differences in operating conditions (i.e. water levels) within the images, the plantations are initially split into two groups: (1) water-bound (≥ 50% relative border to "water") and (2) land-bound (< 50% relative border to "water") plantations and separated into different "map" environments allowing for the application of condition specific classification rules.

Subsequently, the first phase of the classification is performed, designed to remove any objects representing unfavorable operating conditions (i.e. submerged, dormant and mature mangroves), as these were not included by the inversion model.

In step 8, the growth quality classification is carried out, based on the model discussed in section 4.2.2.2.2. For this purpose, the plantations are again split into two planting

period groups, as a biomass-based quality assessment must account for the natural temporal differences in tree development. The threshold conditions used for determining the strata of each image object (only image objects with favorable monitoring conditions are considered) are derived from a customized arithmetic feature referred to as "Stand Biomass" (SB). In turn, each strata has a unique membership function; a membership function allows the user to "define the relationship between feature values and the degree of membership to a class using fuzzy logic" (Trimble, 2012). In this case the "larger than" membership function type was applied.

After the completion of step 8, temporary classes are assigned to their final target classes and a general classification "clean-up" is performed. The clean-up procedure includes the merging of like image objects, with respect to plantation boundaries, and a final series of neighborhood-based classifications. The clean-up process did not involve any image object resizing or smoothing; the image objects were exported as polygons with pixelated boundaries corresponding with the TS-X input pixels.

Table 4-8: Generalized classification steps.

Classification Step	Process Explanation
1	Chessboard segmentation to isolate plantations
2	Classification of plantation type (water- or land-bound) & generation of maps for each type
3	Multi-resolution segmentation of plantation objects
4	Classification of water I
5	Multi-threshold segmentation of plantation objects
6	Classification of water II
7	Classification of Non-planted objects
8	Classification of growth quality based on year of planting
9	Assignment of temporary classes to target classes
10	Clean-up & export to shapefile
11	Final clean-up in ArcGIS

The classification parameters for the temporary and target classes are listed in ***Table 4-9***. The differences in operating conditions between the two TS-X footprints requires, in some cases, slight adjustments to classification thresholds. Therefore, the parameters for both images are listed. ***Figure 4-27*** provides a generalized image analysis workflow diagram.

Table 4-9: Classification parameters used in the study area.

Class	Type	Classification Parameters (Threshold Conditions)	
		24.10.2012 – 04.11.2012	21.11.2012 – 02.12.2012 & 17.02.13
Water (I & II)	Temp	T_1 dB <-17.1	T_3 dB <-17.1
Non-vegetated I	Temp	Coherence > 0.2 T_1 dB ≥ -8.0	Coherence > 0.3 T_3 dB ≥ -6.0
Non-vegetated II	Temp	Number of Pixels > 18 T_1 dB ≥ -6.5 T_2 dB ≤ --12	Number of Pixels > 18 T_3 dB ≥ -6.5 T_2 dB ≤ -10
Mature Mangrove I	Temp	Number of Pixels ≤ 18 Coherence ≥ 0.14 T_1 dB ≥ -8.5	
Mature Mangrove II	Temp	Coherence ≥ 0.14 T_1 dB ≥ -6	Coherence ≥ 0.14 T_1 dB ≥ -6.5
2008/09 plantation	Temp	Based on thematic attribute (YEAR)	
2010/11 plantation	Temp	Based on thematic attribute (YEAR)	
Mature Mangrove	Target	Merger of all mature mangrove classes	
Dormant	Target	Merger of all non-vegetated classes	
Submerged	Target	Merger of all water classes	
Good 2008/09	Target	Water-bound: 205 ∫ 390 SB Land-bound: 260 – 510 SB	230 ∫ 500 SB
Medium 2008/09	Target	Water-bound: 130 ∫ 205 SB Land-bound: 155 ∫ 260 SB	155 ∫ 230 SB
Poor 2008/09	Target	Water-bound: 0 ∫ 130 SB Land-bound: 0 ∫ 155 SB	0 ∫ 155 SB
Good 2010/11	Target	Water-bound: 210 – 445 SB Land-bound: 235 – 445 SB	235 ∫ 440 SB
Medium 2010/11	Target	Water-bound: 125 ∫ 210 SB Land-bound: 144 ∫ 235 SB	150 ∫ 235 SB
Poor 2010/11	Target	Water-bound: 0 ∫ 125 SB Land-bound: 0 ∫ 144 SB	0 ∫ 150 SB

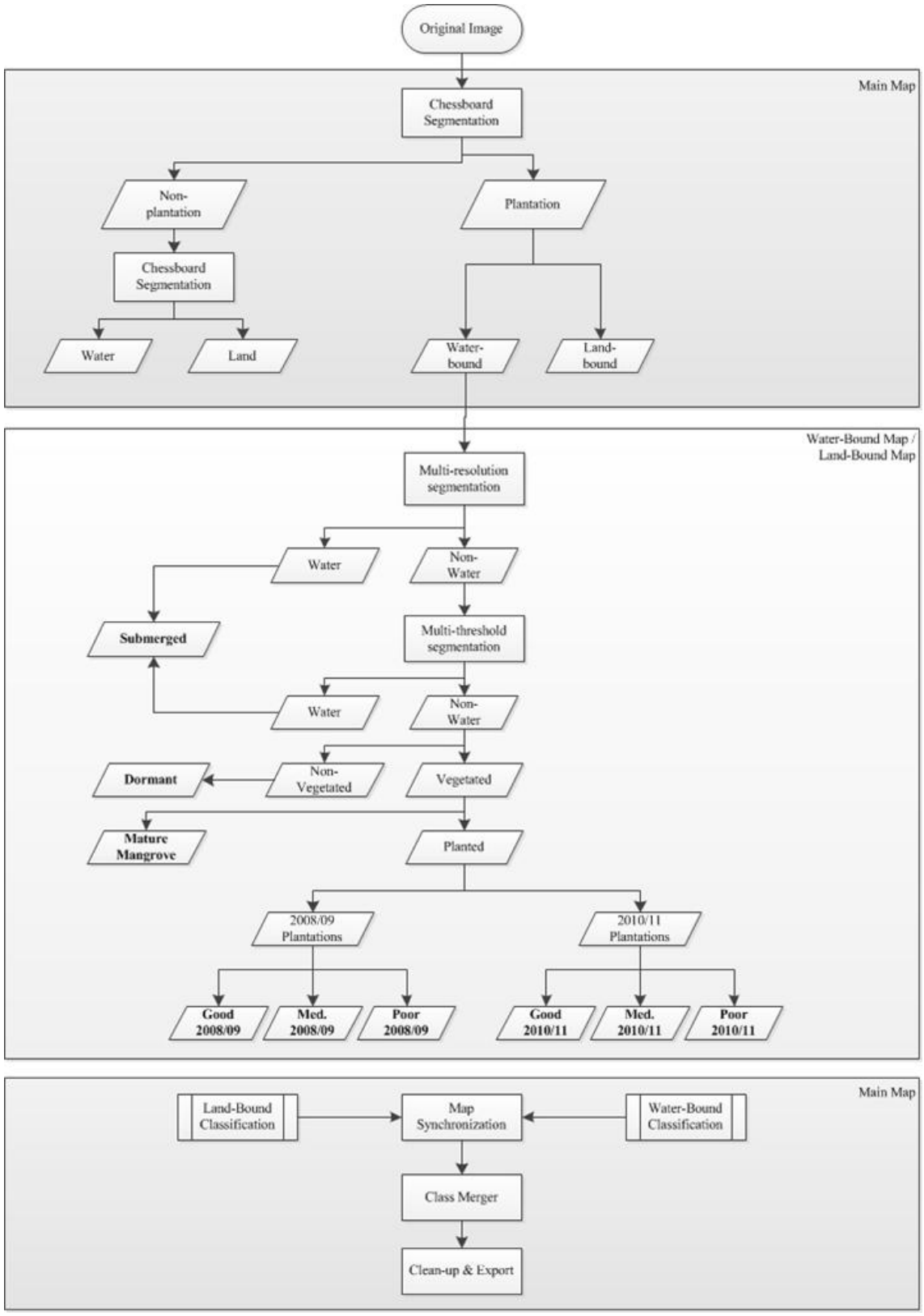

Figure 4-27: Generalized image analysis workflow.

4.2.4 Validation & accuracy assessment

To assess the accuracy of the classification results, a stratified random point approach was applied to the classification results of each TS-X footprint. 201 validation points were generated and randomly distributed throughout each classification data set. The

number of validation points per class was stratified based on the percentage area of each class within the respective footprints. *Table **4-10*** and *Table **4-11*** provide an overview of the stratification of the validation points used for the accuracy assessment of the FP01S and FP04S classifications.

Table 4-10: Distribution of validation points for the assessment of the FP01S classification results.

Class Name	Class Code	Area (m^2)	Area (%)	Number of Points
Good Growth 08/09	1	1907249.5	7	13
Medium Growth 08/09	2	754331.5	3	5
Poor Growth 08/09	3	2690564.5	9	19
Good Growth 10/11	4	4067418.1	14	28
Medium Growth 10/11	5	996064.9	3	7
Poor Growth 10/11	6	10702960.1	37	74
Dormant	7	1096810.0	4	8
Submerged	8	4876294.3	17	34
Mature Mangrove	9	1840441.7	6	12
TOTAL	-	*28932134.6*	-	*201*

Table 4-11: Distribution of validation points for the assessment of the FP04S classification results.

Class Name	Class Code	Area (m^2)	Area (%)	Number of Points
Good Growth 08/09	1	691787.2	5	11
Medium Growth 08/09	2	158593.2	1	2
Poor Growth 08/09	3	1267611.1	10	19
Good Growth 10/11	4	1579481.1	12	24
Medium Growth 10/11	5	254742.8	2	4
Poor Growth 10/11	6	4158263.3	32	63
Dormant	7	577994.31	4	9
Submerged	8	3909298.3	30	60
Mature Mangrove	9	561303.9	4	9
TOTAL	-	*13159075.1*	-	*201*

The validation points were created using the ArcGIS "Create Random Points" tool (ESRI, 2013). Each point corresponds to a single land cover image object and therefore a specific land cover class (i.e. submerged, dormant, etc.). In order to assure a non-biased validation, the class name and class code were not included in the original validation point layer (these were added post-validation).

The validation was performed using three different data sets: (1) the TS-X classification input images, (2) VHR WorldView-2 imagery, where available (see *Figure **4-3*** and *Table **4-2***), and (3) VHR Google Earth imagery acquired in the year 2012 (see *Table **4-2***). The image objects corresponding to each validation point were overlain on the three different image types, without indication of class type. The validation considered the entire image object rather than the pixel containing the point, as the classification was object-based. A visual analysis of each image object (or validation point) was performed and the validated class was recorded in the attribute table of the validation point layer.

The validation of the growth quality classes within the two groups of plantations (i.e. 2008/09 and 2010/11) was performed separately from one another as they were discretely classified.

Finally, the validation results were intersected with the original classification results for statistical analysis. The examination of validation results and the classification accuracy was done in the form of an error matrix (i.e. confusion matrix). This form of analysis has been suggested by numerous researchers and according to Congalton (1991), is the "standard reporting convention". The use of an error matrix allows for the calculation of the errors of commission (User's accuracy) and omission (Producer's accuracy) as well as the overall accuracy and Cohen's kappa coefficient (Cohen, 1960). These statistics can be used for a qualitative assessment of the classification results. The Producer's accuracy is a measure of how well the reference points are classified, whereas the User's accuracy demonstrates the reliability of the classification in comparison to actual ground conditions (Congalton, 1991). The kappa coefficient is a measure of agreement among a set of coders and corrects for chance agreement and is "widely accepted in the field of content analysis (Carletta, 1996). A kappa value of 0 indicates no agreement and a kappa of 1 reflects total agreement.

4.2.4.1 Comparative assessment

In addition to the accuracy assessment of the entire classification data set, a localized comparative assessment of several plantations was performed based field-delineated classifications of growth quality collected with GPS in 2011 by Pôle Carto. The field-delineation only considered four growth quality strata: good, medium, poor and dormant. No information was available on how the classes are defined. Unfortunately, only four plantations were fully mapped in the field, three of which were within the classifiable footprints. One plantation overlaps the classification of FP01S and two overlap the classification of FP04S.

4.3 Tools

This research utilized a variety of different software tools such as ArcGIS 10.1 (ESRI, 2013), Trimble eCognition 8.8 (Trimble, 2013), ENVI 4.8 (Exelis Visual Information Solutions, 2013), R 2.15.2 (R Development Core Team, 2008) and MS Excel 2010.

ArcGIS 10.1 was used during the pre-processing and analysis of the field survey data as well as for the analysis of the image classification results and the generation of various maps and figures.

The Trimble eCognition software was used to perform the object-based segmentation and classification of the TerraSAR images. A rule set was developed within the Developer portion of the software.

ENVI 4.8 was used during the pre-processing procedure to re-scale the TerraSAR images. It was also used for basic visualizations and image comparison.

The R 2.15.2 open source statistics software was used for the computation of zonal statistics and the generation of the sigma-0 images.

Finally, MS Excel was used for exploratory data analysis – the generation of plots and the quantification of results.

The processing, analysis and quantification of results, using the tools mentioned above, were implemented using a standard desktop PC.

5 RESULTS

This chapter presents the results obtained through the method adopted for this research. It begins with a presentation of the results, followed by the outcome of the validation and accuracy assessment. Subsequently, the overall achieved results and the corresponding accuracies are discussed and interpreted.

5.1 Presentation of Results

The results are presented in three parts: (1) section 5.1.1 provides a review of the classification results for footprint FP01S, (2) section 5.1.2 provides a review of the classification results derived for footprint FP04S and (3) section 5.2 presents the cumulative overall classification results.

5.1.1 Classification of 24.10.2012 Image

The classification of footprint FP01S was based on the images acquired on 24.10.2012 (T_1) and 04.11.2012 (T_2). In total, 730 plantations were found within this TS-X footprint; 226 plantations were established between 2008 and 2009 and 504 were planted in the years 2010 and 2011. The plantations cover an area of 28.93 km^2, of which 21.12 km^2 (73%) represented favorable operating conditions (i.e. flooded) and 7.81 km^2 (27%) represented unfavorable conditions and mature mangrove (see ***Table 5-1***).

The stratification of growth quality classes within areas representing favorable operating conditions revealed that the majority of plantations were of poor growth quality (64%) followed by good quality (28%); only 9% of the plantations demonstrated medium growth quality conditions.

The 7.81 km^2 of plantations that demonstrated unfavorable monitoring conditions were comprised of three classes: dormant, submerged and mature mangrove. Nearly two thirds of these areas were submerged (62%), whereas 14% reflected dormant conditions. Mature mangroves made up 24% of the unfavorable monitoring area. Overall, the mature mangrove class made up only 6% of the established plantation area.

Table 5-1: Hierarchal breakdown of classification results for footprint FP01S.

Operating Condition	Area (km^2)	Area* (%)	Class	Area (km^2)	Area** (%)	Area* (%)
Favorable	21.12	73	Good 08/09	1.91	9	7
			Med. 08/09	0.75	4	3
			Poor 08/09	2.69	13	9
			Good 10/11	4.07	19	14
			Med. 10/11	1.00	5	3
			Poor 10/11	10.70	51	37
Unfavorable	7.81	27	Dormant	1.10	14	4
			Submerged	4.88	62	17
			Mature Mangrove	1.84	24	6
TOTAL	*28.93*	*100*	-	*28.93*	-	*100*

* Percentage of the entire area; ** Percentage of the operating condition area.

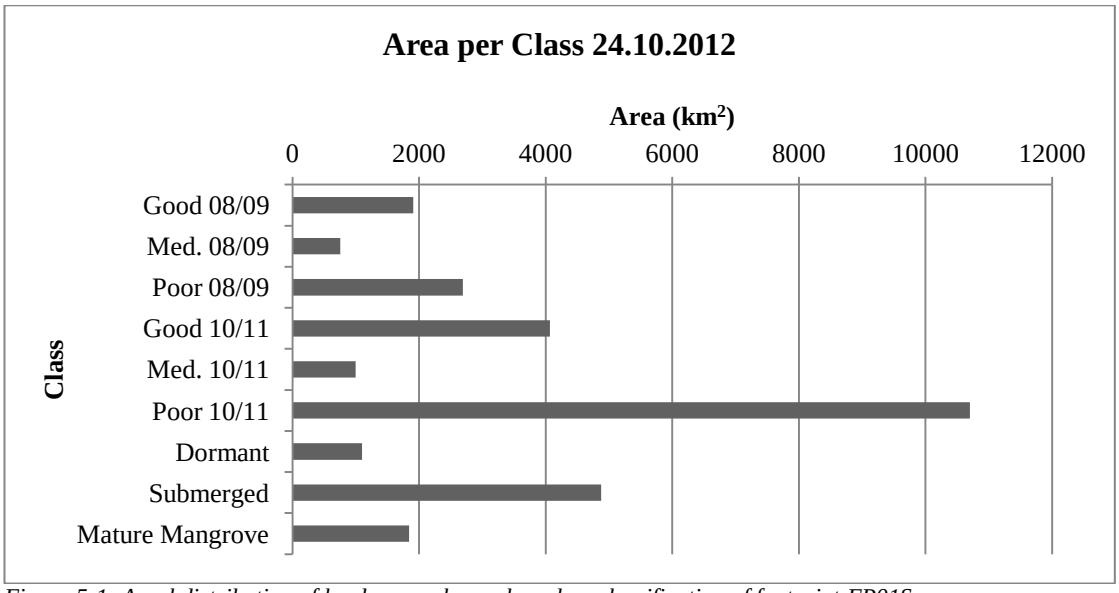

Figure 5-1: Areal distribution of land cover classes based on classification of footprint FP01S.

Figure 5-2 provides a comparative analysis of the stratification results based on the year of plantation establishment. Both periods demonstrated similar general growth quality stratification trends; poor growth accounted for the largest percentage, followed by good growth, then medium growth.

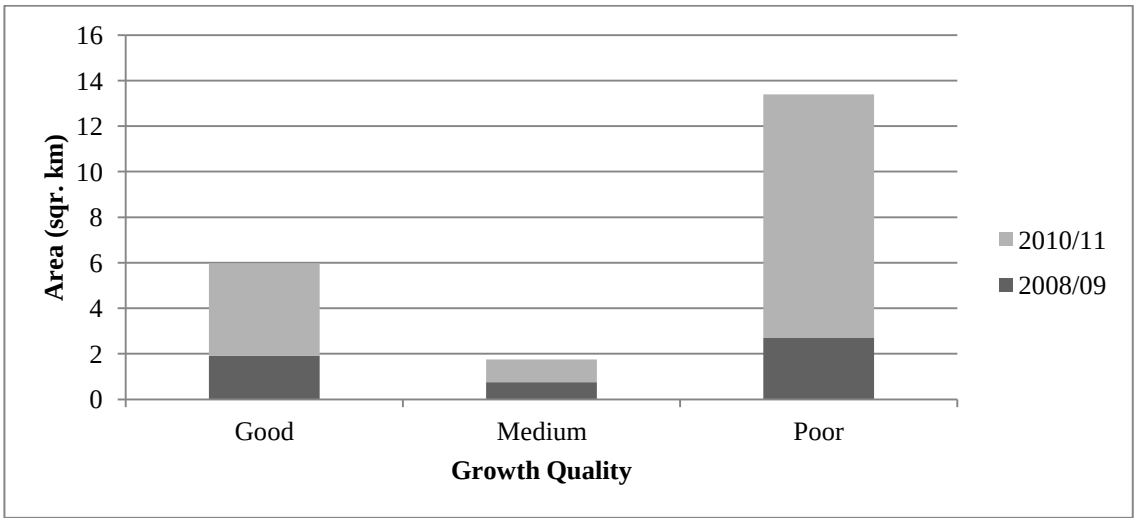

Figure 5-2: Stratification results of areas with favorable operating conditions by year of plantation establishment.

A breakdown of the classification of unfavorable monitoring areas by year of planting is shown in *Figure **5-3***. Plantations established between 2010 and 2011 contained a significantly higher percentage of land in all three classes than plantations planted between 2008 and 2009. The largest difference appeared in the submerged class, where the submerged class made up 57% of the unfavorable area in 2010/11 plantations as opposed to only 6% in 2008/09 plantations.

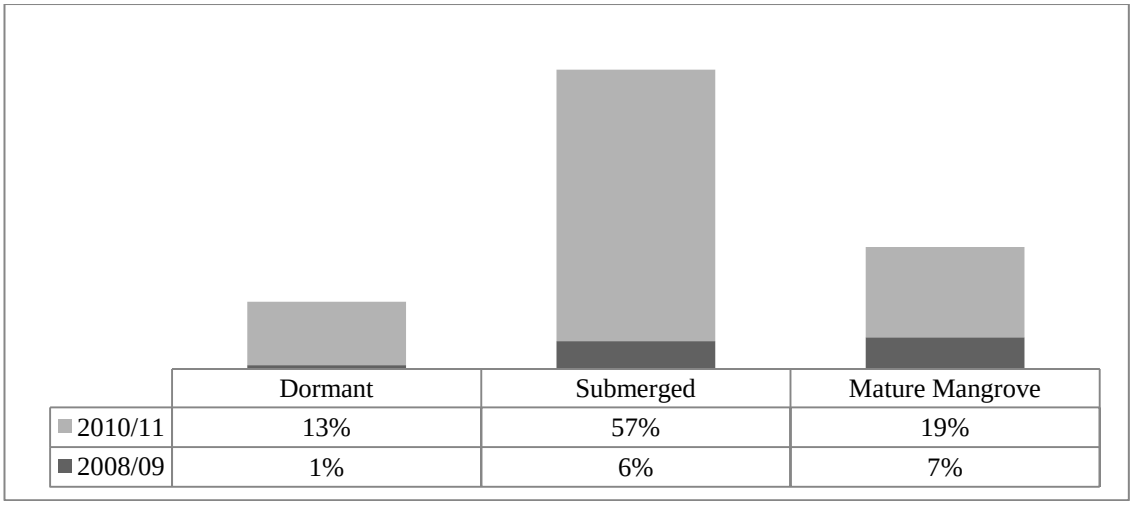

	Dormant	Submerged	Mature Mangrove
2010/11	13%	57%	19%
2008/09	1%	6%	7%

Figure 5-3: Comparison of the classification distribution (percentage) of unfavorable operating conditions by year of plantation establishment.

*Figure **5-4*** provides a detailed map showing a representative portion of the qualitative stratification (a full size version of the map can be found in the Appendix, see *Figure A **3***).

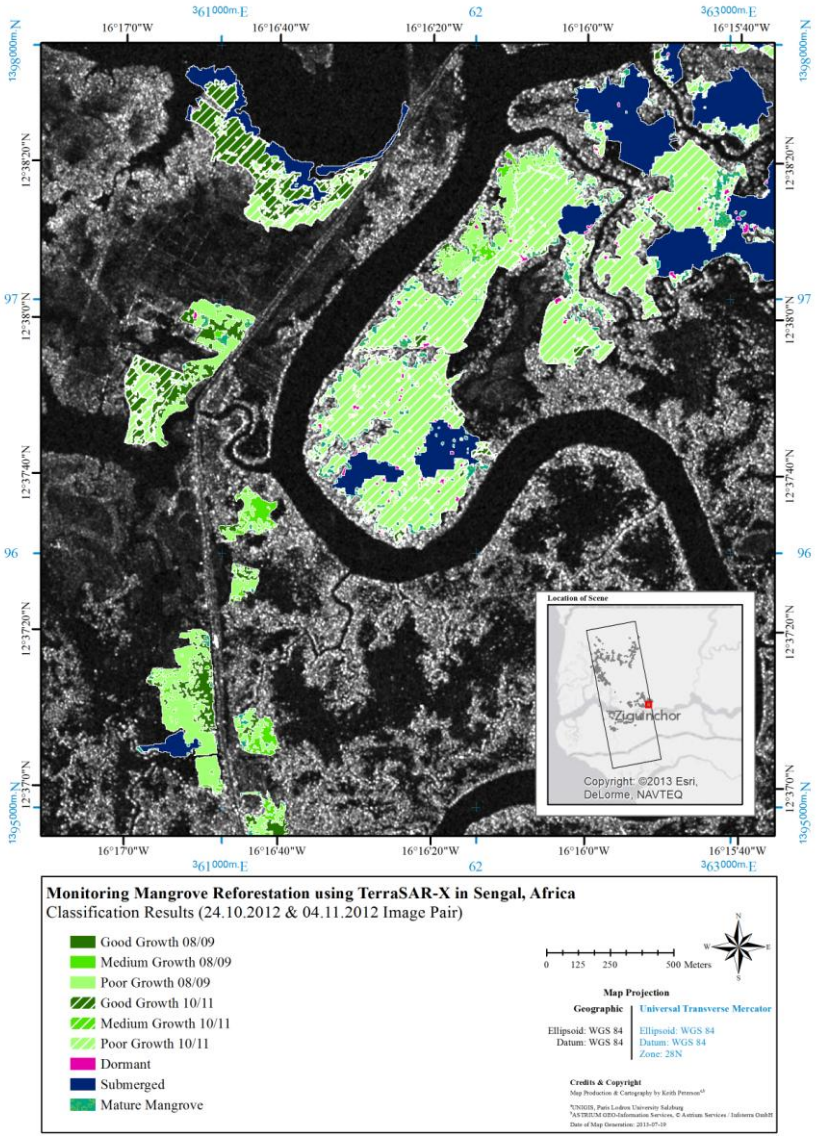

Figure 5-4: Map showing representative classification results in footprint FP01S.

5.1.1.1 Validation & accuracy of FP01S

An overall accuracy of 72% was achieved with the classification of footprint FP01S. The confusion matrix in ***Table 5-2*** shows the results of the analysis based on 201 stratified random validation points. The corresponding Producer's and User's accuracies, calculated for each of the nine classes, are shown in ***Table 5-3***.

Of the six growth quality stratification classes, poor growth 2008/09 (100%) was the most accurate in terms of Producer's accuracy, followed by poor growth 2010/11 (93%) and good growth 2008/09 (80%). The three classes representing unfavorable monitoring conditions showed considerably lower Producer's accuracies, particularly the dormant class (8%).

Four of the six classes demonstrated a lower User's accuracy than Producer's accuracy: good growth 2008/09, poor growth 2008/09, good growth 2010/11 and poor growth 2010/11. Both the medium growth classes had a higher User's accuracy than Producer's

accuracy. Of the six growth quality classes, the class poor growth 2008/09 (84%) had the highest User's accuracy. The three classes representing unfavorable monitoring conditions all had higher User's accuracies than Producer's accuracies; the highest being 91% for the submerged class.

The classification resulted in a kappa confident of 69%, indicating a level of disagreement between the classes.

Table 5-2: Confusion Matrix for the classification from 24.10.2012.

		Validation Data									
		1	**2**	**3**	**4**	**5**	**6**	**7**	**8**	**9**	*TOT.*
Classification Data	**1**	8	2	0	0	0	0	1	0	2	*13*
	2	1	4	0	0	0	0	0	0	0	*5*
	3	0	2	16	0	0	0	0	1	0	*19*
	4	0	0	0	15	0	0	6	0	7	*28*
	5	0	0	0	4	3	0	0	0	0	*7*
	6	0	0	0	0	6	54	0	14	0	*74*
	7	0	0	0	1	0	1	4	0	2	*8*
	8	0	0	0	0	0	3	0	31	0	*34*
	9	1	2	0	0	0	0	1	0	9	*13*
	TOT.	*10*	*10*	*16*	*20*	*9*	*58*	*12*	*46*	*20*	*201*

Key: 1 = Good Growth 08/09, 2 = Medium Growth 08/09, 3 = Poor Growth 08/09, 4 = Good Growth 10/11, 5 = Medium Growth 10/11, 6 = Poor Growth 10/11, 7 = Dormant, 8 = Submerged & 9 = Mature Mangrove.

Table 5-3: Producer's and User's accuracies resulting from the 24.10.2012 classification.

Class Name	**Producer's Accuracy**	**User's Accuracy**
Good Growth 08/09	80%	62%
Medium Growth 08/09	40%	80%
Poor Growth 08/09	100%	84%
Good Growth 10/11	75%	54%
Medium Growth 10/11	33%	43%
Poor Growth 10/11	93%	73%
Dormant	8%	50%
Submerged	67%	91%
Mature Mangrove	45%	69%

Only one field-delineated plantation overlaps a portion of the FP01S classification (see *Figure **5**-**5***). The plantation was established in 2009 in the Thiobon region. Due to slight differences in extent, a direct comparison of the two stratifications was not possible; the field-based stratification examined an area of 43,125.39 m^2, whereas model-based method considered a plantation area of 42,917.80 m^2. Furthermore, the field-based stratification did not include a mature mangrove class.

Despite the differences in the stratifications, a comparative analysis reveals several interesting differences. First of all, the model-based classification results show a much larger percentage of good and poor growth, whereas the majority of the plantation was considered medium growth by the field team (see *Table **5**-**4***). In addition, the field team identified 1,803.43 m^2 (4%) as dormant; the model-based method did not classify any part of the plantation as dormant.

Table 5-4: Comparison of field- and model-based stratification results.

	Field-based stratification		Mode-based stratification	
Class Name	**Area (m^2)**	**Area (%)**	**Area (m^2)**	**Area (%)**
Good Growth	8020.31	19	23556.51	55
Medium Growth	32410.82	75	5936.31	14
Poor Growth	890.84	2	7943.03	19
Dormant	1803.43	4	0	0
Mature Mangrove	0	0	5481.95	13
TOTAL	*43125.39*	*100*	*42917.80*	100

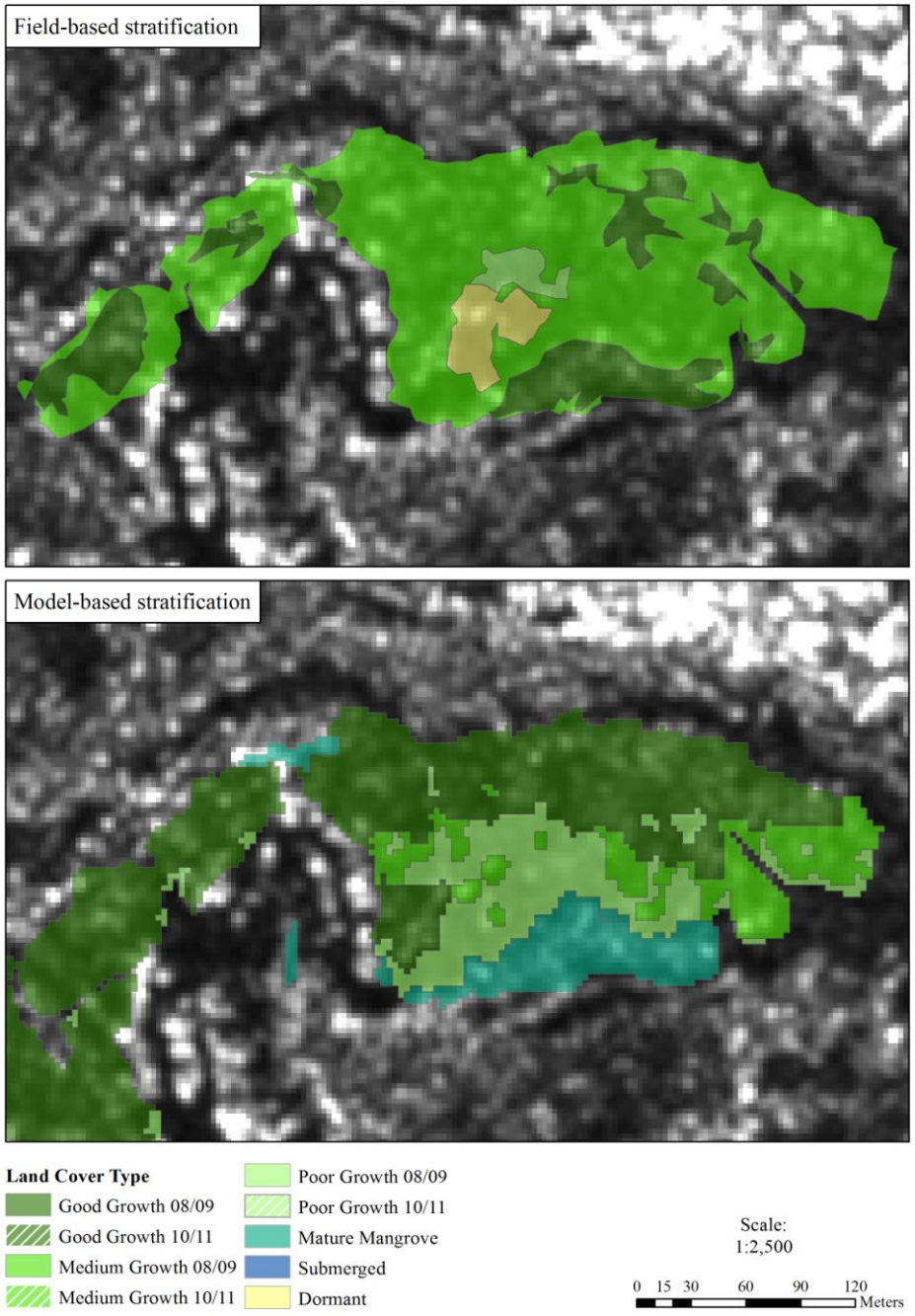

Figure 5-5: Comparison of field- and model-based stratification results.

5.1.2 Classification of 17.02.2013 Image

The classification of footprint FP04S was based on the images acquired on 21.11.2012 (T_1), 03.12.2012 (T_2) and 17.02-2013 (T_3). The third image was added to the classification rule set due to the very high tide levels present at the time of acquisition in T_1 and T_2; the image acquired on 17.02.2013 displayed favorable operating conditions and was the primary scene for the classification. A total of 296 plantations were located within this TS-X footprint; 108 plantations were established between 2008 and 2009 and 188 were planted in the years 2010 and 2011. The plantations comprised a total area of 13.16 km^2, of which 8.11 km^2 (62%) were classified as having favorable monitoring conditions and 5.05 km^2 (38%) represented unfavorable monitoring conditions and mature mangrove (see *Table **5-5***).

Like in the classification of FP01S, the stratification of growth quality classes within areas representing favorable operating conditions in FP04S revealed that a majority of plantations were of poor growth quality (67%), followed again by good quality (28%); only 5% of the plantations demonstrated medium growth quality conditions.

The three classes comprising unfavorable monitoring conditions (dormant, submerged and mature mangrove) covered an area of 5.05 km^2. The majority (77%) of this area was submerged, whereas 11% was dormant and an additional 11% was mature mangrove. Overall, these two classes made up only 4% of the established plantation area, respectively.

Table 5-5: Hierarchal breakdown of classification results for footprint FP04S.

Operating Condition	**Area (km^2)**	**Area* (%)**	**Class**	**Area (km^2)**	**Area** (%)**	**Area* (%)**
Favorable	8.11	62	Good 08/09	0.69	9	5
			Med. 08/09	0.16	2	1
			Poor 08/09	1.27	16	10
			Good 10/11	1.58	19	12
			Med. 10/11	0.25	3	2
			Poor 10/11	4.16	51	32
Unfavorable	5.05	38	Dormant	0.58	11	4
			Submerged	3.91	77	30
			Mature Mangrove	0.56	11	4
TOTAL	*13.16*	*100*	-	*13.16*	-	*100*

* Percentage of the entire area; ** Percentage of the operating condition area.

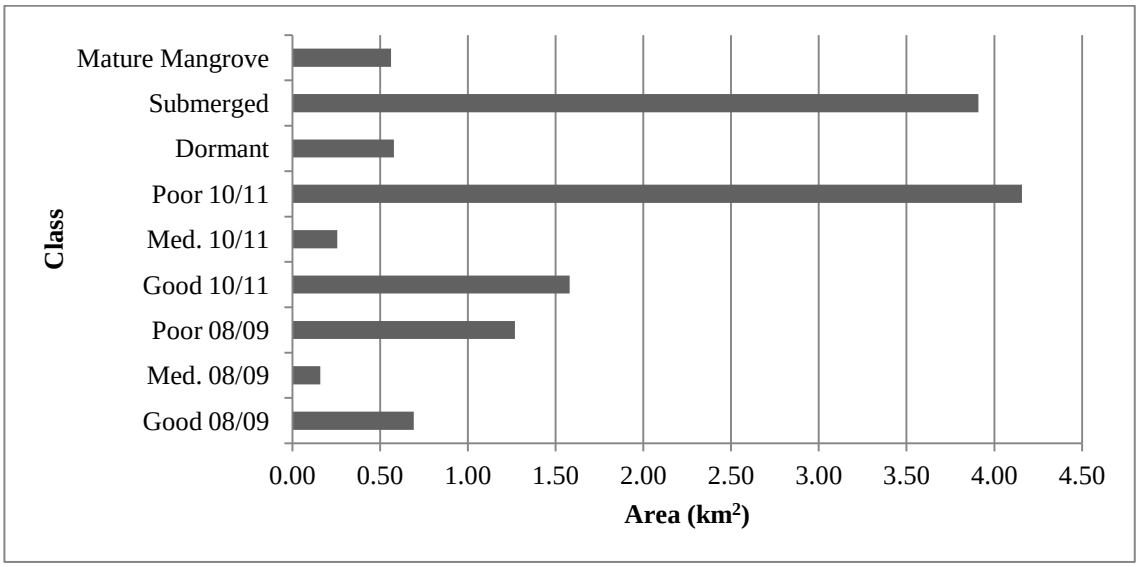

Figure 5-6: Areal distribution of land cover classes based on classification of footprint FP04S.

Figure ***5-7*** compares the stratification results based on the year of plantation establishment. Both periods, as seen in FP01S, demonstrated similar general growth quality stratifications trends; poor growth accounted for the largest percentage, followed by good growth, then medium growth.

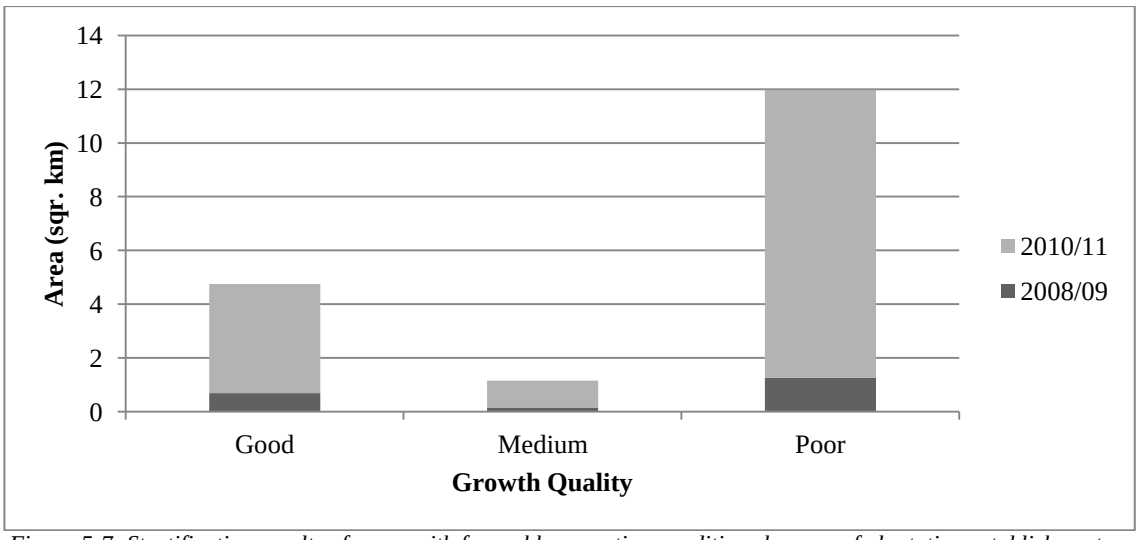

Figure 5-7: Stratification results of areas with favorable operating conditions by year of plantation establishment.

An analysis of the classification of unfavorable monitoring areas by planting year (see ***Figure 5-8***) revealed that plantations established between 2010 and 2011 contained a significantly higher percentage of land in all three classes than plantations planted between 2008 and 2009; this trend was also observed for footprint FP01S. The largest difference appeared in the submerged class, where the submerged class made up 70% of the unfavorable area in 2010/11 plantations as opposed to only 8% in 2008/09 plantations.

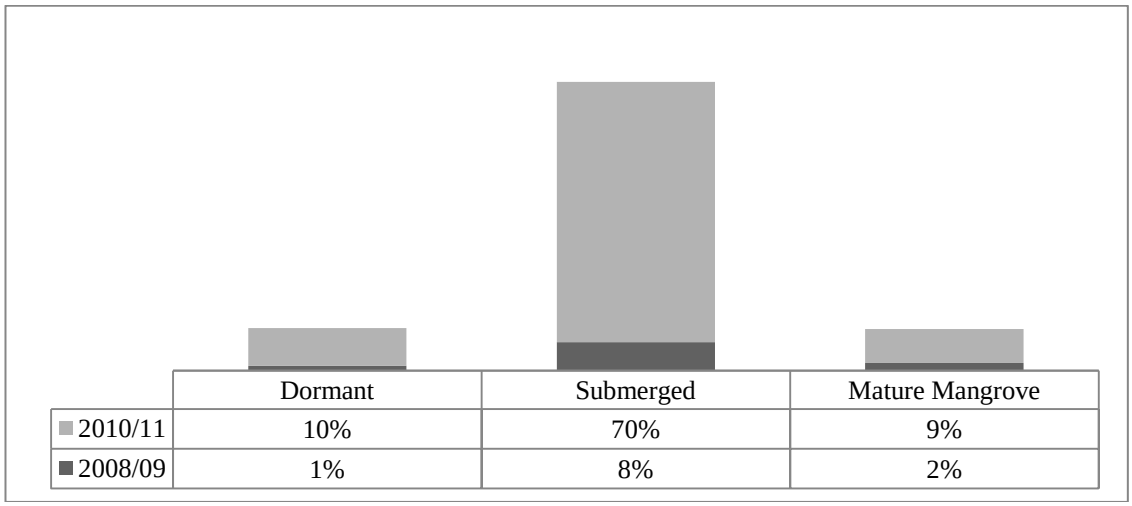

	Dormant	Submerged	Mature Mangrove
2010/11	10%	70%	9%
2008/09	1%	8%	2%

Figure 5-8: Comparison of the classification distribution (percentage) of unfavorable operating conditions by year of plantation establishment.

A map showing a representative portion of the qualitative classification is shown in *Figure **5-9*** (a full size version of the map can be found in the Appendix, see *Figure A **4***).

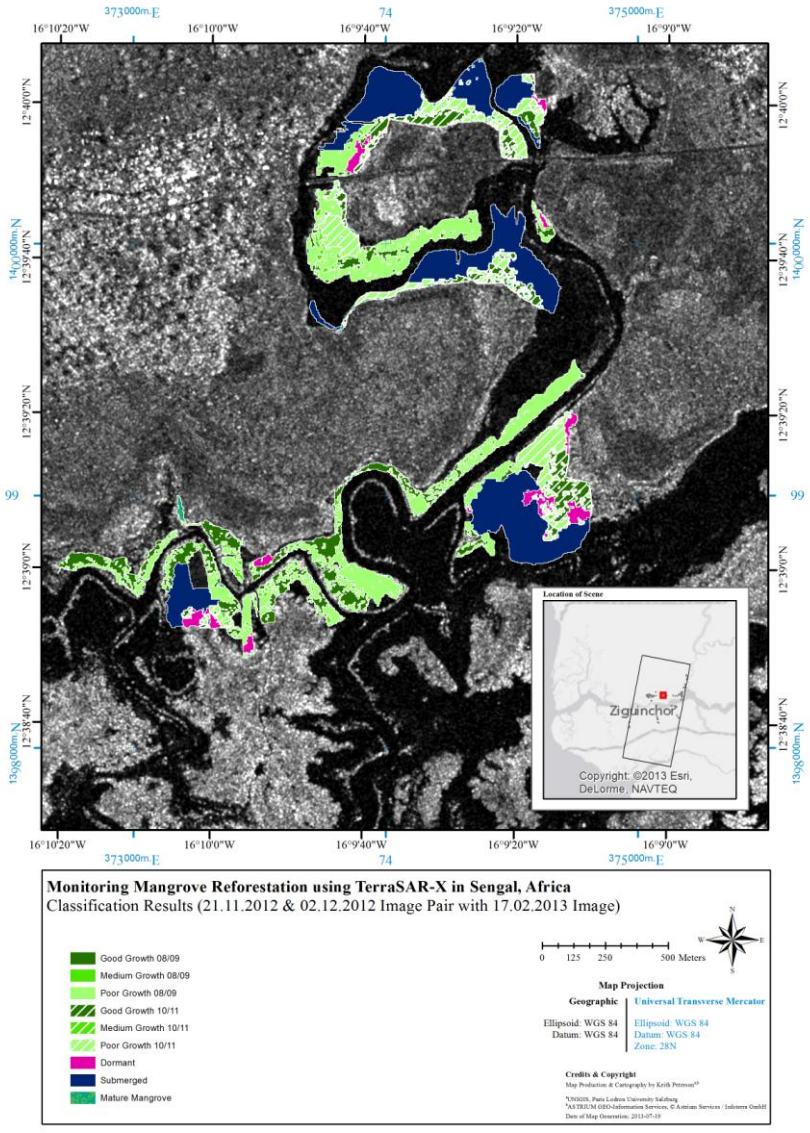

Figure 5-9: Map showing representative classification results in footprint FP04S.

5.1.2.1 Validation & accuracy of FP04S

The classification of the 17.02.2013 image revealed an overall accuracy of 83%. The confusion matrix in ***Table 5-6*** illustrates the results of the analysis based on 201 stratified random validation points. The Producer's and User's accuracies are provided for each of the nine classes in ***Table 5-7***.

Of the six growth quality stratification classes, poor growth 2008/09 (100%) was, as in FP01S, the most accurate in terms of Producer's accuracy. The second highest Producer's accuracy is 95%, for poor growth 2010/11, followed by good growth 2010/11 (87%). The medium growth 2008/09 class had the lowest Producer's accuracy; all the validation points were interpreted as good growth 2008/09. The Producer's accuracy for the three classes representing unfavorable monitoring conditions was mixed; the submerged class was highly accurate (92%), whereas the dormant and mature mangrove classes were significantly lower.

Three of the six growth classes had a lower User's accuracy than Producer's accuracy: good growth 2008/09, good growth 2010/11 and poor growth 2010/11. The poor growth 2008/09 had the same User's accuracy as Producer's accuracy and at the same time the highest User's accuracy (100%). The three classes representing unfavorable monitoring conditions all had higher User's accuracies than Producer's accuracies, the highest being 97% for the submerged class.

The classification results demonstrated a high level of agreement, with a kappa coefficient of 82%.

Table 5-6: Confusion Matrix for the classification from 17.02.2013.

		Validation Data									
		1	**2**	**3**	**4**	**5**	**6**	**7**	**8**	**9**	*TOT.*
Classification Data	**1**	6	0	0	0	0	0	2	0	3	*11*
	2	2	0	0	0	0	0	0	0	0	*2*
	3	0	0	19	0	0	0	0	0	0	*19*
	4	0	0	0	13	1	1	4	0	5	*24*
	5	0	0	0	1	3	0	0	0	0	*4*
	6	0	0	0	0	2	56	0	5	0	*63*
	7	0	0	0	0	0	0	8	0	1	*9*
	8	0	0	0	0	0	2	0	58	0	*60*
	9	0	0	0	1	1	0	3	0	4	*9*
	TOT.	*8*	*0*	*19*	*15*	*7*	*59*	*17*	*63*	*13*	***201***

Key: 1 = Good Growth 08/09, 2 = Medium Growth 08/09, 3 = Poor Growth 08/09, 4 = Good Growth 10/11, 5 = Medium Growth 10/11, 6 = Poor Growth 10/11, 7 = Dormant, 8 = Submerged & 9 = Mature Mangrove.

Table 5-7: Producer's and User's accuracies resulting from the 17.02.2013 classification.

Class Name	**Producer's Accuracy**	**User's Accuracy**
Good Growth 08/09	75%	55%
Medium Growth 08/09	-	0%
Poor Growth 08/09	100%	100%
Good Growth 10/11	87%	54%

Medium Growth 10/11	43%	75%
Poor Growth 10/11	95%	89%
Dormant	12%	89%
Submerged	92%	97%
Mature Mangrove	31%	44%

Two field-delineated plantations overlapped a portion of the FP04S classification (see *Figure **5-10***). The plantation was established in 2009 in the Thiobon region. Due to slight differences in extent, a direct comparison of the two stratifications was not possible; the field-based stratification examined an area of 332,826.05 m^2, whereas the model-based method considered a plantation are of 365,594.23 m^2. Furthermore, the field-based stratification did not include a mature mangrove class.

A comparative analysis again revealed that the model-based classification resulted in much larger percentages of good and poor growth, whereas the majority of the plantation was deemed medium growth by the field team (see *Table **5-8***). In addition, the field team identified 66% of the two plantations as dormant; the model-based method classified only 22% as dormant and 9% as submerged.

Table 5-8: Comparison of field- and model-based stratification results.

	Field-based stratification		**Mode-based stratification**	
Class Name	**Area (m^2)**	**Area (%)**	**Area (m^2)**	**Area (%)**
Good Growth	6484.93	2	84155.54	23
Medium Growth	108158.73	32	10769.07	3
Poor Growth	0	0	149661.98	41
Dormant	218182.39	66	81319.58	22
Mature Mangrove	0	0	6821.43	2
Submerged	0	0	32866.63	9
TOTAL	*332826.05*	*100*	*365594.23*	*100*

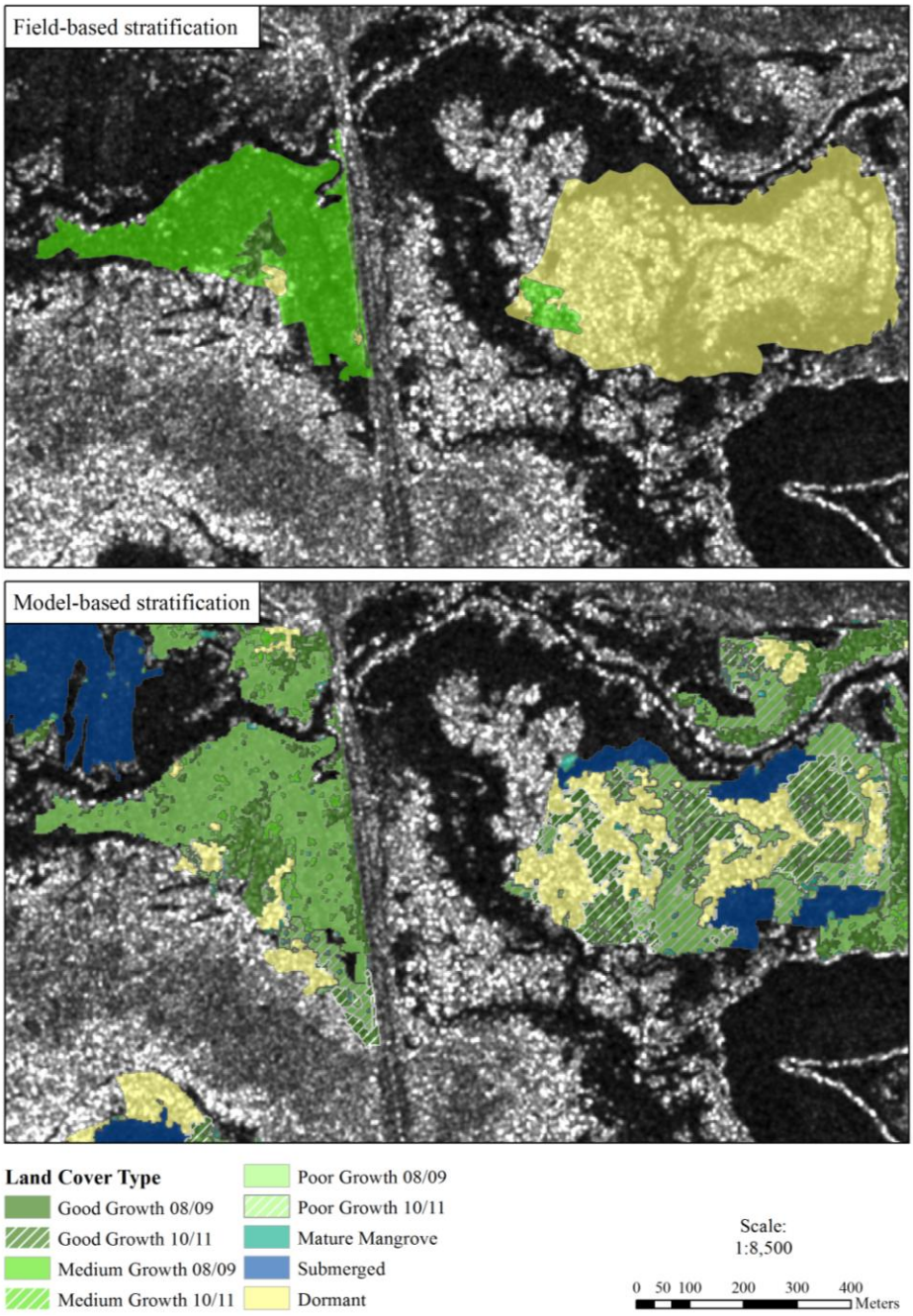

Figure 5-10: Comparison of field delineated (above) and model-based stratifications (below).

5.2 Interpretation of overall classification results

A total of 878 plantations were examined between the two footprints (148 plantations were located in the overlap area of the two footprints and were accounted for accordingly), comprising a total area of 34.44 km^2. Overall, 72% of the examined plantations had favorable operating conditions; 28% were comprised of unfavorable operating conditions and mature mangroves. A hierarchal breakdown of the overall classification results (without overlap) is listed in ***Table 5-9*** and illustrated in *Figure **5-11***.

Table 5-9: Overview of classification results by class and operating condition.

Operating Condition	Area (km^2)	Area* (%)	Class	Area (km^2)	Area** (%)	Area* (%)
Favorable	24.74	72	Good 08/09	2.29	7	9
			Med. 08/09	0.84	2	3
			Poor 08/09	3.51	10	14
			Good 10/11	4.80	14	19
			Med. 10/11	1.09	3	4
			Poor 10/11	12.20	35	49
Unfavorable	9.70	28	Dormant	1.59	5	16
			Submerged	6.07	18	63
			Mature Mangrove	2.05	6	21
TOTAL	*34.44*	*100*	-	*34.44*	-	*100*

* Percentage of the entire area; ** Percentage of the operating condition area.

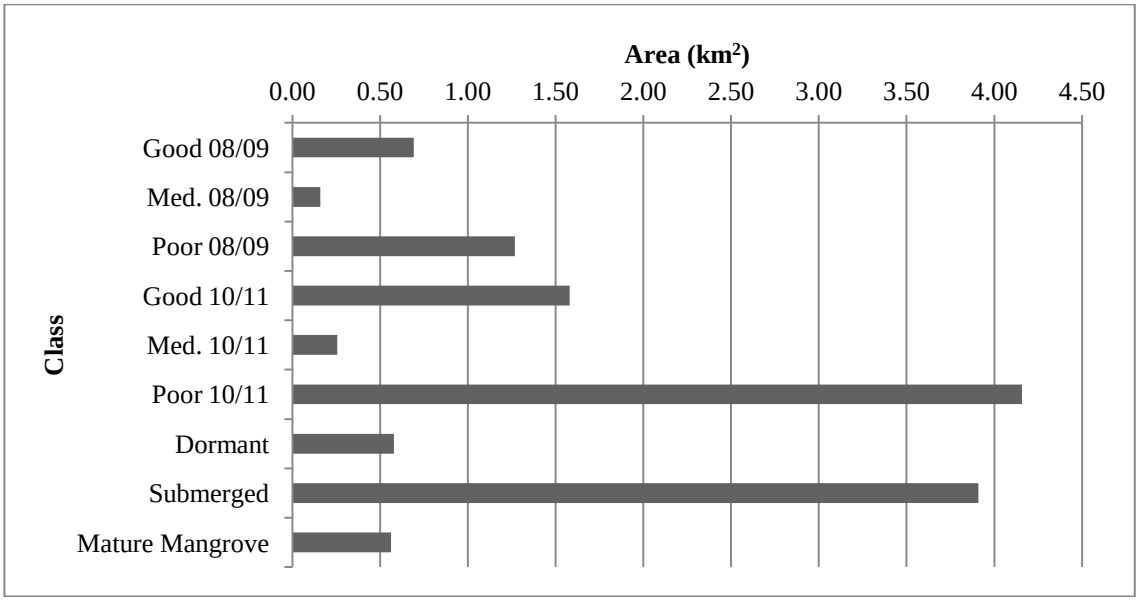

Figure 5-11: Areal distribution of land cover classes within in the classified portion of the study area.

5.2.1 Favorable operating conditions

A series of trends were observed in the growth quality stratification results. A comparison of the growth quality stratification results showed that the three 2010/11 growth quality classes consistently comprised a higher amount of the land with favorable operating conditions than 2008/09 growth quality classes (see *Figure **5-12***). This is simply due to the fact that the study area contains more plantations established between 2010 and 2011 (see *Figure **3-2*** in chapter 3). 63% of the plantations in the entire study area were planted in 2010 and 2011, whereas only 37% were planted in 2008 and 2009. Therefore, the continually higher distribution values for the three growth quality stratifications representing 2010/11 plantations is expectable.

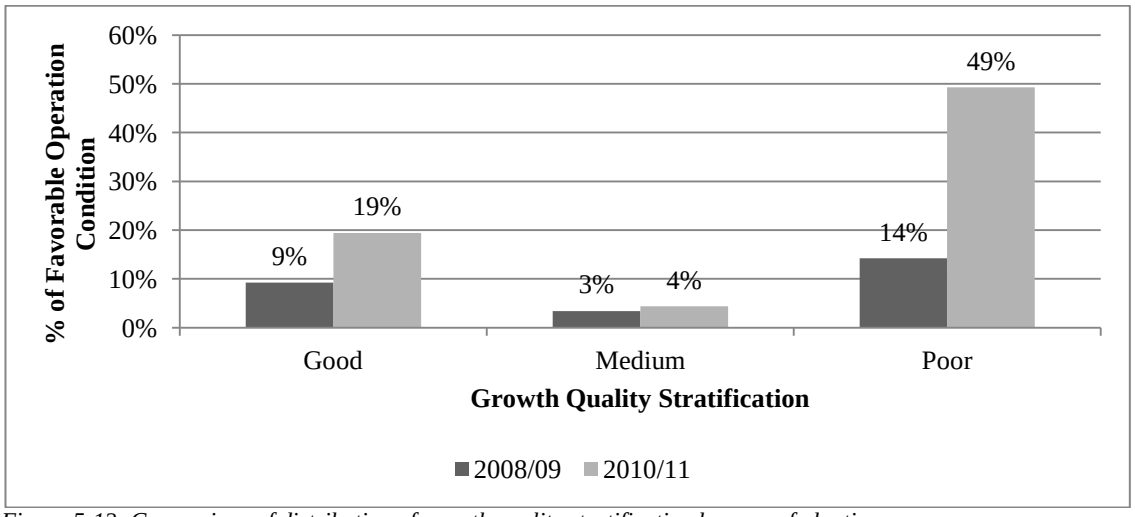

Figure 5-12: Comparison of distribution of growth quality stratification by year of planting.

An additional tendency, illustrated in *Figure **5-12***, was that the medium growth class made up a significantly smaller overall percentage of the favorable operating condition classification than both good and poor growth in both planting periods. The poor growth class made up the largest portion of plantations, regardless of year of planting. This was especially true for 2010/11 plantations, where 49% of plantations with favorable operating conditions were considered to reflect poor tree growth.

The under-representation of medium growth was also apparent in the comparisons of the model- and field-based stratification results (see *Table **5-4*** and *Table **5-8*** above). Overall, 35% of the mapped plantations were considered medium growth by the field team in the 2011 survey, whereas only 3% reflected medium growth conditions according to the model-based stratification.

This underestimation can be explained by four factors: (1) discrepancies in growth quality definitions between the field team and the author, (2) tree growth between the time of the field survey and the current study, (3) operating conditions at the time of TS-X image acquisition, or (4) model-based stratification parameters.

Despite not having full knowledge of the growth quality definitions used by the field team, there is little reason to believe that potentially small inconsistencies could lead to such differences in results. It is additionally unlikely that temporal differences could cause such discrepancies; approximately one year separates the field delineation and the TS-X image acquisition.

The operating conditions, especially the presence and depth of water, greatly influenced the growth quality stratification. If the tide level is high, less vertical tree structure is available to interact with the SAR signal, resulting in a lower backscatter value. Similarly, smaller, less developed vegetation also has a lower backscatter, as demonstrated in the field measurement-based statistical modeling (see *Figure **4-17*** in

section 4.2.2.2.2). Therefore, the tree height to water level ratio plays a critical role, directly impacting the growth quality stratification. ***Figure 5-13*** demonstrates this problem; as the tide level increases the perceived size of the tree decreases, eventually leading to a miss-classification since the water level was an unknown variable.

The likelihood for such miss-classifications is greater in plantations established between 2010 and 2011, as the trees are generally smaller (the mean height of trees measured in 2011/12 plantations during the 2012 field campaign was 32.29 cm compared to 70.08 cm in 2008/09 plantations). Hence, they are more likely to be nearly (situation c in ***Figure 5-13***) or completely submerged, even during generally favorable operation conditions. This results in lower backscatter, which is directly associated with poorer growth.

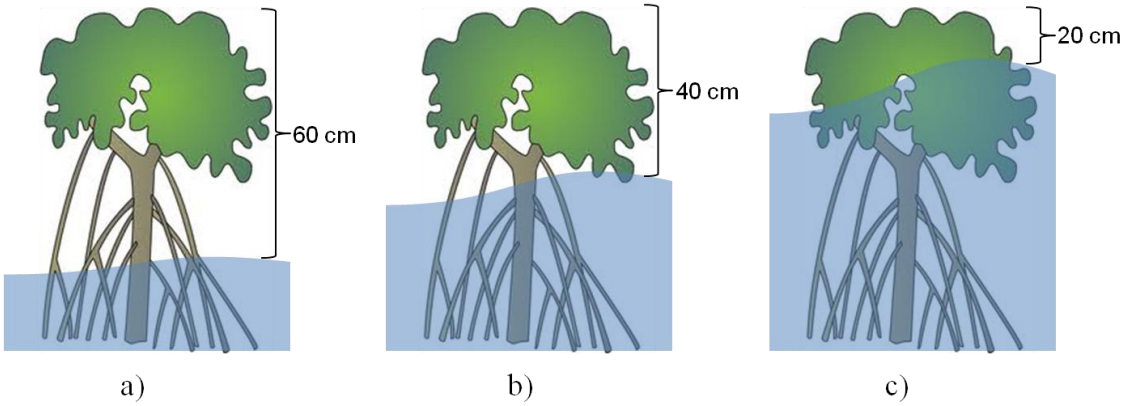

Figure 5-13: The effect of water depth on perceived tree height and growth quality; a) favorable operation conditions, b) moderate operating conditions, c) unfavorable operation conditions.

This factor could explain the high percentage of poor growth present in the model-based stratification, but not the larger percentage of good growth. Therefore, the under-representation of medium growth is primarily associated with the stratification parameters. An examination of the membership functions revealed that the medium growth class continually had a smaller membership function range (see *Table **5-10***), which reduced the number of image objects that could fulfill the threshold conditions.

Table 5-10: Class membership analysis.

Footprint	Planting Period	Class Name*	Membership Function**		
			Minimum	Maximum	Range
FP01S	2008/09	Good (WB)	205	390	185
		Medium (WB)	130	205	75
		Poor (WB)	0	130	130
		Good (LB)	260	510	250
		Medium (LB)	155	260	105
		Poor (LB)	0	155	155
	2010/11	Good (WB)	210	445	235
		Medium (WB)	125	210	85
		Poor (WB)	0	125	125
		Good (LB)	235	445	210
		Medium (LB)	144	235	91
		Poor (LB)	0	144	144
FP04S	2008/09	Good	230	500	270
		Medium	155	230	75
		Poor	0	155	155
	2010/11	Good	235	440	205
		Medium	150	235	85
		Poor	0	150	150

* WB = Water bound; LB = Land Bound

**the minimum and maximum values of the membership function represent fuzzy threshold conditions.

5.2.2 Unfavorably operating conditions

Of the three classes representing unfavorable operating conditions, the submerged class accounted for the 6.07 km^2, making up 63% of unfavorable operating conditions and 18% of all land classified. In comparison, the dormant class only accounted for 1.59 km^2 (16%). These two classes were particularly vulnerable to the tidal conditions present at the time of image acquisition and the characteristics of the plantations in the study area. Plantations established between 2010 and 2011 contain smaller trees, hence they had a greater chance of submersion, even during favorable operating conditions. Likewise, the presence of water prevents dormant portions of a plantation from being considered dormant, as the ground conditions are not visible. Hence, the class submerged will contain dormant areas that are merely underwater at the time of image acquisition.

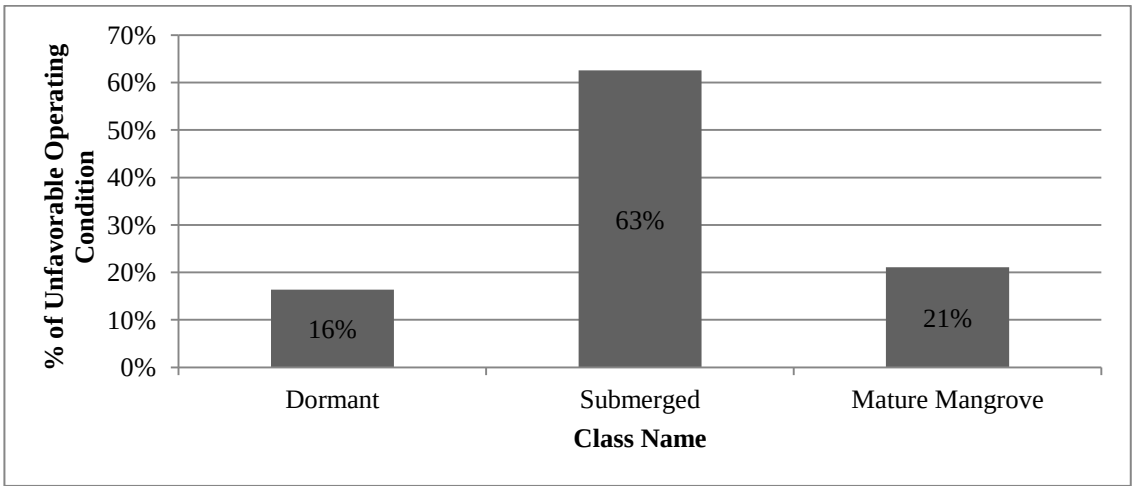

Figure 5-14: Overall percent distribution of unfavorable operating conditions.

5.2.3 Interpretation of the accuracy assessment

The classifications of the individual footprints demonstrated relatively high accuracies. In total, 402 validation points were examined, yielding a cumulative overall accuracy of 77%.

An analysis of the Producer's and User's accuracies, in ***Table 5-12***, which are indications of (1) how well reference points are classified (Producer's accuracy) and (2) the probability, or reliability, that a point classified on the map actually represents that class on the ground (User's accuracy) (Congalton, 1991), revealed the quality of the classification method for each class.

The poor growth classes both had high Producer's and User's accuracies. This indicates that the model-based stratification method was well suited for the identification of poor growth quality and that the stratification was reliable. On the other hand, the model-based good and medium growth quality stratification results warrant more caution. For example, although 78% of good growth areas in plantations established between 2008 and 2009 were correctly identified, only 58% them were actually good growth. The classification of medium growth yields even lower accuracies: only 40% of medium growth areas in plantations established between 2008 and 2009 were correctly classified and 57% of them were actually medium growth. A more detailed examination of the error matrix (see *Table* ***5-11***) shows that there was significant confusion in discriminating medium from good growth. This was also found to be true in the comparison of model- and field-based classification results.

Of the three unfavorable operating condition classes, submerged areas resulted in the highest Producer's and User's accuracies – meaning these image objects were well-classified and that the probability that they were correctly classified is high. The identification of this ground cover class is relatively straightforward and it has a strong

contrast to the other unfavorable classes. The only confusion occurs with the poor growth classes, as the water surface tends to have a stronger influence in this class due to the smaller size of the trees and lower densities.

The dormant and mature mangrove classes displayed considerably more confusion, which is reflected in the lower accuracies. The single-pol SAR characteristics of these two classes make them, in some cases, particularly difficult to discriminate from one another. Furthermore, the validation of these two classes is difficult without the VHR optical imagery (see the confusion between mature mangrove and dormant and plantations with good growth in the confusion matrix).

Overall, a kappa coefficient of 75% was achieved, indicating a majority level of agreement between the classes.

Table 5-11: Cumulative confusion matrix considering the validation points from both footprints.

		Validation Data									
		1	**2**	**3**	**4**	**5**	**6**	**7**	**8**	**9**	*TOT.*
Classification Data	**1**	14	2	0	0	0	0	3	0	5	*24*
	2	3	4	0	0	0	0	0	0	0	*7*
	3	0	2	35	0	0	0	0	1	0	*38*
	4	0	0	0	28	1	1	10	0	12	*52*
	5	0	0	0	5	6	0	0	0	0	*11*
	6	0	0	0	0	8	110	0	19	0	*137*
	7	0	0	0	1	0	1	12	0	3	*17*
	8	0	0	0	0	0	5	0	89	0	*94*
	9	1	2	0	1	1	0	4	0	13	*22*
	TOT.	*18*	*10*	*35*	*35*	*16*	*117*	*29*	*109*	*33*	***402***

Key: 1 = Good Growth 08/09, 2 = Medium Growth 08/09, 3 = Poor Growth 08/09, 4 = Good Growth 10/11, 5 = Medium Growth 10/11, 6 = Poor Growth 10/11, 7 = Dormant, 8 = Submerged & 9 = Mature Mangrove.

Table 5-12: Cumulative Producer's and User's accuracies.

Class Name	**Producer's Accuracy**	**User's Accuracy**
Good Growth 08/09	78%	58%
Medium Growth 08/09	40%	57%
Poor Growth 08/09	100%	92%
Good Growth 10/11	80%	54%
Medium Growth 10/11	38%	55%
Poor Growth 10/11	94%	80%
Dormant	10%	71%
Submerged	82%	95%
Mature Mangrove	39%	59%

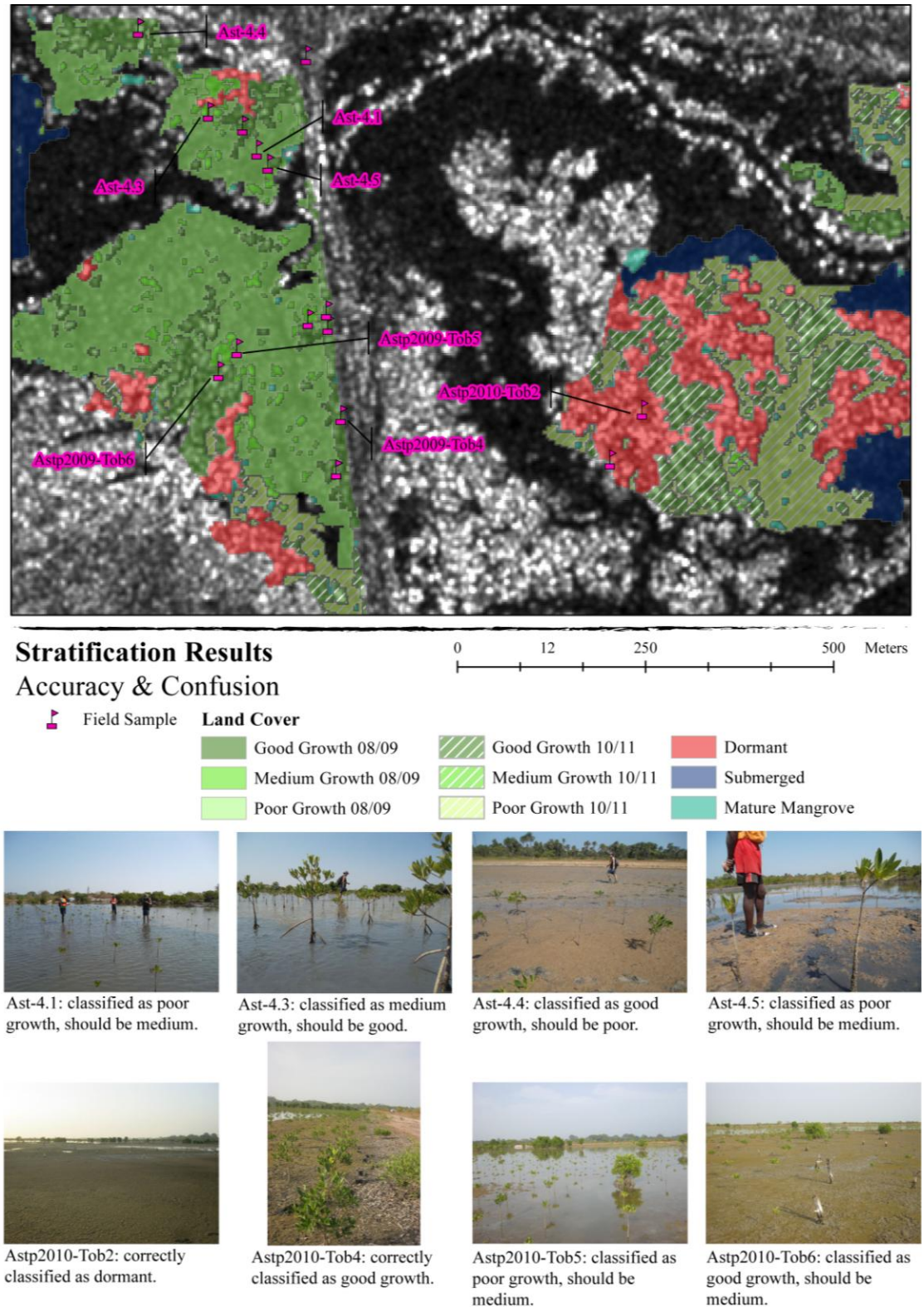

Figure 5-15: Representative examples of classification accuracy and class confusion.

6 DISCUSSION

This chapter presents a discussion of the conducted research methodology, addressing limiting factors as well as potential sources of error and reviewing the methodology implemented as it relates to the posed research questions. Subsequently, the initial research statement will be discussed. The chapter will conclude with an exploration of potential improvements to the methodology and probable opportunities for future research.

6.1 Limiting factors & potential sources of error

The mangrove ecosystem, particularly the young mangrove plantation environment, is versatile, subject to acute changes caused by daily tidal fluctuations, making it difficult to characterize over time. The Casamance River system is strongly influenced by complex tidal cycles. Furthermore, the tidal range leaves the sand and mud banks along the river, where the mangrove plantations are often established, dry at low tide or flooded to a depth of a few meters at high tide (Blesgraaf et al., 2006). Such changing and inconsistent environmental conditions, in combination with the extremely sensitive remote sensing characteristics of young plantation trees, make for challenging monitoring circumstances. These changes are reflected in the applied methodology as well as the potential operational requirements.

A primary limitation to the research method stems from the water depth to tree height ratio, which plays a significant role in the stratification of plantation growth quality. These ever changing conditions represent, in this case, critical unknown variables in the developed methodology. Unfortunately, very little water depth data was recorded by the field survey team and the information provided only corresponded to a single TS-X image acquisition. Therefore, the resulting stratification results must be considered with these limitations in mind.

An additional source of error in this study stems from the thematic input data on which it is based upon, namely the plantation boundaries and field sample location. Both data sets originate from field measurements and include displacements associated with the accuracy of the GPS device (3 to 15 m). According to the Project CDM-PDD (2010), such displacements were corrected based on Google Earth imagery during the generation of the plantation boundary files (the exact methodology for the correction is

unknown). Potential displacements in the location of field sample locations were not accounted for by the field team and remain unknown.

The operationalism of the project is driven by the need for two key pieces of information: (1) regeneration control recordings and (2) an estimation of carbon stock (i.e. biomass). As demonstrated in section 4.2.2.2.1, it was not possible to develop a quantitative model that could be accurately applied to the entire study area based on the field sampling data provided. Although the generated model demonstrated a relatively high R^2 and low RMSE, it was only applicable to select plantations. Furthermore, the quantitative calculation (i.e. the retrieval of plant and stand parameters) is impeded by the small tree sizes which often do not provide enough vertical structure to overwhelmingly influence the backscatter. In many such cases, the received SAR signal is increasingly influenced by background surface parameters (i.e. soil roughness, the presence of water or other vegetation).

The small tree sizes also impact the biomass assessment, in that the formula developed by Medeiros and Sampaio (2007) is primarily intended for larger mangrove trees (DBH $\geq$ 2 cm). Trees with a DBH under 2 cm negatively impact the applicability of the inversion model as the biomass calculation might be less representative of such small trees.

6.2 Discussion of applied method

Despite the limiting factors and sources of error, the methodology developed through this research is efficiently designed, considering the prototype status of development. Many of the pre-processing steps, particularly the image pre-processing, can be automated for integration into a fully operational service. The statistical pre-processing and development of the inversion model currently poses the principal problem. This critical step is presently operator driven and relies heavily on an individual's image interpretation skills, experience with SAR and familiarity with the study area. Furthermore, the development of the inversion model is dependent on operating conditions and only accounts for favorable conditions. Of the 850 zonal statistics, only 35 were finally deemed usable for the inversion model. The extremely variable operating conditions lead to the exclusion of five TS-X scenes that reflected either very high tide levels or very low tide (dry); it was important to use scenes acquired during flooded conditions to maximize the potential for double-bounce returns.

The supervised image-object based data processing method proved effective and efficient for the stratification of the plantations. The eCogniton rule set allowed for

input image substitution with minimal adjustment to individual classifiers as well as flexible segmentation strategies that could be tailored to the general plantation characteristics.

The accuracy assessment was designed to give an unbiased analysis of the stratification quality. Nevertheless, the method chosen contains several weaknesses. First of all, the validation process was not fully based on an independent data source, as wall-to-wall WorldView-2 and temporally relevant Google Earth data was not available. In some cases the classification outputs were validated with the input data set, resulting in a bias. Secondly, and more importantly, the validation was performed by the author and therefore, cannot be completely free of biases, despite his best efforts. A validation based on a complete secondary data source and performed by an independent expert would have been less biased.

6.3 Operational potential

Ideally, an operational EO-based service is based on an efficient, transferable and accurate methodology. For this methodology to be operational, a quantitative or qualitative product must be achieved that is cost efficient. Therefore, three general criterions have to be recognized regarding the data on which this methodology is based: (1) ideally, the use of single-source EO input data, (2) the use of practicable (i.e. applicable for a wall-to-wall monitoring scenario) image parameters and (3) timely temporal coverage.

The use of single-pol TerraSAR-X StripMap imagery met these three criterions. TS-X was determined superior to optical data during the pilot study phase (Tewkesbury et al., 2012). The plantations in the project area were often small, narrow and scattered, requiring large coverage, high resolution data – the single-pol TS-X StripMap mode imagery has a spatial resolution up to 3 m as well as a swath width of 30 km (Infoterra, 2009). In addition, the use of single-pol TS-X data was temporally more efficient, exhibiting twice the swath width of the dual-pol mode. With only one orbit in the ascending and descending direction being available for the Casamance study site and the large extent of the area in a West to East direction, the acquisition time was twice as long (132 days for this specific project site) for dual-pol as for single-pol data.

Principally, the developed method is transferable, when statistically relevant field sampling for all operating conditions in the coverage area are available. Although it was possible to generate an accurate quantitative model, the model was not transferable and the statistical pre-processing was not efficient. The qualitative model, although limited

by the efficiency of the statistical pre-processing, was applicable for over 70% of the examined area, where the plantations are partially flooded (i.e. a significant amount of the vertical vegetation structure was still above the water surface). In the remaining 30% of the study area, conventional field sampling will need to be applied. A more robust and representative set of field plots is needed to fully characterize the different plantation periods and quality stratum. The method was successfully applied to two different TS-X footprints within the study area, yet it is difficult to make any qualified conclusions as to its suitability in other parts of Senegal and the world.

Given the operational conditions and data available for the study, a relatively high overall accuracy of 77% was achieved. Notwithstanding, some classification confusion remains between growth quality strata as a result of critical unknown variables, particularly fluctuations in water depth and the water depth to tree height ratio. This is reflected in the overall kappa value of 75% - according to Krippendorff (1980), a $\kappa >$ 80% indicates "good" reliability in terms of content analysis.

Due to these factors, the developed method cannot yet be considered fully operational. Particularly, the statistical pre-processing and development of the inversion model have to be improved and reconfigured to account for water level. Such changes would ideally lead to a more productive use of acquired data.

6.4 Reflection on research goals

The main goal of this research has been to establish to what extent a TerraSAR-X based monitoring mechanism can efficiently supplement the traditional field-measurement based monitoring plan currently be implemented. Thereby, the research question concentrated on the exploration of operational parameters. Given the field data made available for this study, a standalone TerraSAR-X based approach has several weaknesses which impede the efficiency, accuracy and hence reliability of the methodology. First of all, the applied method was based on the stand-alone use of single-pol SAR data, the characteristics of which made it difficult to accurately differentiate between mature mangrove stands and bare soil. As previously established, the use of single-pol TS-X StripMap data was effective and met the operational requirements, nevertheless, the benefits from dual-pol data could be advantageous. Furthermore, the severe influence of the tidal range, particularly the temporal occurrence of tidal ranges and the seasonal influence on tide levels was not fully understood at the outset of this research and corrective measures are outside the considerations of this thesis.

Despite these factors, this study yields meaningful and useful results, given that the monitoring of mangrove reforestation environments with remote sensing technologies has been practically unexplored (Field, 1999). Still, there is a fair amount of room for further developments and future improvements, ranging from the quality of the *in situ* data to the type of EO input data sets.

Improvements that could be implemented to this particular research include the strengthening of the field sampling methodology – the inconsistencies and layout of the field data can be improved through the documentation of required information as well as the establishment and introduction of a data dictionary into the GPS. Such steps will prevent the need of manual editing in the future and gaps in the attribute data. In addition, a GPS accuracy threshold should be set to limit the effects of displacement and guarantee a sufficient level of accuracy. Furthermore, the distribution of field samples should focus on plantations with an average tree height greater than 40 cm and be constrained to areas known to demonstrate favorable operating conditions. A great improvement to the field sampling would be the future recording of water depth at the time of measurement.

General improvements to the operationalism of the method should consider the fusion of different EO data sets rather than the stand alone use of either optical or SAR data. For example, the integration of VHR optical imagery, such as Pléiades, could be used to introduce important and useful information to the image objects such as the Normalized Differenced Vegetation Index (NDVI) and Green Vegetation Index (GVI) or Green Vegetation Cover Fraction (GVCF). Although the addition of such information would lead to increased costs, they could especially improve the discrimination of mature mangrove and dormant image objects and potentially enhance the growth quality stratification in plantations older than 4 years– leading to more accurate and reliable results. An additionally interesting, yet costly, combination, particularly for very young ($\leq$ 2 years in age) plantations, would be that of SAR and blue-green waveform LiDAR information (such as that provided by the Experimental Advance Airborne Research LiDAR (EAARL)) due to its proven use in the evaluation of submerged environments and coastal vegetation.

Finally, future research should consider the integration of dual-pol SAR data, combining HH and VV polarizations (a comparative analysis of the effects of dual-pol SAR data was not feasible within the framework of this Masters thesis). According to a recent DLR study by Schmitt et al. (2012), the use of dual-polarized data allows for the "identification of two scattering mechanisms: surface and double-bounce". Such

information would be beneficial for the accurate classification of image objects with unfavorable operating conditions, specifically the discrimination of mangrove from dormant image objects. According to Janoth et al. (2013), VHR (up to 0.25 m spatial resolution) X-band polarimetric SAR data will be available through the TerraSAR-X Next Generation mission slated for 2014.

7 CONCLUSIONS

The aim of this study was to explore the potential of a TerraSAR-X based monitoring mechanism in a young mangrove plantation environment and thereby to establish to what extent it can efficiently supplement the current field-measurement based monitoring plan.

For this purpose, a linear inversion model was developed based on a correlation between the TS-X StripMap imagery acquired over the study site in southwestern Senegal and field samples acquired during the same period. The model established a relatively good correlation between TS-X sigma-0 backscatter and stand biomass; a R^2 of 0.57 and RMSE of 32% were achieved. This model was, in turn, applied to an image object based classification, designed to produce four growth quality strata: good, medium, poor and dormant.

Despite the difficult monitoring conditions, resulting from small tree sizes, the large tidal range and highly dissimilar hydrological parameters, the monitoring methodology developed by this research was applicable to 72% of the examinable study area. Furthermore, the cumulative image classification results revealed an overall accuracy of 77%. Based on these findings, the need for conventional field sampling can be reduced to account for approximately 30% of the project site, making wall-to-wall monitoring efforts far more realistic.

The results demonstrated by this research represent a positive development in the monitoring of mangrove reforestation with remote sensing techniques and provide a solid foundation for future studies. Yet, several sources of error need to be considered in subsequent studies: (1) the accuracy of GPS devices for the field survey, (2) the appropriateness of the biomass model, and (3) the influence of and integration of water depth into the modeling. These three factors can greatly improve the stratification results. Furthermore, in order for this method to become fully operational, the development of the inversion model must be optimized to eliminate the need of manual selection and fine tuning.

This being said, from a research perspective, the developed methodology can be considered successful. It provides valuable and relatively accurate information on the growth quality of young mangrove plantations; the image object-based rule set was successfully transferred to other TS-X scenes in the project area despite radical differences in hydrologic operating conditions and yielded comparable results. From an operational standpoint, the method still lacks decisive efficiency and the results of this

study do not fully establish the extent of transferability (i.e. to other parts of Senegal or similar projects sites in Southeast Asia).

Prospective work on the analysis and monitoring of mangrove reforestation should examine the potential of hybrid remote sensing data sets (i.e. a combination of SAR and optical data) as well as the use of VHR polarimetric SAR, like that anticipated within the framework of the TerraSAR-X Next Generation mission, or LiDAR data. The increased costs associated with the use of such data sets may affect the operationalism, but the expected improvements would be extremely interesting from a scientific perspective.

Nearly 15 years have passed since Field's publication, entitled *Mangrove rehabilitation: choice and necessity* (1999), in which he addressed the important, yet then restrictively expensive, role of remote sensing in mangrove reforestation monitoring. Since that time, remote sensing data has witnessed significant spatial, temporal as well as spectral improvements and has become cost effective. As a result, scientists can overcome past barriers; this research has achieved just that.

LIST OF REFERENCES

Adeel, Z., & Pomeroy, R. (2002). Assessment and management of mangrove ecosystems in developing countries. *Trees, 16*(2-3), 235-237.

Alongi, D. M. (2002). Present state and future of the world's mangrove forests. *Environmental Conservation, 29*, 331-349.

Alongi, D. M. (2008). Mangrove forests: Resilience, protection from tsunamis, and responses to global climate change. *Estuarine, Coastal and Shelf Science, 76*(1), 1-13.

Blesgraaf, R., Geilvoet, A., van der Hout, C., Smoorenburg, M., & Sottewes, W. (2006). Salinity in the Casamance Estuary: Occurrence and Consequences: Delft University of Technology.

Bosire, J. O., Dahdouh-Guebas, F., Walton, M., Crona, B. I., III, R. R. L., Field, C. D., . . . Koedam, N. (2008). Functionality of restored mangroves: A review. *Aquatic Botany, 89*(2), 251-259.

Brisco, B., Schmitt, A., Murnaghan, K., Kaya, S., & Roth, A. (2011). SAR polarimetric change detection for flooded vegetation. *International Journal of Digital Earth, 6*(2), 103-114.

Cafforio, C., Prati, C., & Rocca, F. (1991). SAR data foucusing using seismic migration techniques. *IEEE Transactions on Aerospace and Electronic Systems, 27*(2), 194-207.

Carletta, J. (1996). Assessing agreement on classification tasks: The kappa statistic. *Computational Linguistics, 22*(2), 249-254.

Cohen, J. (1960). A coefficient of agreement for nominal scales. *Educ. Psychol. Measurement, 20*(1), 37-46.

Conchedda, G., Durieux, L., & Mayaux, P. (2008). An object-based method for mapping and change analysis in mangrove ecosystems. *ISPRS Journal of Photogrammetry & Remote Sensing, 63*(5), 578-589.

Congalton, R. G. (1991). A Review of Assessing the Accuracy of Classifications of Remotely Sensed Data. *Remote Sensing of Environment, 37*(1), 35-46.

Cormier-Salem, M. C. (1999). The mangrove: an area to be cleared... for social scientists. *Hydrobiologia, 413*, 8.

DLR.). F-SAR - The New Airborne SAR System Retrieved 27. August, 2013, from http://www.dlr.de/hr/en/desktopdefault.aspx/tabid-2326/3776_read-5691/

DLR. (2011). TanDEM-X - die Erde in drei Dimensionen Retrieved 28.03, 2013, from http://www.dlr.de/dlr/desktopdefault.aspx/tabid-10378/566_read-426/

Duke, N. C., Meynecke, J.-O., Dittmann, S., Ellison, A. M., Anger, K., Berger, U., . . . Dahdouh-Guebas, F. (2007). A World Without Mangroves? *Science, 317*, 41-43.

Eineder, M., Fritz, T., Mittermayer, J., Roth, A., Börner, E., Breit, H., & Bräutigam, B. (2010). TerraSAR-X Ground Segment Basic Product Specification Document (1.7 ed.): DLR.

ESA. (2008). TIGER Initiative: Priniciples of Remote Sensing Retrieved 07.03., 2013, from http://www.tiger.esa.int/TrainingCds/cd_01/content_2/sez_2_2/pg2_2_04.htm

ESA. (2013). RADAR and SAR Glossary, 2013, from https://earth.esa.int/handbooks/asar/CNTR5-2.htm

ESRI. (2013). ArcGIS Desktop: Release 10.1. Redlands, CA: Environmental Systems Research Institute.

FAO. (2007). The world's mangroves 1980-2005. *FAO Forestry, 153*.

Faye, S., Faye, S. C., Ndyoe, S., & Faye, A. (2003). Hydrogeochemistry of the Saloum (Senegal) superficial coastal aquifer. *Environmental Geology, 44*, 127-136.

Field, C. D. (1999). Mangrove rehabilitation: choice and necessity. *Hydrobiologia, 413*(0), 47-51.
GARMIN. (2006). eTrex color series Retrieved 05.04, 2013, from http://www8.garmin.com/specs/eTrexspec0406.pdf
Hess, L. L., Melack, J. M., Filoso, S., & Wang, Y. (1995). Deliniation of Inundated Area and Vegetation Along the Amazon Floodplain with SIR-C Synthetic Apertature Radar. *IEEE TRANSACTIONS ON GEOSCIENCE AND REMOTE SENSING, 33*(4), 896-904.
Hijmans, R., & Etten, J. v. (2013). Raster: Geographic data analysis and modeling Retrieved 05.04., 2013, from http://cran.r-project.org/package=raster
Infoterra. (2009). TerraSAR-X Services - Image Product Guide. In Astrium (Ed.), (1 ed.). Friedrichshafen, Germany.
Janoth, J., Gantert, S., Schrage, T., & Kaptein, A. (2013). *TerraSAR Next Generation - Mission Capabilities*. Paper presented at the IGARSS, Melbounre, Australia.
Jones, H. G., & Vaughan, R. A. (2010). *Remote sensing of vegetation: principles, techniques, and applications*. New York: Oxford University Press Inc.
Kasischke, E. S., Melack, J. M., & Dobson, M. C. (1997). The use of imaging radars for ecological applications—A review. *Remote Sensing of Environment, 59*(2), 141-156.
Komiyama, A., Ong, J. E., & Poungparn, S. (2008). Allometry, biomass, and productivity of mangrove forests: A review. *Aquatic Botany, 89*(2), 128-138.
Krippendorff, K. (1980). *Content Analysis: An introduction to its Methodology*. London, U.K.: Sage Publications.
Livelihoods. (2010). Clean Development Mechanism Project Design Document Form for A/R CDM project activities (CDM-AR-PDD).
Livelihoods. (2012a). http://www.livelihoods.eu/casamance-senegal.html Retrieved 2012-12-26, 2012
Livelihoods. (2012b). Livelihoods Charter. In Livelihoods (Ed.).
Livelihoods. (2012c). Livelihoods Fund Panorama. In Livelihoods (Ed.).
Lopez-Sanchez, J. M., Ballester-Berman, J. D., & Hajnsek, I. (2012). First Results of Rice Monitoring Practices in Spain by Means of Time Series of TerraSAR-X Dual-Pol Images. *IEEE JOURNAL OF SELECTED TOPICS IN APPLIED EARTH OBSERVATIONS AND REMOTE SENSING, 4*(2), 412-423.
Massonnet, D., & Souyris, J.-C. (2008). *Imaging with Synthetic Aperature Radar*. Florida: CRC Press.
Mazda, Y., Wolanski, E., & Ridd, P. V. (2007). *The Role of Physical Processes in Mangrove Environments: Mannual for the Preservation and Utilization of Mangrove Ecosystems*. Tokyo: Terrapub.
McSweeney, C., New, M., & Lizcano, G. (2010). UNDP Climate Change Country Profiles: Senegal Retrieved 30 October 2013, from http://country-profiles.geog.ox.ac.uk/
Medeiros, T. C. C., & Sampaio, E. V. S. B. (2007). Allometry of aboveground biomasses in mangrove species in Itamaracá, Pernambuco, Brazil. *Wetlands Ecology and Management, 16*(4), 323-329.
Mollins, J., & Verchot, L. (2013). Bonn climate talks tackle emissions verification stumbling block. Retrieved from http://blog.cifor.org/17406/bonn-climate-talks-tackle-emissions-verification-stumbling-block#.Ulz15lNoiiQ
Ndour, J. P. N., Diédiou, C. M., & Fall, M. (2009). Developing a technique to plant Avicennia at La Somone lagoon (Senegal). *Nature & Faune, 24*(1), 74-80.
Olson, J., C.E. (2008). *Is 80% accuracy good enough?* Paper presented at the PECORA17, Denver, Colorado, U.S.A. http://ww.asprs.org/a/publications/proceedings/pecora17/0026.pdf

Proisy, C., Maugin, E., Fromard, F., & Karam, M. A. (2000). Interpretation of Polarimetric Radar Signatures of Mangrove Forests. *Remote Sensing of Environment, 71*, 11.

Richards, J. A. (2009). *Remote Sensing with Imaging Radar*. Berlin: Springer-Verlag.

Sakho, I., Mesnage, V., Deloffre, J., Lafite, R., Niang, I., & Faye, G. (2011). The influence of natural and anthropogenic factors on mangrove dynamics over 60 years: The Somone Estuary, Senegal. *Estuarine, Coastal and Shelf Science, 94*(1), 93-101.

Schmitt, A., Leichtle, T., Huber, M., & Roth, A. (2012). *On the use of dual-co-polarized TerraSAR-X data for wetland monitoring* Paper presented at the XXII ISPRS Congress, Melbourne, Australia.

Sendling, P. d. (2012, Jan. 12, 2012). ESA's Dordain Restates Sentinel Launch Cancellation Threat, from http://www.spacenews.com/article/esas-dordain-restates-sentinel-launch-cancellation-threat

Sensing, C. C. f. R. (2007). Advanced Radar Polarimetry Turorial Retrieved 08.03., 2013, from http://www.nrcan.gc.ca/sites/www.nrcan.gc.ca.earth-sciences/files/pdf/resource/tutor/polarim/pdf/polarim_e.pdf

Solutions, E. V. I. (2004). ENVI User's Guide (pp. 466). Boulder, Colorado, U.S.A: Exelis Visual Information Solutions.

Solutions, E. V. I. (2013). ENVI: Release 4.8. Boulder, CO.

Spalding, M. D., Blasco, F., & Field, C. D. (1997). *World Mangrove Atlas*. Okinawa, Japan: Ther International Society for Mangrove Ecosystems.

Team, R. D. C. (2008). R: A language and environment for statistical computing. Vienna, Austria: R Foundation for Statistical Computing. Retrieved from http://www.R-project.org

Tewkesbury, A., Von Poncet, F., & Brown, S. (2012). Satellite Monitoring of Mangrove Regeneration: Astrium Services.

Toan, T. L. (2005). *SAR image information content: Scattering physics.* Paper presented at the ESA-MOST Dragon Programme Advanced training course in Land Remote Sensing, Beijing.

Townsend, P. A. (2001). Mapping seasonal flooding in forested wetlands using multi-temporal Radarsat SAR. *Photogrammetric Engineering & Remote Sensing, 67*(7), 857-863.

Townsend, P. A. (2002). Estimating forest structure in wetlands using multitemporal SAR. *Remote Sensing of Environment, 79*(2-3), 288-303.

Trimble. (2012). eCognition Developer 8.8: User Guide.

Trimble. (2013). eCognition Developer: Release 8.8. Munich, Germany.

Kyoto Protocol to the United Nations Framework Convention on Climate Change (1998).

Valiela, I., Bowen, J. L., & York, J. K. (2001). Mangrove Forests: One of the World's Threatened Major Tropical Environments. *BioScience, 51*(10), 807-815.

Woodhouse, I. H. (2006). *Introduction to Microwave Remote Sensing*. Boca Raton, Florida, U.S.A.: CRC Press.

Woodroffe, C. D., & Grindrod, J. (1991). Biogeography: The Role of Quaternary Environmental and Sea-Level Change. *Journal of Biogeography, 18*(5), 479-492.

APPENDIX

Table A 1: Field data - shapefile configuration. Note the differences in file type and attributes.

Shapefile	Attributes	Definition
2008 & 2009 plantations (point.shp)	GPS Name	Point name
	Site Name	Name of the planted plot
	Year	Year of plantation establishment
	Density	Number of planted trees in the plot area (314 m^2)
	Photos	Range of corresponding photo numbers
	Date	Date of plot collection
	Time	UCT time of the GPS point acquisition
	Comments	Any additional information on the plot
2011 & 2012 plantations (point.shp)	GPS Name	As above
	Site Name	As above
	Year	As above
	Density	As above
	Photos	As above
	Date	As above
	Time	As above
Tide level field plots (poin.shp)	GPS Name	As above
	Site Name	As above
	Year	As above
	Density	As above
	Photos	As above
	Date	As above
	Time	As above
	Tide Level	Tide level in cm
	Comments	As Above
Biomass field plot (polygon.shp)	GPS Name	As Above
	Site Name	As Above
	Year	As Above
	Date	As Above
	Density	Number of planted trees within the plot area
	Surface ha	Area of the plot in hectares
	Comments	As Above

Table A 2: Field data – tabular field sheet configuration. Note the dissimilarities in the fields (attributes).

Excel Sheet	Fields	Definitions
2012 plantations	Date	Date of plot collection
	Village	Village associated with the plantation
	Site	Name of the planted plot
	Height	Tree height in cm (3-5 representative trees were measured)
	Diameter	Stem/trunk diameter in cm (3-5 representative trees were measured)
	GPS Point Name	Point name
	Photos	Range of corresponding photo numbers for the plot
	Density	Number of planted trees in the plot area (314 m^2)
	Density per hectare	Number of planted trees per hectare extrapolated from the plot density (i.e. plot density*10000/314,159)
	Species	Species of mature mangrove trees within the plot
	Estimation of plants inside the plot	Number of mature mangrove trees within the plot
	Height of vegetation inside plot	Height of mature mangrove trees within the plot
	Photo of vegetation inside plot	Range of corresponding photos of mature mangrove trees within the plot
	Height of vegetation outside plot	Height of mature mangrove trees around the plot
	Photos of vegetation outside plot	Range of corresponding photos of mature mangrove trees around the plot
2011 plantations	Date	As Above
	Village	As Above
	Site	As Above
	Height	As Above
	Diameter	As Above
	GPS Point Name	As Above
	Photos	As Above
	Density	As Above
	Density per hectare	As Above
	Height of vegetation outside plot	As Above
	Photos of vegetation outside plot	As Above

Table A 3: Field data – tabular field sheet configuration (continued).

Excel Sheet	Fields	Definitions
2008 & 2009 plantations	Date	As Above
	Village	As Above
	Site	As Above
	Year	Year of plantation establishment
	GPS Point Name	As Above
	Photos	As Above
	Density	As Above
	Density per hectare	As Above
	Tide Level	Tide level in cm at time of plot collection
	Height	As Above
	Diameter	As Above
	Species	As Above
	Height of vegetation inside plot	As Above
	Estimation of plants inside the plot	As Above
	Photo of vegetation inside plot	As Above
	Comments	Comments on growth quality etc.
Biomass monitoring	Date	As Above
	Village	As Above
	Site	As Above
	Year	As Above
	Plot (Polygon) Name	
	Density	Number of planted trees within the plot area
	Density per hectare	Number of planted trees per hectare extrapolated from the plot density
	Height	Tree height in cm (all trees within the plot were measured)
	Stem Diameter	Stem/trunk diameter in cm (all trees within the plot were measured)
	Crown Diameter	Crown diameter in cm(all trees within the plot were measured)
	Comments	Growth quality comments

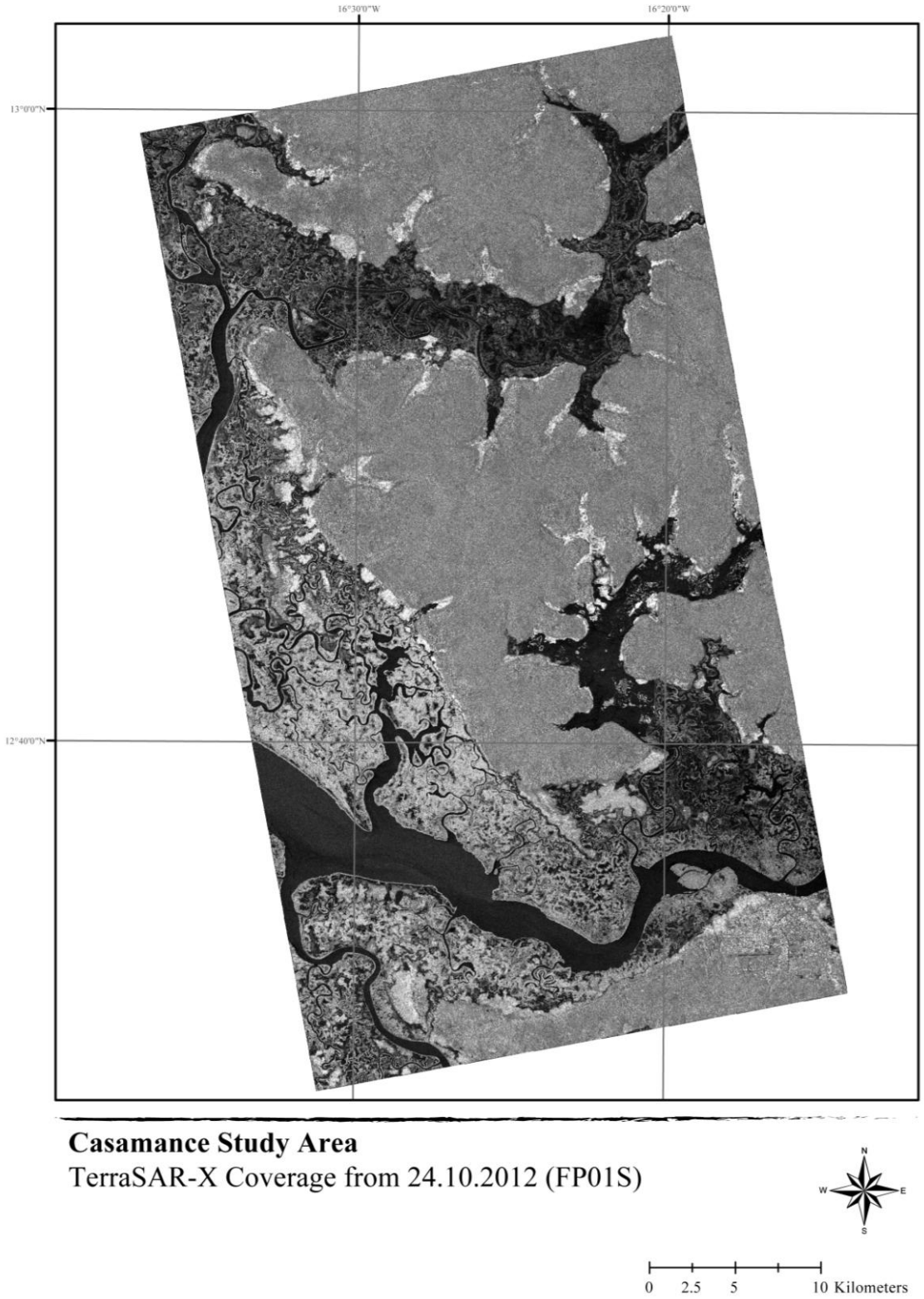

Figure A 1: TS-X scene acquired on 24.10.2012 used for the classification of footprint FP01S.

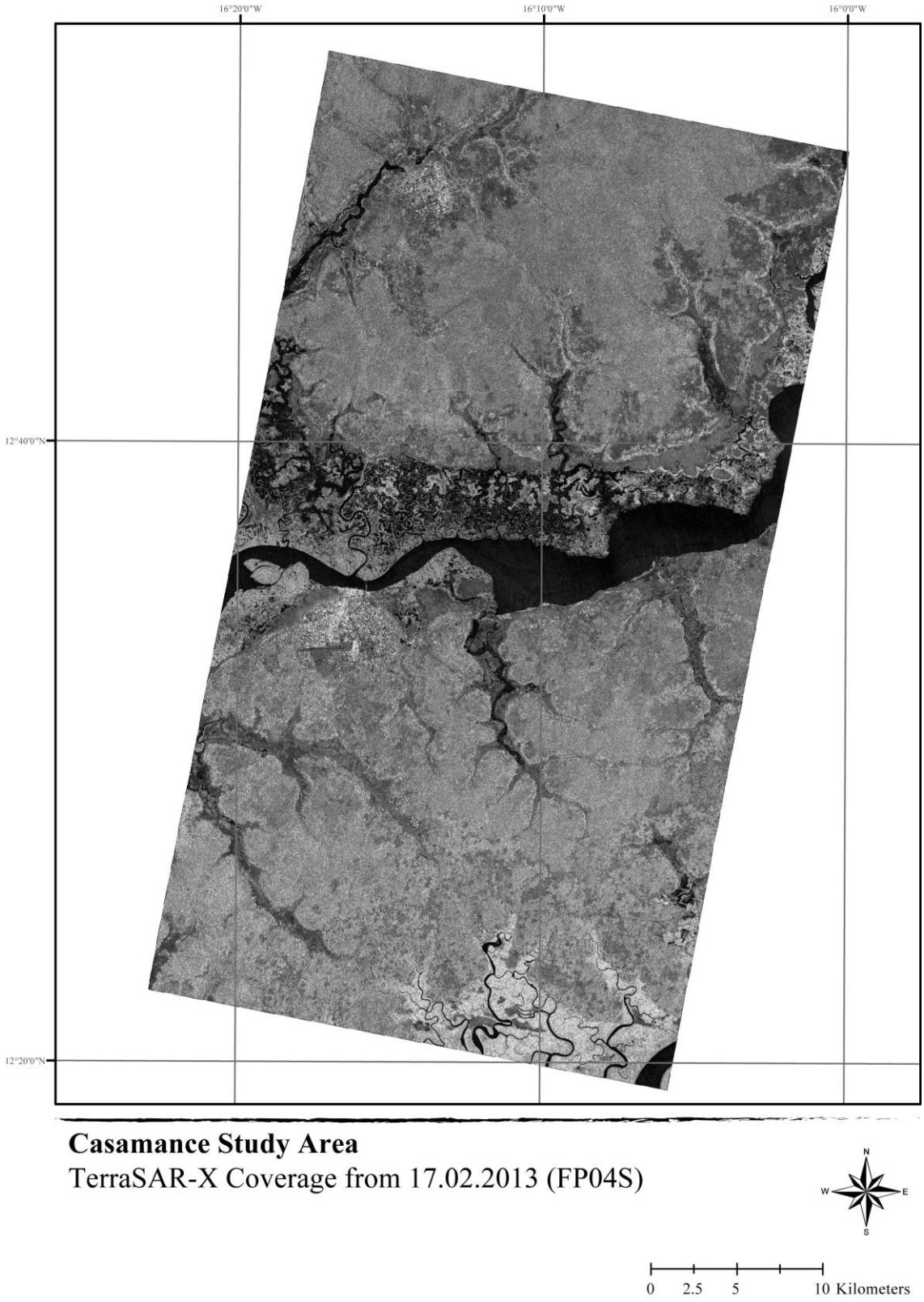

Figure A 2: TS-X scene acquired on 17.02.2013 used for the classification of footprint FP04S.

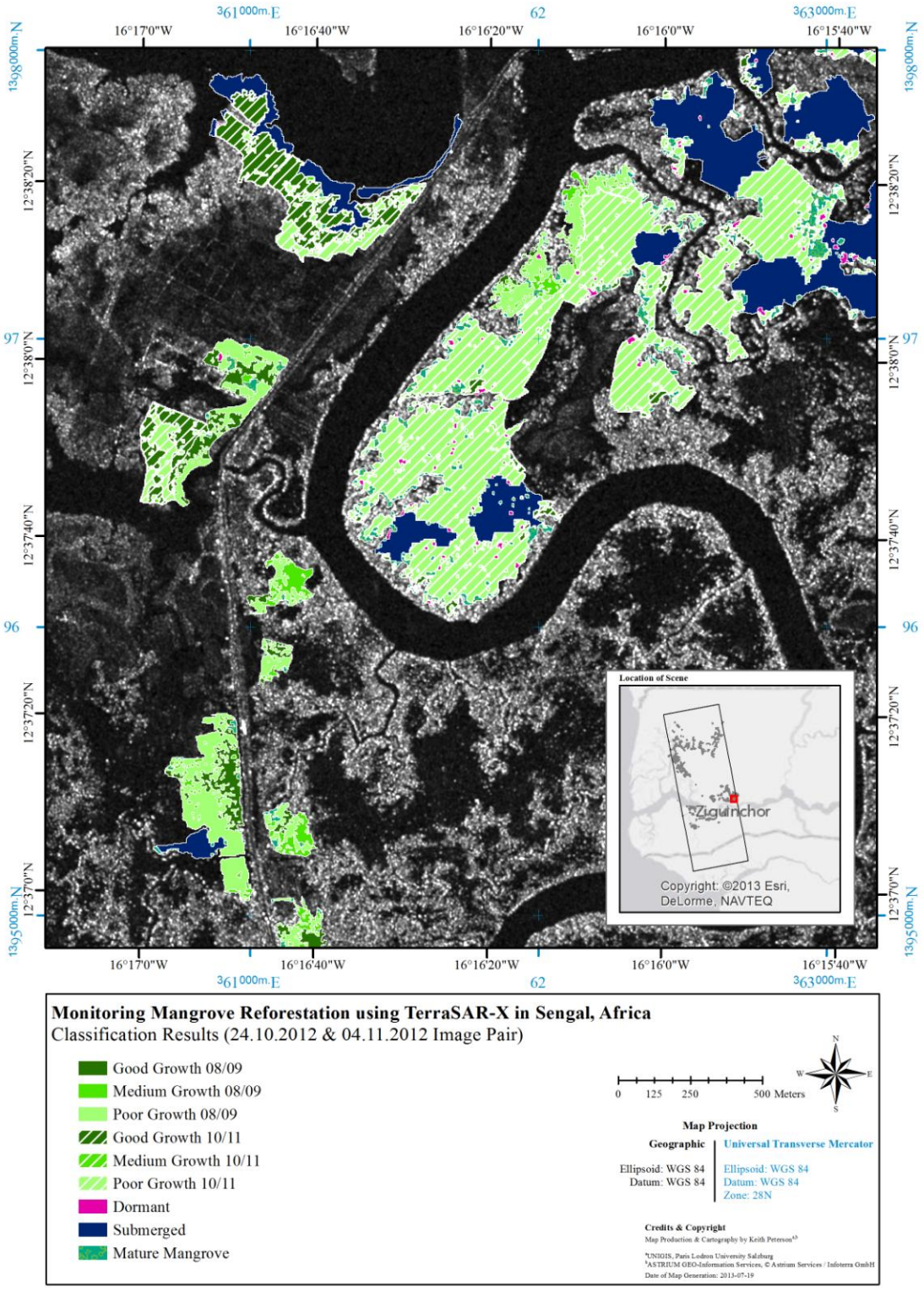

Figure A 3: Classification results from TS-X footprint FP01S.

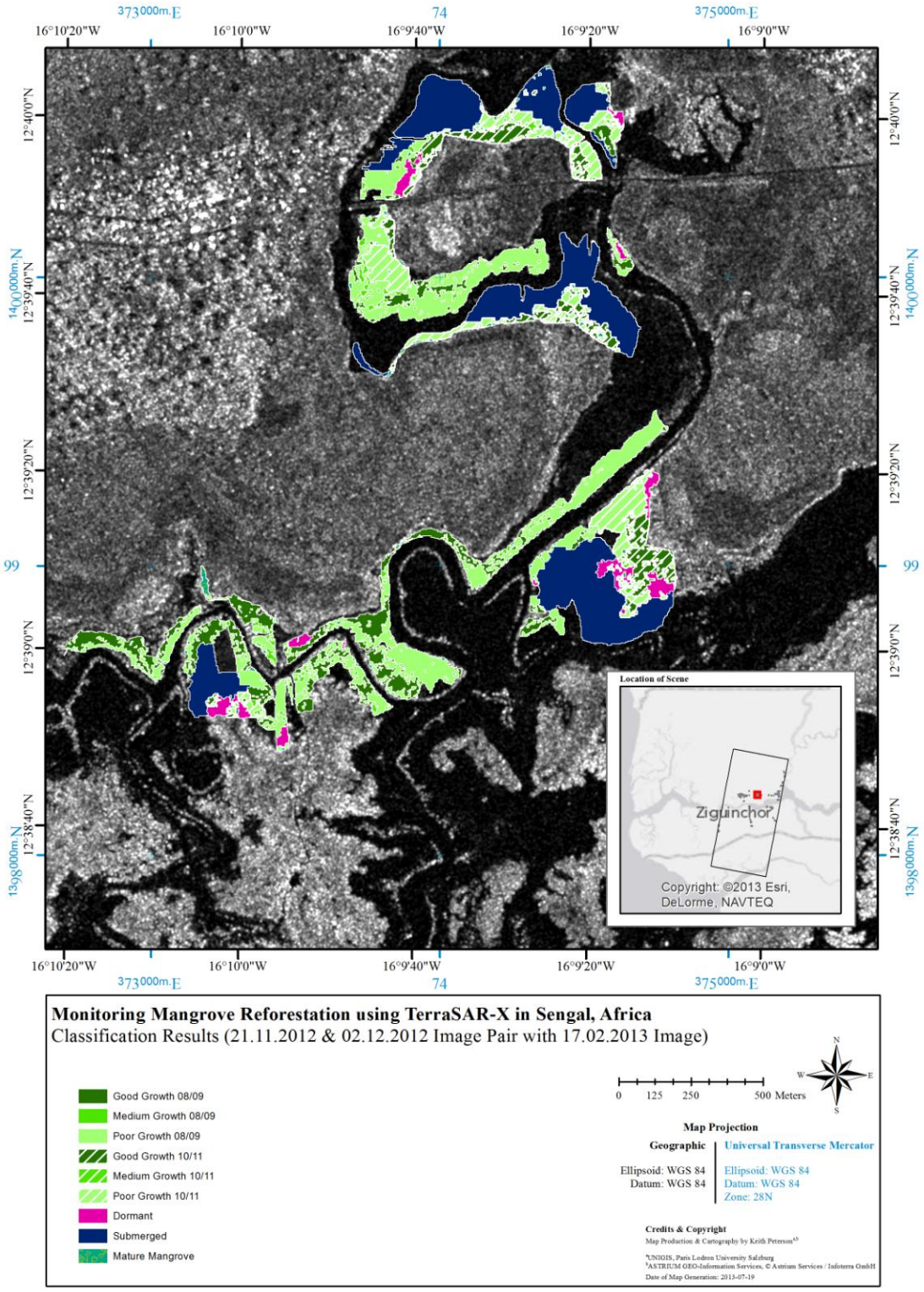

Figure A 4: Classification results from TS-X footprint FP04S.